

CAPITAL UNIVERSITY OF SCIENCE AND  
TECHNOLOGY, ISLAMABAD



# Supercritical Carbon Dioxide Power Cycles for Waste Heat Recovery of Gas Turbine

by

Abubakr Ayub

A thesis submitted in partial fulfillment for the  
degree of Master of Science

in the

Faculty of Engineering

Department of Mechanical Engineering

2018

Copyright © 2018 by Abubakr Ayub

All rights reserved. No part of this thesis may be reproduced, distributed, or transmitted in any form or by any means, including photocopying, recording, or other electronic or mechanical methods, by any information storage and retrieval system without the prior written permission of the author.

*This Thesis is dedicated to Professor Dr. Nadeem Ahmed Sheikh for his continuous advices, guidance, motivation and technical support.*



CAPITAL UNIVERSITY OF SCIENCE & TECHNOLOGY  
ISLAMABAD

**CERTIFICATE OF APPROVAL**

**Supercritical Carbon Dioxide Power Cycles for Waste  
Heat Recovery of Gas Turbine**

by

Abubakr Ayub

MME163001

**THESIS EXAMINING COMMITTEE**

S. No.	Examiner	Name	Organization
(a)	External Examiner	Dr. Muhammad Bilal Sajid	NUST, Islamabad
(b)	Internal Examiner	Dr. Muhammad Irfan	CUST, Islamabad
(c)	Supervisor	Dr. M. Mahabat Khan	CUST, Islamabad

---

Supervisor Name

Dr. M. Mahabat Khan

September, 2018

---

Dr. Liaquat Ali Khan

Head

Dept. of Mechanical Engineering

September, 2018

---

Dr. Imtiaz Ahmed Taj

Dean

Faculty of Engineering

September, 2018

## *Author's Declaration*

I, **Abubakr Ayub** hereby state that my MS thesis titled “**Supercritical Carbon Dioxide Power Cycles for Waste Heat Recovery of Gas Turbine**” is my own work and has not been submitted previously by me for taking any degree from Capital University of Science and Technology, Islamabad or anywhere else in the country/abroad.

At any time if my statement is found to be incorrect even after my graduation, the University has the right to withdraw my MS Degree.

**Abubakr Ayub**

Registration No: MME163001

## *Plagiarism Undertaking*

I solemnly declare that research work presented in this thesis titled “**Supercritical Carbon Dioxide Power Cycles for Waste Heat Recovery of Gas Turbine**” is solely my research work with no significant contribution from any other person. Small contribution/help wherever taken has been dully acknowledged and that complete thesis has been written by me.

I understand the zero tolerance policy of the HEC and Capital University of Science and Technology towards plagiarism. Therefore, I as an author of the above titled thesis declare that no portion of my thesis has been plagiarized and any material used as reference is properly referred/cited.

I undertake that if I am found guilty of any formal plagiarism in the above titled thesis even after award of MS Degree, the University reserves the right to withdraw/revoke my MS degree and that HEC and the University have the right to publish my name on the HEC/University website on which names of students are placed who submitted plagiarized work.

**Abubakr Ayub**

Registration No: MME163001

## *List of Publications*

It is certified that following publication(s) has been made out of the research work that has been carried out for this thesis:-

1. **Ayub, A.** , Sheikh, N. A., Tariq, R., Khan, M. M., & Invernizzi, C. M. (2018). Exergetic optimization and comparison of combined gas turbine supercritical CO2 power cycles. *Journal of Renewable and Sustainable Energy*, 10(4), 044703.
2. **Ayub, A.** , Sheikh, N. A., Tariq, R., Khan, M. M., Thermodynamic Optimization of Air Bottoming Cycle for Waste Heat Recovery, in 2nd International Conference on Energy Systems for Sustainable Development (ESSD-2018), 2018, pp. 5962.

**Abubakr Ayub**

Registration No: MME163001

## *Acknowledgements*

Firstly, Thanks a lot to ALLAH ALMIGHTY for giving me skills and strengths to carry out all the tasks of this research work successfully. I am deeply grateful to my beloved mother who supports and encourages me at all times, and always prays for my success in this life and the life hereafter.

I would also like to acknowledge my deep thanks and appreciation to Professor Dr. Nadeem Ahmed Sheikh of Department of Mechanical Engineering at International Islamic University Islamabad (IIUI), Pakistan for keeping me motivated throughout the course of this research work with his kind remarks and technical support. It's an honor for me to work under his supervision. May ALLAH ALMIGHTY grant countless blessings on him, Ameen.

I would also like to thank Mr. Muhammad Saeed from Kyungpook National University, South Korea and Prof. Costante Mario Invernizzi from University of Brescia, Italy for their generous support and guidance during this research work. Thanks also to Capital University of Science and Technology (CUST), Islamabad for granting me full tuition fee waiver in all semesters of my MS degree.

It is a great pleasure to express my deepest thanks and gratitude to my friends and research colleagues specifically Rasikh Tariq from HITEC University, Taxila and Raja Awais Liaqat from Capital University of Science and Technology, Islamabad for their continuous review and positive feedback on my research work. Without their input, this work could not have been completed successfully.

Lastly, Thanks to my family members for their endless love and support.

---

# *Abstract*

For developing a sustainable power system, the key is to maximize the use of available resources with minimal impact on the environment. One technique of achieving this is waste heat recovery. In this study, the combined cycles are proposed based on the concept of gas turbine waste heat recovery which comprise of two parts: topping gas turbine and bottoming sCO<sub>2</sub> Brayton power cycles. The combined cycle configurations selected for thermodynamic analysis are the combined gas turbine simple regenerative sCO<sub>2</sub> cycle (CGTSRC), the combined gas turbine recompression sCO<sub>2</sub> cycle (CGTREC) and the combined gas turbine preheating sCO<sub>2</sub> cycle (CGTPHC). The energy and exergy analysis are conducted to investigate the power production, exhaust heat recovery, energetic and exergetic efficiencies of selected cycles for variation in mass flow rate, mass split percentage and compression ratio. Using Engineering Equation Solver (EES) software, the thermodynamic calculations and optimization are carried out to find the design point which provide maximum exergetic efficiency.

In addition to determination of design point, the comparison of selected combined cycles is performed with simple gas turbine cycle (SGT) and conventional air bottoming combined cycle (ABC) to highlight the thermodynamic and environmental significance of sCO<sub>2</sub> bottoming power cycles. For comparison, heat recovery, power output of combined and bottoming cycles, mass flow rate, energetic efficiency, exergetic efficiency and environmental impact are considered as the key performance parameters. The results and comparison indicate that optimum cycle configuration is CGTPHC which provide energy efficiency of 46.8%, exergy efficiency of 64.8% and 47.3 MW combined power output. Moreover, the energetic and exergetic performance of combined supercritical CO<sub>2</sub> cycles are better than ABC cycle and SGT cycle.

The turbomachinery (compressor and turbine) of optimum bottoming sCO<sub>2</sub> power cycle are designed which include the determination of accurate geometry and efficiency using preliminary and 1D mean line design methods. A robust design code is developed in MATLAB<sup>®</sup> coupled with REFPROP property library for retrieval

of sCO<sub>2</sub> properties. The compressor design code is validated with experimental results taken from literature. The efficiency of compressor and turbine calculated from the turbomachinery design code are 81.2% and 86.17%, respectively.

# Contents

Author's Declaration	iv
Plagiarism Undertaking	v
List of Publications	vi
Acknowledgements	vii
Abstract	viii
List of Figures	xiii
List of Tables	xv
Abbreviations	xvi
Symbols	xvii
Subscripts	xviii
<b>1 Introduction</b>	<b>1</b>
1.1 Overview of Gas Turbine Waste Heat Recovery . . . . .	1
1.2 Supercritical Carbon Dioxide Power Cycles . . . . .	4
1.3 Problem Statement . . . . .	6
1.4 Scope of the Work . . . . .	7
1.5 Thesis Outline . . . . .	7
<b>2 Literature Review</b>	<b>10</b>
2.1 Summary . . . . .	22
<b>3 Methodology</b>	<b>24</b>
3.1 Combined Gas Turbine Supercritical CO <sub>2</sub> Power Cycles . . . . .	24
3.2 Thermodynamic Modeling . . . . .	27

---

3.2.1	Exergy of a System . . . . .	28
3.2.2	Turbomachinery Thermodynamic Model . . . . .	29
3.2.2.1	Topping Cycle Compressor (CI) . . . . .	29
3.2.2.2	Topping Cycle Turbine (TI) . . . . .	30
3.2.2.3	Bottoming sCO <sub>2</sub> Cycle Compressor (C2) . . . . .	30
3.2.2.4	Bottoming sCO <sub>2</sub> Cycle Recompressor (C3) . . . . .	30
3.2.2.5	Bottoming sCO <sub>2</sub> Cycle Turbine (T2) . . . . .	31
3.2.3	Combustion Chamber Thermodynamic Model . . . . .	31
3.2.4	Integrated Heat Exchanger (IHX) Thermodynamic Model . . . . .	32
3.2.5	Recuperators Thermodynamic Model . . . . .	33
3.2.5.1	HTR . . . . .	33
3.2.5.2	LTR . . . . .	33
3.2.5.3	Cooler . . . . .	33
3.2.5.4	Mixer Model . . . . .	34
3.3	Performance Parameters . . . . .	34
3.3.1	Energy Efficiency . . . . .	34
3.3.2	Exergy Efficiency . . . . .	35
3.3.3	Environmental Impact . . . . .	36
3.4	Calculation Methodology . . . . .	36
3.5	Validation . . . . .	40
<b>4</b>	<b>Thermodynamic Results and Analysis</b> . . . . .	<b>41</b>
4.1	Combined Gas Turbine Recompression Brayton Cycle . . . . .	42
4.2	Combined Gas Turbine Preheating Brayton Cycle . . . . .	47
4.3	Comparison of Results . . . . .	52
4.3.1	Performance Comparison with Combined Gas Turbine Simple Regenerative Cycle (CGTSRC) . . . . .	52
4.3.2	Performance Comparison with Air Bottoming Combined Cycle (ABC) . . . . .	54
4.4	Summary . . . . .	57
<b>5</b>	<b>Turbomachinery Design</b> . . . . .	<b>60</b>
5.1	Compressor Design . . . . .	60
5.1.1	Selection of Type of Compressor . . . . .	62
5.1.2	Preliminary Sizing . . . . .	63
5.1.3	1D Mean Line Compressor Design . . . . .	67
5.1.4	Impeller Inlet . . . . .	68
5.1.5	Impeller Outlet . . . . .	71
5.1.6	Enthalpy Loss Models . . . . .	72
5.1.7	Internal Loss Models . . . . .	73
5.1.7.1	Incidence Loss . . . . .	73
5.1.7.2	Blade Loading Loss . . . . .	74
5.1.7.3	Skin Friction Loss . . . . .	74
5.1.7.4	Clearance Loss . . . . .	74

---

5.1.8	External Loss Models . . . . .	75
5.1.8.1	Recirculation Loss . . . . .	75
5.1.8.2	Disc Friction Loss . . . . .	75
5.1.8.3	Mixing Loss . . . . .	76
5.1.9	Updated Compressor Efficiency . . . . .	77
5.1.10	Diffuser and Volute Section . . . . .	77
5.1.11	Pressure Ratio Convergence . . . . .	78
5.1.12	Compressor Design Results . . . . .	78
5.1.13	Validation of Compressor Design Code . . . . .	79
5.2	Turbine Design . . . . .	80
5.2.1	Preliminary Sizing . . . . .	81
5.2.2	1D Mean Line Turbine Design . . . . .	83
5.2.3	Revised Performance Evaluation of BPHC and CGTPHC . . . . .	88
<b>6</b>	<b>Conclusion and Recommendations</b>	<b>90</b>
	<b>Bibliography</b>	<b>93</b>
	<b>EES Code for CGTREC</b>	<b>104</b>
	<b>MATLAB Code for Compressor Design</b>	<b>117</b>

# List of Figures

1.1	Variation of specific heat ( $C_p$ ) of CO <sub>2</sub> near the critical point. . . . .	5
1.2	Variation of density of CO <sub>2</sub> near the critical point. . . . .	5
3.1	Schematic of combined gas turbine simple regenerative sCO <sub>2</sub> cycle (CGTSRC). . . . .	26
3.2	Schematic of combined gas turbine recompression sCO <sub>2</sub> cycle (CGTREC). . . . .	27
3.3	Schematic of combined gas turbine preheating sCO <sub>2</sub> cycle (CGT-PHC). . . . .	28
3.4	Methodology for thermodynamic calculations of CGT-sCO <sub>2</sub> power cycles. . . . .	39
4.1	Behavior of (a) thermal efficiency and (b) net power output of bottoming recompression cycle (BREC) and combined gas turbine recompression cycle (CGTREC) with change in MFRR, keeping 'x' constant ( $x = 60\%$ ). . . . .	42
4.2	Behavior of (a) specific heat $C_p$ of sCO <sub>2</sub> in BREC, turbine inlet temperature ( $T_3$ ) and (b) heat recovery of BREC with change in MFRR keeping 'x' constant ( $x = 60\%$ ). . . . .	43
4.3	Variation of (a) energetic and (b) exergetic efficiencies with change in both MFRR and $x$ for CGTREC. . . . .	43
4.4	Optimum T-s diagram of BREC. . . . .	45
4.5	(a) Component level exergy destruction in BREC (b) Exergy destruction and exergy loss in CGTREC compared to SGT. . . . .	46
4.6	Variation of (a) first law efficiency, (b) net power output, (c) $T_3$ and (d) heat recovery for CGTPHC with change in MFRR keeping 'x' constant ( $x = 65\%$ ). . . . .	48
4.7	Variation of (a) thermal, (b) exergetic efficiency and heat recovery of CGTPHC with change in 'x' at MFRR = 1.6. . . . .	48
4.8	Variation of (a) energy efficiency and (b) exergy efficiency of CGTPHC for variation in MFRR and 'x'. . . . .	49
4.9	Optimum T-s diagram of BPHC. . . . .	51
4.10	Component level exergy destruction in BPHC (b) Exergy destruction and exergy loss in CGTPHC compared to SGT. . . . .	52
4.11	Comparison of combined cycle energy efficiency at (a) $r_c = 2.7$ , (b) $r_c = 3$ , keeping $x = 45\%$ for CGTREC and CGTPHC. . . . .	53
4.12	Comparison of combined cycle exergy efficiency at (a) $r_c = 2.7$ , (b) $r_c = 3$ , keeping $x = 45\%$ for CGTREC and CGTPHC. . . . .	54

---

4.13	Schematic of Air Bottoming cycle (ABC). . . . .	54
4.14	Results validation of ABC combined cycle. . . . .	55
5.1	Effect of compressor's isentropic efficiency on the first law efficiency of BPHC. . . . .	62
5.2	Single stage radial compressor in r-plane [69]. . . . .	63
5.3	Balje's $N_S$ - $D_S$ diagram for compressors [81]. . . . .	64
5.4	1D Mean line design methodology. . . . .	66
5.5	1D Mean line path of a radial compressor [67]. . . . .	67
5.6	Method to compute impeller inlet static density. . . . .	70
5.7	Impeller inlet velocity triangle. . . . .	70
5.8	Impeller outlet velocity triangle. . . . .	73
5.9	Balje's $N_S$ - $D_S$ diagram for Turbines. . . . .	82
5.10	(a) Meridional view showing main stations of the radial turbine; (b) Rotor inlet velocity triangle;(c) Rotor outlet velocity triangle. . . . .	87

# List of Tables

2.1	Review of literature on supercritical CO <sub>2</sub> power cycles for applications in nuclear, solar and biomass energy sources. . . . .	12
2.2	Review of literature on supercritical CO <sub>2</sub> power cycles for applications in waste heat recovery. . . . .	19
3.1	Operating parameters for combined cycle calculations. . . . .	38
3.2	Comparison between the present work and those of Ref. [37] for BREC. . . . .	40
4.1	Objective function and ranges of decision parameters for BREC. . . . .	44
4.2	Optimum results of CGTREC. . . . .	44
4.3	Bounds and objective function for CGTPHC. . . . .	49
4.4	Optimum results of CGTPHC. . . . .	50
4.5	Summary and comparison of the results. . . . .	56
5.1	Preliminary design results of the radial compressor of BPHC. . . . .	65
5.2	Input thermodynamic parameters from BPHC. . . . .	68
5.3	Input geometric parameters [65, 71]. . . . .	68
5.4	Compressor geometry and performance results for supercritical CO <sub>2</sub> BPHC. . . . .	78
5.5	Geometry and operating conditions of the compressor in Sandia National Laboratory [52]. . . . .	79
5.6	Comparison of results from 1D Mean line design code with experimental results. . . . .	80
5.7	Preliminary design results of the radial turbine of BPHC. . . . .	83
5.8	Input parameters and design conditions for turbine 1D mean line design code. . . . .	84
5.9	Radial turbine design results for BPHC. . . . .	88
5.10	Comparison of thermodynamic results of CGTPHC from two methods (a) Assumed compressor efficiency method (b) Predicted compressor efficiency using 1D mean line design method. . . . .	89

# Abbreviations

<b>ABC</b>	Air bottoming cycle
<b>BPHC</b>	Bottoming supercritical CO <sub>2</sub> preheating cycle
<b>BREC</b>	Bottoming supercritical CO <sub>2</sub> recompression cycles
<b>BSRC</b>	Bottoming supercritical CO <sub>2</sub> simple regenerative cycle
<b>CGT-sCO<sub>2</sub></b>	Combined gas turbine supercritical CO <sub>2</sub> cycles
<b>CGTPHC</b>	Combined gas turbine preheating cycle
<b>CGTREC</b>	Combined gas turbine recompression cycle
<b>CGTSRC</b>	Combined gas turbine simple regenerative cycle
<b>REFPROP</b>	Reference Fluid Properties (NIST database)
<b>sCO<sub>2</sub></b>	Supercritical carbon dioxide
<b>SGT</b>	Simple gas turbine cycle

# Symbols

$C$	Heat capacity (kW/K)
$E_x$	Exergy (kW)
$h$	Specific enthalpy (kJ/kg)
IRR	Rate of exergy destruction of combined cycle components (kW)
$\dot{m}$	Mass flow rate (kg/s)
$Q$	Thermal power (kW)
$r_c$	Compression ratio of bottoming sCO <sub>2</sub> power cycles
$r_s$	Shroud radius (m)
$r_t$	Blade tip radius (m)
$r_h$	Hub radius (m)
$S$	Specific entropy (kJ/kg.K)
$T$	Temperature (K)
$T_{wh}$	Exhaust waste heat temperature (K)
$W$	Power (W)
$x$	Split mass percentage in case of CGTPHC Recompression mass percentage in case of CGTREC
$\varepsilon$	Effectiveness
$\eta$	Efficiency
$\alpha$	Inlet swirl angle
$\beta$	Relative velocity angle
$U$	Blade tangential velocity
$W$	Flow relative velocity
$Z$	Number of blades

# Subscripts

<i>b</i>	Referring to bottoming cycle
<i>c</i>	Compressor
<i>df</i>	Disc friction
<i>exh</i>	Exhaust gases
<i>f</i>	Fuel
<i>g</i>	Flue gas
<i>inc</i>	Incidence
<i>LHV</i>	Lower heating value (kJ/kg)
<i>o</i>	Reference state
<i>rc</i>	Recirculation
<i>sf</i>	Skin friction
<i>s</i>	Isentropic
<i>T</i>	Referring to topping cycle
<i>t</i>	Turbine
<i>tt</i>	Total to total

# Chapter 1

## Introduction

### 1.1 Overview of Gas Turbine Waste Heat Recovery

In many countries, large portion of power production is shared by gas turbines. The design as well as performance of gas turbines have been improved due to considerable efforts in research and development. The improvements in materials and cooling technologies allowed gas turbine to work at large temperatures and pressures which significantly enhances the power capacity and efficiency of the gas turbine cycle. The technology advancements and development of new gas turbines has increased the efficiency of the standalone gas turbine cycle up to 40% [1]. To enhance the specific work of the gas turbine cycle, reheat and inter-cooling are employed by various manufacturers. Reheating increases the expansion work of the turbine, whereas inter-cooling decreases the compression work (or back work ratio) of the gas turbine cycle, consequently the specific work increases.

Gas turbines work on the principle of Brayton cycle in which there are four processes; compression, combustion, expansion and exhaust. The air at ambient conditions enter the compressor and is compressed to high pressure. Air is then transferred to combustion chamber where combustion gases are produced at high temperature and pressure. The combustion gases then travel to the turbine where

expansion occurs and power is produced. After expansion process in turbine, the exhaust gases are lost to the environment. These exhaust gases carry combustion products at high mass flow and temperature and they are major source of pollution and global warming. The temperature of exhaust gases is usually in the range of 400 °C to 600 °C [1, 2] and they have enough thermodynamic potential (exergy) to produce more power.

The performance of gas turbine cycle can significantly be improved by recovering the high temperature exhaust gases for useful purposes. Recuperation is one of the common techniques used for many years, in which heat from exhaust gases is extracted with the help of a recuperator to preheat the air entering the combustion chamber. The recuperation increases the fuel efficiency of gas turbine cycle; however, it is limited by the compressor outlet temperature. Recuperation is adopted by several commercial gas turbines which experienced approximately 10% increase in thermal efficiency [1].

An alternative technique to utilize high temperature exhaust gases is by employing heat recovery power cycle known as bottoming cycle [3]. Integration of bottoming cycle not only increases the fuel efficiency of the gas turbine but also takes part in the reduction of environmental emissions [4]. A well-known combined cycle is gas turbine-steam Rankine cycle, also known as conventional combined cycle. The conventional cycle comprises of topping cycle gas turbine and steam Rankine bottoming cycle. The exhaust heat from topping cycle is utilized to produce steam in a heat recovery steam generator which in turn is transferred to steam turbines for power production. Heat recovery at two or three pressure levels is mostly applied to enhance power capacity of the combined cycle. Power output in the range of 500-600 MWe with efficiency of almost 58-60% can be produced using conventional combined cycle [1]. However, the conventional combined cycle needs large capital investment and maintenance cost due to presence of two or more heat recovery steam generators, heavy duty gas turbines and water purification system to maintain steam quality. Therefore, the steam Rankine bottoming cycle is not proved to be an economically feasible option in the power production range of 40-50 MW [5, 6].

To improve the performance of small scale gas turbines, air bottoming cycle (ABC) is recently industrialized [7]. ABC [8–10] has comparatively simple configuration, it comprises of a compressor, a heat exchanger and an expander. It has simple operation because of absence of heavy steam equipment and water purification system. Various studies showed the thermodynamic and economic feasibility of ABC [5, 10–13]. ABC has ability to enhance the specific work of gas turbine by 15.4% and provide 13.3% average reduction in the specific fuel consumption (SFC) of the gas turbine [4]. However, it is reported that ABC requires large and heavy regenerator; a regenerator weighing 45 tons is required for 6.6 MW gas turbine [12].

In recent decades, organic Rankine cycles (ORCs) are investigated as a bottoming cycle for utilization of waste heat from various sources. Organic fluids such as R123, R113, R12 and ammonia can be used as a working fluid in these cycles [14, 15]. An extensive research has been done on thermodynamic analysis and comparison of different configurations of ORCs [16–18]. Different choices of organic fluids are suggested by researchers for different kinds of heat sources. R123 is found to be the best option among R12, R123, R134a and R717 for power conversion from low grade heat source [19]. Similarly, cyclohexane working fluid was suggested for ORCs coupled with biomass heat source [20]. To recover biogas waste heat, the subcritical and supercritical ORCs are also investigated using R245fa as working fluid [21]. Although there is an active research going in the field of ORCs based on different working fluids for power generation, however, some of the limitations of the organic fluids are yet challenging. For example, organic fluids such as R11, R12, R113 and R123 are expensive and contain chloro-fluoro carbons (CFCs) which are harmful for ozone layer [22]. Organic fluids are limited to low grade waste heat mainly because of their low chemical stability. Moreover, the selection and screening procedure of organic fluids for different temperature ranges of heat sources is difficult. Their turbine designs are challenging especially for some wet organic fluids which, after expansion in turbine, cause erosion of the turbine blades [23]. In addition, the constant temperature heat addition process in the heat

recovery heat exchanger of ORC creates pinching which restricts the performance of the heat exchanger.

## 1.2 Supercritical Carbon Dioxide Power Cycles

Due to the depletion of fossil fuels and serious environmental concerns, the researchers and industrialists are working on the environment friendly alternatives. Supercritical carbon dioxide (from here referred to as sCO<sub>2</sub>) got attention of the researchers because of its unique thermo-physical properties near critical point. CO<sub>2</sub> attains supercritical state above 31 °C (304 K) and 7.4 MPa. The properties of carbon dioxide especially specific heat ( $C_p$ ) and density ( $\rho$ ) near the critical point show large variations as shown in Figures 1.1 and 1.2. Because of these variations, ideal gas assumption is invalid and use of latest thermodynamic property data should be used for calculations. The thermodynamic data in this study is taken from Engineering equation solver (EES) and Reference Fluid Thermodynamic and Transport Properties (REFPROP) [24] for sCO<sub>2</sub> cycle analysis and turbomachinery design respectively. Also, the compressibility factor of sCO<sub>2</sub> near critical point is lower, i.e. 0.2-0.5 due to which less compression work is required which is reflected in high thermal efficiency of sCO<sub>2</sub> cycle. In case when conditions are far away from the critical point, i.e. at large temperatures and pressures, the properties show comparatively smooth (linear) behaviour as shown in Figures 1.1 and 1.2. Hence, ideal gas relations can be employed for operation far from critical point as in the case of sCO<sub>2</sub> turbine. sCO<sub>2</sub> offers benefits as clean working fluid for power production because it has zero ozone depletion potential [25]. It is relatively inexpensive, nontoxic and abundant in nature [26, 27]. Compared to steam, sCO<sub>2</sub> is less corrosive at the same temperature which is helpful in maintaining large turbine inlet temperature (TIT). In addition, sCO<sub>2</sub> power cycles require 10 times smaller turbo machinery because of large pressure (>7.4 MPa) and density (shown in Fig 1.2) compared to the steam Rankine cycle [28].

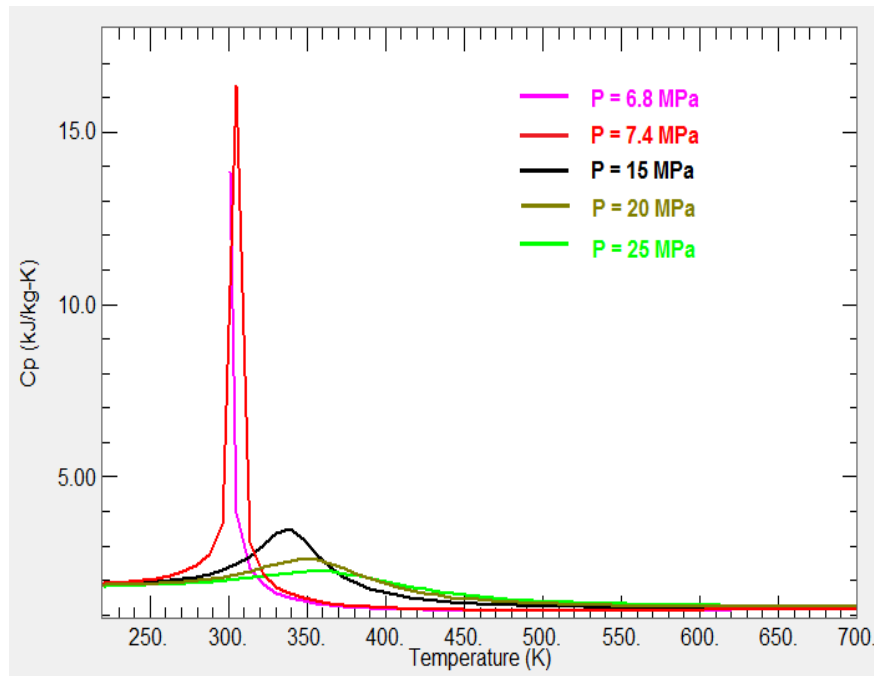


FIGURE 1.1: Variation of specific heat ( $C_p$ ) of  $\text{CO}_2$  near the critical point.

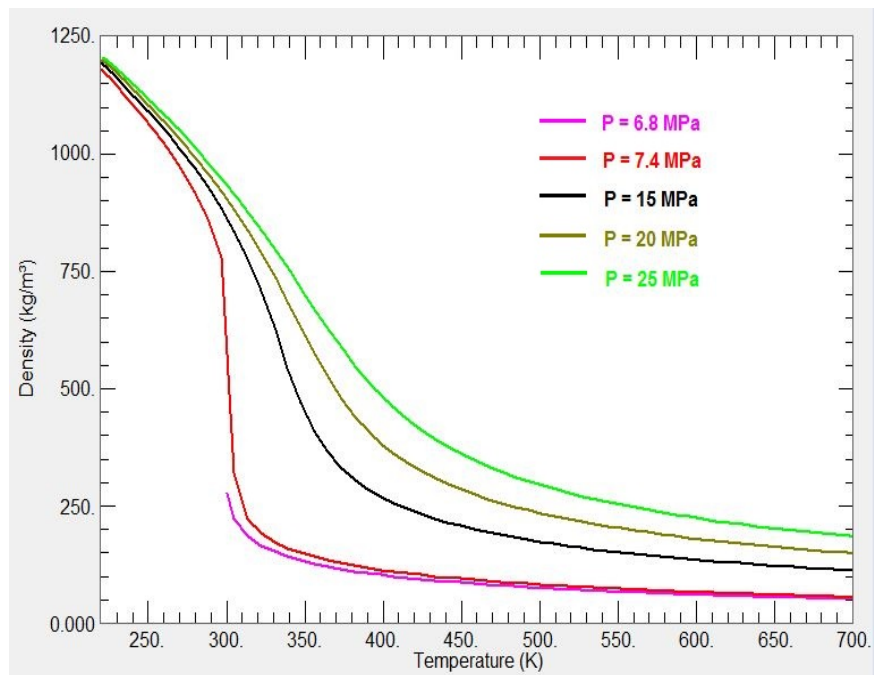


FIGURE 1.2: Variation of density of  $\text{CO}_2$  near the critical point.

Supercritical  $\text{CO}_2$  power cycle was first proposed by Sulzer in 1948 [29]. Later on, Feher [30] studied the feasibility of supercritical  $\text{CO}_2$  regenerative cycle for power and propulsion. A number of theoretical and experimental studies are carried out on  $\text{sCO}_2$  cycles for applications in nuclear, solar, wind, geothermal and waste heat sources. Researchers have analyzed the performance of  $\text{sCO}_2$  power

cycles at different turbine inlet temperatures and performed a comparison with the conventional steam Rankine cycle. Similarly, Klemencic et al. [31] compared the performance of supercritical and transcritical CO<sub>2</sub> cycles with steam Rankine cycle for waste heat recovery of cement industry. They concluded that power output and thermal efficiency of both supercritical and transcritical CO<sub>2</sub> cycles are better than the steam Rankine cycle. Dostal et al. [26, 32, 33] investigated the thermodynamic performance of supercritical CO<sub>2</sub> cycles and found that sCO<sub>2</sub> cycles can achieve higher efficiency compared to steam Rankine cycle when TIT > 550 °C. Moreover, studies have also revealed that sCO<sub>2</sub> cycle has simpler structure and requires less space because of the compact turbomachinery and heat exchangers as compared to the steam Rankine cycle [28, 34]. sCO<sub>2</sub> cycles can yield 38 to 50% thermal efficiency at mild turbine inlet temperatures of 450 to 600 °C [26, 35].

### 1.3 Problem Statement

From the above discussion it can be concluded that sCO<sub>2</sub> cycle is the most viable option for exhaust heat recovery of gas turbine cycle. So, in this study sCO<sub>2</sub> power cycles are presented for improving the thermal efficiency of the medium scale gas turbine using waste heat recovery. The objective of this work is

- To improve the efficiency of gas turbine cycle with the help of waste heat recovery using sCO<sub>2</sub> bottoming power cycles.
- To study the performance of bottoming and combined sCO<sub>2</sub> power cycles.
- To identify the optimal sCO<sub>2</sub> bottoming cycle configuration based on energy, exergy and environmental impact analysis.
- To compare the performance of combined sCO<sub>2</sub> power cycles with Air bottoming cycle (ABC).
- To design the turbomachinery for optimal sCO<sub>2</sub> power cycle configuration.

## 1.4 Scope of the Work

In this study, three configurations of sCO<sub>2</sub> power cycle are selected as bottoming cycle of gas turbine cycle. The thermodynamic (energy and exergy) performance of the selected cycles is compared and optimal cycle is selected based on thermodynamic optimization. In first stage, energy analysis is carried out to investigate heat recovery, power output and energy efficiency of the bottoming and combined cycle. In second stage exergy analysis is performed to compute exergy efficiencies and component wise exergy destruction rates. The environmental benefit of sCO<sub>2</sub> cycles as a result of waste heat recovery is also computed. The optimum performance point of each cycle is determined using Genetic method. The energy and exergy performances of sCO<sub>2</sub> cycles are compared with standalone gas turbine cycle and air bottoming cycle (ABC) to quantify the advantages of waste heat recovery. In the third stage, comparative analysis is carried out to determine the best possible configuration (or optimal configuration) of sCO<sub>2</sub> bottoming cycle for the waste heat recovery of the gas turbine. The compressor of optimal cycle configuration is designed using preliminary and 1D mean line design method in the fourth stage. Finally, turbine design for optimal cycle configuration is done using preliminary and 1D mean line design method. Moreover, the compressor and turbine design codes are linked with the thermodynamic analysis of the optimal cycle to compute updated energy and exergy performance parameters.

## 1.5 Thesis Outline

The entire thesis is divided into following chapters:

### **Chapter 2:**

In this chapter, detailed literature on the thermodynamic analysis and optimization of supercritical carbon dioxide cycles is presented.

**Chapter 3:**

This chapter first describes the configurations of combined gas turbine-supercritical CO<sub>2</sub> cycles. Then, the energy and exergy models of each component of the cycle are developed. The methodology adopted to analyze and optimize the performance of the combined cycles is delineated along with description of operating parameters and assumptions. In addition, validation of the methodology is performed with the data in literature.

**Chapter 4:**

This chapter presents the detailed analysis of the results obtained from the thermodynamic optimization. Moreover, comparative analysis is described based on certain performance criteria to find the optimal cycle configuration.

**Chapter 5:**

This chapter focuses on the compressor and the turbine design for optimal configuration of sCO<sub>2</sub> bottoming cycle. First of all, type of compressor is specified based on operating conditions from thermodynamic analysis. Then, preliminary sizing approach is adopted to estimate the size and efficiency of the compressor. After that, accurate geometry and efficiency of the compressor is computed using 1D mean line design technique and validation of the design code is carried out using experimental results from literature.

For turbine design, type of turbine is specified based on operating conditions from the thermodynamic analysis. Then, preliminary sizing approach is adopted to estimate the size and efficiency of the turbine. Moreover, accurate geometry and efficiency of the turbine is computed using 1D mean line design technique.

Lastly, the updated performance of turbomachinery computed from the design codes is linked with thermodynamic analysis code of sCO<sub>2</sub> cycles for calculation of accurate cycle performance.

**Chapter 6:**

This chapter presents conclusions and highlight the key areas for improvement as a future work.

# Chapter 2

## Literature Review

Supercritical carbon dioxide power cycles have proved to be a promising technology owing to non-toxic nature of  $s\text{CO}_2$  working fluid, smaller size footprint and higher efficiency of the power cycle as compared to the conventional steam Rankine cycle. Ahn et al. [28] showed that  $s\text{CO}_2$  power cycle exhibit higher efficiency for large range of temperatures as compared to the steam Rankine cycle, air Brayton cycle, ORCs and combined cycle gas turbine. Hence,  $s\text{CO}_2$  power cycles have ample potential to be realized as bottoming cycle of topping gas turbine cycle. Various bottoming power cycle technologies for waste heat recovery of topping gas turbine are summarized in Chapter 1. In this Chapter, the prior studies on thermodynamic analysis and feasibility of supercritical carbon dioxide power cycles in various applications are discussed.

Feher [30] proposed and analyzed the first  $s\text{CO}_2$  power cycle with regeneration and identified the problem of pinch point in the regenerator which create large irreversibility in heat transfer. To eliminate the pinch point problem and enhance the cycle thermal efficiency, various layouts of  $s\text{CO}_2$  cycles are investigated by researchers. Dostal et al. [26] conducted an extensive study on  $s\text{CO}_2$  power cycles for nuclear reactors and proposed recompression cycle layout to overcome pinch point problem in regenerators. Similarly, Angelino [36] also studied different layouts of  $s\text{CO}_2$  power cycles and found that the most efficient cycle layout is the recompression cycle layout. Later on, numerous studies adopted recompression cycle for

nuclear, solar and low-grade waste heat sources. Fahad et al. [37] analyzed and compared the thermal efficiency and power output of five layouts of sCO<sub>2</sub> power cycles integrated with solar power tower-heliostat field. They concluded that re-compression cycle layout produced higher power output and thermal efficiency compared to simple, simple recuperated, pre-compression and split expansion cycle layouts. Various prominent studies on supercritical CO<sub>2</sub> power cycles in the arena of nuclear, solar and biomass energy sources are summarized in Table 2.1.

Several other sCO<sub>2</sub> power cycle layouts are suggested and investigated by authors for different type of heat sources. These power cycle layouts are designed using combinations of intercooling, reheating and recuperation processes with a goal to enhance the thermal performance of the sCO<sub>2</sub> power cycles. The layouts are broadly classified into two types: single flow and split flow layouts. The simpler one is the simple regenerative sCO<sub>2</sub> power cycle or simple recuperative sCO<sub>2</sub> power cycle usually considered as the benchmark to compare the performance of other recuperative layouts. Ahn et al. [28, 38] carried out a thermodynamic performance analysis and comparison of twelve layouts of sCO<sub>2</sub> power cycles for sodium-cooled fast reactor (SFR) application which include six single flow and six split flow cycle layouts. The single flow layouts are intercooling, reheating, inter-recuperation, precompression and split expansion layouts. Whereas, split flow layouts are re-compression, preheating, modified recompression, turbine split flow-1, turbine split flow-2 and turbine split flow-3 cycle layouts. The results showed the recompression sCO<sub>2</sub> cycle layout as the highest efficiency layout but at the expense of larger heat transfer area (or larger size of recuperator).

TABLE 2.1: Review of literature on supercritical CO<sub>2</sub> power cycles for applications in nuclear, solar and biomass energy sources.

Study	Configurations	Heat Source	Analysis Type	Outcomes/Conclusions
Sarkar and Bhat-tacharyya (2009) [39]	Recompression sCO <sub>2</sub> Brayton cycle with re-heater.	600 MW heat input from nuclear reactor, TR = 800 °C.	Effect of operating pressure ratio, operating temperatures, maximum operating pressure, LTR and HTR effectiveness on the performance of recompression cycle (with and without reheating).	Maximum thermal efficiency without reheating = 45.28% and with reheating = 46.15% at optimum pressure ratio of 3.08 and 3.25, respectively.
Ahn et al. (2015) [28]	Twelve different sCO <sub>2</sub> cycle configurations.	Heat input from sodium-cooled fast reactor (SFR).	First law analysis and comparison based on heat recovery, size and thermal efficiency.	Maximum thermal efficiency of 44% is exhibited by Recompression sCO <sub>2</sub> cycle.

Study	Configurations	Heat Source	Analysis Type	Outcomes/Conclusions
Sarkar (2009) [40]	Recompression sCO <sub>2</sub> cycle.	600 MW heat input from nuclear reactor, TR = 800 °C.	Investigated the effect of isentropic efficiency, recuperator effectiveness and component pressure drop on the second law efficiency of the recompression sCO <sub>2</sub> Brayton cycle.	Irreversibility contribution of heat exchangers and recuperators are more significant as compared to turbomachinery. Maximum second law efficiency in range of 55-60%.
Kulhanek et al. (2011) [33]	Four different sCO <sub>2</sub> cycle layouts.	3600 MW thermal power input from European sodium fast reactor.	Thermodynamic first law analysis and comparison of four different sCO <sub>2</sub> cycle layouts for TIT = 550 °C, Pressure = 25 MPa, 3600 MW thermal input and flowrate = 3200 kg/s.	Optimal thermodynamic performance of 46.48% exhibited by recompression sCO <sub>2</sub> cycle.

Study	Configurations	Heat Source	Analysis Type	Outcomes/Conclusions
Mahmoudi et al. (2014) [41]	sCO <sub>2</sub> recompression cycle, Combined recompression sCO <sub>2</sub> /ORC	Nuclear heat input of 600 MW. WHR by bottoming ORC from topping pre-cooler. 8 working fluids are considered.	Thermo-economic analysis and comparison of sCO <sub>2</sub> recompression Brayton cycle and combined sCO <sub>2</sub> recompression Brayton/ORC.	11.7% increase in exergy efficiency for SCRBC/ORC as compared to SCRBC. 5.7% decrease in product unit cost for SCRBC/ORC (RC318) as compared to SCRBC.
Belmonte et al. (2016) [42]	sCO <sub>2</sub> Recompression cycle.	Solar central particles receiver (T = 630 - 680 °C).	Thermodynamic analysis, Optimization of first law efficiency based on HTR and LTR effectiveness.	Optimum range of first law efficiency = 40 to 50%.
Wang et al. (2017) [43]	Cascaded recompression/simple sCO <sub>2</sub> cycle.	Solar-Biomass hybrid heat source (T = 550 - 880 °C).	Energy and Exergy analysis.	Maximum thermal efficiency = 40.1%
Maio et al. (2015) [44]	sCO <sub>2</sub> recompression cycle. sCO <sub>2</sub> simple Brayton cycle.	300 MW Lead cooled fast reactor (LFR).	Energy analysis	sCO <sub>2</sub> recompression cycle efficiency >40%.

Study	Configurations	Heat Source	Analysis Type	Outcomes/Conclusions
Yiping Dai et al. (2016) [45]	sCO <sub>2</sub> recompression cycle, t-CO <sub>2</sub> partial cooling cycle, Four Combined sCO <sub>2</sub> /ORC cycle.	Nuclear heat input of 600 MW.	Energy, exergy and economic analysis of 2 standalone and 4 combined sCO <sub>2</sub> /ORC.	Partial cooling is an optimal stand-alone cycle under $P_{max} = 20$ MPa and TIT = 550 °C). Simple t-CO <sub>2</sub> /ORC is an optimal combined cycle.

Various authors endeavor to improve the energy efficiency and power output of sCO<sub>2</sub> bottoming power cycles for gas turbine exhaust heat recovery. Kim et al. [46] compared the thermodynamic performance of nine different layouts of sCO<sub>2</sub> bottoming cycles for exhaust heat recovery of 5 MWe landfill gas fired gas turbine. The comparison is done based on the first law of thermodynamics and plant size. They concluded that the recompression cycle layout is not suitable as a bottoming cycle because of smaller heat recovery from the gas turbine exhaust which also reduced its specific work compared to other layouts. However, they suggested partial heating cycle (in some literature known as preheating cycle) and dual heated and flow split cycle as the optimum bottoming power cycles because of higher power output and smaller size footprint. Mohagheghi et al. [47] conducted the thermodynamic optimization of sCO<sub>2</sub> simple recuperated and recompression cycle layouts based on waste heat stream at mass flow rate of 100 kg/s. They emphasized that the prime objective in the optimization of bottoming sCO<sub>2</sub> cycles should be to maximize heat recovery and power output of the power cycle rather than thermal efficiency. Furthermore, they concluded that recompression bottoming cycle produce smaller power output compared to simple recuperated cycle.

Wright et al. [48] studied the thermo-economic performance of four recuperated bottoming cycle in conjunction with LM-2500PE gas turbine (a 25 MWe general electric gas turbine). The analyzed layouts are simple recuperated, cascaded, dual recuperated and preheating cycles. Although, the authors didn't explained the methodology they adopted but concluded that the selected sCO<sub>2</sub> bottoming cycles increased the efficiency of gas turbine from 35.5% to nearly 49%. Moreover, the authors found that the maximum combined cycle efficiency with reasonable increase in annual revenue is shown by preheating bottoming cycle. In an effort to enhance the waste heat recovery utilization and power output of the bottoming sCO<sub>2</sub> cycle, Marchionni et al. [49] proposed preheating with precompression bottoming cycle layout and compared it with previously proposed sCO<sub>2</sub> cycle layouts as discussed earlier. They found that the preheating with precompression layout is able to achieve comparatively higher power output, whereas, the highest economic effectiveness is achieved by simple recuperated cycle layout owing to lower size foot

print. An extensive comparative analysis on large scale bottoming sCO<sub>2</sub> power cycles is conducted by Cho et al. [50]. They evaluated the performance of simple, combined and cascade sCO<sub>2</sub> bottoming power cycles integrated with topping 288 MW gas turbine (Siemens SGT5-4000F). Furthermore, they compared the power output as well as the size of sCO<sub>2</sub> bottoming cycles with steam Rankine bottoming cycle and found that cascade cycle produce greater power output than steam Rankine bottoming cycle and other sCO<sub>2</sub> cycle layouts adopted in this study. In addition, they also concluded that combination of two cycles as bottoming cycle is not prove to be an attractive option owing to smaller power output and larger size. Kimzey [51] also presented a comparison between sCO<sub>2</sub> bottoming power cycles and steam Rankine bottoming power cycles (SRBC) integrated with topping gas turbine (Siemens H-class and LM6000) and found that both simple and intercooled sCO<sub>2</sub> bottoming cycles displayed larger power output compared to the SRBC in case of LM6000 gas turbine. Further studies on sCO<sub>2</sub> power cycles in the scope of waste heat recovery from gas turbine and other industrial sources are summarized in Table 2.2.

In addition to the theoretical analysis and optimization of sCO<sub>2</sub> power systems, experimental work is also going on in various institutes and research centers around the world. Sandia National laboratories (SNL) in US developed a 240 kWe experimental test loop comprise of recompression cycle run at pressure ratio of 1.65, revolution speed of 50,000, 67% compressor isentropic efficiency and 87% turbine isentropic efficiency [52]. Moreover, SNL also constructed the simple Brayton cycle test loop having power capacity of 10MWe at cycle TIT of 550 °C [53]. The test loop performed well in situations of variable conditions. Similarly, Echogen power system designed a 250 kW sCO<sub>2</sub> cycle experimental test system based on waste heat recovery [54]. The main focus of these test loops is to identify and minimize the losses occurring in the components, to improve the performance of turbomachinery and heat exchangers and to scale up the power capacity of the cycle. These experimental test loop plays important role in validation of cycle thermodynamic and component design codes. Some other test loops are functional in Korea Advanced Institute of Science and Technology (KAIST, Korea) [28] and Institute of

Applied Energy (IAE) in Japan.

The design of turbomachinery (turbine and compressor) of sCO<sub>2</sub> cycle is equally important as the cycle thermodynamic optimization since the overall efficiency of the sCO<sub>2</sub> power cycle is influenced by the efficiency of turbomachinery. So far, the practice is to assume efficiency of the compressor and turbine and kept as constant during thermodynamic analysis at different operating conditions. Though, the turbine and compressor efficiency depend on the cycle operating parameters. Thus, the turbomachinery performance should be calculated in conjunction with cycle thermodynamic analysis in order to obtain realistic results at variable operating conditions.

Both theoretical and experimental works are being done on performance prediction of the compressor and turbine of sCO<sub>2</sub> power cycles. However, more attention is made on the design of compressor since it operates near the critical point where there are sharp variations in density and specific heat of CO<sub>2</sub>. Due to large variations in properties near critical point, the sCO<sub>2</sub> compressor design method is different from the previous methods. The previous design methods adopted for compressors of air and steam cycle are based on ideal gas assumption but these methods cannot be applicable for sCO<sub>2</sub> compressor because of nonideal behavior of CO<sub>2</sub> near critical point as explained in **Chapter 1**. In literature, the theoretical design of turbomachinery is followed using four steps: 1) Preliminary sizing, 2) 1D Mean Line design 3) CFD simulation and 4) Validation. Giuseppe et al. [55] used the preliminary sizing and CFD simulation to design the radial turbomachinery for simple regenerative sCO<sub>2</sub> power cycle. They computed 70% turbine efficiency and 76% compressor efficiency. Lee et al. [56] employed the preliminary design method to design the compressor, recompressor and turbine for recompression sCO<sub>2</sub> cycle layout integrated with small modular nuclear reactor.

TABLE 2.2: Review of literature on supercritical CO<sub>2</sub> power cycles for applications in waste heat recovery.

Study	Configurations	Heat Source	Analysis Type	Outcomes/Conclusions
Banik et al. (2016) [57]	Recompression tCO <sub>2</sub> and sCO <sub>2</sub> Brayton cycle.	Low grade waste heat source (T < 240 °C).	Energy and Exergy Analysis. Parametric study with respect to recompression mass ratio and pressure ratio.	tCO <sub>2</sub> cycle maximum thermal efficiency = 13.6% at recompression mass ratio of 0.26, $r_p = 2.4$ and TIT = 443 K.
Matteo Marchionni et al. (2017, 2018) [49, 58]	sCO <sub>2</sub> preheating, sCO <sub>2</sub> preheating split expansion, sCO <sub>2</sub> preheating pre-compression, sCO <sub>2</sub> split heating split expansion.	High grade waste heat.	1 <sup>st</sup> law, 2 <sup>nd</sup> law and economic analysis.	Highest net power output produced by Preheating Pre-compression (PHPC) cycle. SR scheme gives the highest economic effectiveness i.e. 770 \$/kWe and payback period of 1.86 years.

Study	Configurations	Heat Source	Analysis Type	Outcomes/Conclusions
Hou et al. (2018) [59]	sCO <sub>2</sub> recompression cycle.	Gas turbine exhaust heat.	Exergoeconomic analysis and multiobjective optimization based on genetic algorithm.	Exergoeconomic factor is 31.88%, optimal exergy efficiency is 62.23%, and optimal unit cost of electricity is 3.95 cents/kWh.
Hou et al. (2018) [60]	sCO <sub>2</sub> recompression cycle.	Gas turbine exhaust heat.	Multiobjective optimization to find optimal zeotropic mixture.	R236fa/R227ea (0.46/0.54) is the optimal zeotropic mixture for sCO <sub>2</sub> recompression cycle.
Zhang et al. (2018) [61]	sCO <sub>2</sub> Brayton cycle.	Coal fired boiler.	Three improved cycle layouts are presented for a better utilization of the exhaust heat of the flue gas from the coal fired boiler are analyzed.	Second split flow to the boiler is the most effective and an optimized first law efficiency of 50.71% is reported.

Study	Configurations	Heat Source	Analysis Type	Outcomes/Conclusions
Park et al. (2018) [62]	sCO <sub>2</sub> Brayton power cycle.	Coal fired power plant.	Thermodynamic analysis and evaluating levelized cost of electricity.	Power generation efficiency is improved by 6.2-7.4% compared to steam Rankine cycle.
Manjunath et al. [63]	sCO <sub>2</sub> regenerative Brayton cycle/tCO <sub>2</sub> vapor compression cycle.	Shipboard gas turbine waste heat recovery.	Exergy and parametric analysis to evaluate the augmentation in performance of shipboard gas turbine due to waste heat recovery.	34% gain in energy efficiency and 30% gain in exergy efficiency of the combined power plant compared to standalone topping gas turbine cycle.

Lee et al. [64] also suggested the modified 1D mean line design method for design of radial turbomachinery for water cooled small modular nuclear reactors. In this study, they considered the enthalpy losses occurring in the turbomachinery and based on that performance is evaluated and results are validated with experimental results of Sandia National laboratories (SNL). Spazzoli [65] developed 1D mean line design code combined with cycle thermodynamic analysis for design of axial and radial turbomachinery. He validated the design code with experimental results and applied it to design the turbomachinery of recompression sCO<sub>2</sub> cycle integrated with solar power tower. Recent studies on design of sCO<sub>2</sub> turbomachinery includes the study of Liu et al. [66], Khadse et al. [67], Lee et al. [68], Sanghera et al. [69], Oh et al. [70] and Monje et al. [71]. The main intent of these authors is to develop accurate design codes which are capable to analyze the performance of the turbomachinery both in design and off design (variable) conditions.

## 2.1 Summary

To summarize, the literature reports extensive research being done on theoretical analysis and optimization of sCO<sub>2</sub> power cycles for nuclear, biomass, solar and waste heat recovery applications. Meanwhile, experiments have also been performed to test the turbomachinery, heat exchangers and overall performance of the power cycles. Furthermore, efforts are also underway to augment the power capacity of the experimental test loops which will help in commercialization of the sCO<sub>2</sub> power system in future. However, there is still room to study the performance of bottoming sCO<sub>2</sub> power cycles for waste heat recovery applications. Most of the studies conducted so far on bottoming sCO<sub>2</sub> cycles are based on the energy analysis (or First Law of Thermodynamics) and the comparison of cycle layouts is done based solely on net power output. It should be noted that the energy analysis only deals with quantity of energy, it doesn't tell us about the losses occurring inside the system components and changes in the quality of energy during the process. However, second law of thermodynamics provide information about entropy generation and energy degradation due to different processes in components of the

thermal power system. Therefore, this study considers both the first law (energy analysis) and the second law of thermodynamics (exergy analysis) to optimize and evaluate the performance of bottoming sCO<sub>2</sub> power cycles and the combined sCO<sub>2</sub> power cycles. Comparison of three combined cycle configurations (or layouts) is conducted to identify the optimum cycle layout based on energy analysis, exergy analysis and reduction in exhaust gas emissions. In addition, this study also aims to design the compressor and turbine for optimum layout of bottoming sCO<sub>2</sub> power cycle. Radial turbomachinery is selected and both preliminary method and 1D mean line design method are used to determine the size and performance of the turbomachinery.

# Chapter 3

## Methodology

This chapter starts with description of combined gas turbine  $s\text{CO}_2$  power cycle configurations selected for thermodynamic analysis. After that, the thermodynamic models for each component of the cycle are delineated along with operating conditions and assumptions needed to carry out the calculations. In addition, the methodology adopted for analysis and optimization is illustrated with the help of flow diagram.

### 3.1 Combined Gas Turbine Supercritical $\text{CO}_2$ Power Cycles

The combined gas turbine (CGT) supercritical carbon dioxide ( $s\text{CO}_2$ ) power cycles chosen for waste heat recovery application are delineated in this section. As discussed in introduction section, there are many configurations available for  $s\text{CO}_2$  bottoming cycles; however, here the objective is to analyze and argue their thermodynamic behavior based on their comparison. Therefore, three specific configurations are selected such that they are an overall representative of all other presented configurations in literature. Moreover, these specific configurations have smaller size foot print as compared to other layouts in literature [28, 46]. Two split flow configurations and one single flow configuration are selected for parametric

analysis and optimization. The combined system comprises of a topping conventional gas turbine and bottoming  $s\text{CO}_2$  cycle. The topping gas turbine constitutes a compressor (C1), a combustion chamber (CC) and a turbine (T1). The integrated heat exchanger(s) are present which connects the bottoming cycle with topping gas turbine. The purpose of IHX is to recover exhaust gas heat expelling out of the topping cycle gas turbine. The bottoming cycle turbine inlet temperature ' $T_3$ ', work output and energetic and exergetic efficiencies depends on the amount of heat absorbed in integrated heat exchanger(s). The schematics of the combined systems of bottoming supercritical  $\text{CO}_2$  cycles are shown in Figure 3.1 to 3.3.

The combined gas turbine simple regenerative  $s\text{CO}_2$  cycle (CGTSRC) is shown in Figure 3.1. The bottoming cycle is a single flow layout consist of a single IHX and single recuperator in addition to turbine (T2) and a compressor (C2). The  $s\text{CO}_2$  stream absorbed heat in IHX resulted in the increase of bottoming turbine inlet temperature ( $T_3$ ). After expansion in turbine (T2), the  $s\text{CO}_2$  stream flow towards the recuperator which recuperates the heat energy exist in the stream, thus, increases the cycle efficiency. Because of simple recuperation process, this cycle is considered as the reference configuration in this study for comparing the results from other configurations.

The two split flow layouts considered are CGT-recompression  $s\text{CO}_2$  cycle and CGT-preheating  $s\text{CO}_2$  cycle. The exhaust temperature of  $s\text{CO}_2$  turbine is very high because of low pressure ratio of  $s\text{CO}_2$  cycles as compared to steam Rankine cycle and air Brayton cycle, this demand heat recuperation for enhancing thermal efficiency. Therefore, the purpose of split flow layouts is to enhance recuperation inside the  $s\text{CO}_2$  cycle and to augment the heat recovery from exhaust gases. The combined gas turbine recompression  $s\text{CO}_2$  cycle (CGTREC) consist of two compressors, i.e. C2 and C3 and two recuperators, i.e. LTR and HTR in the bottoming cycle. As shown in the Figure 3.2, the  $s\text{CO}_2$  stream after heated in IHX expands in the turbine T2 and produces work. The expanded stream then flows to the high temperature recuperator (HTR) to heat the stream at state 8 and afterward to low temperature recuperator (LTR) to heat the stream at state 2 coming from

the compressor (C2). As a result of mass split before the cooler, the difference in pressures and mass flow created the difference in the specific heats between hot and cold streams in LTR which improves heat recuperation and improves the first law efficiency of the cycle [45]. The combined gas turbine preheating  $s\text{CO}_2$  cycle (CGTPHC) as shown in Figure 3.3 comprises of two heat recovery units (IHX-1 and IHX-2) for enhancement in heat recovery and one recuperator for collection of heat from  $s\text{CO}_2$  turbine in the bottoming cycle. The mass split occurs after compressor 'C2'; one stream goes to recuperator and the other one towards IHX-2. The main difference between CGT-preheating cycle and CGT-recompression cycle is that in former case the mass flow is split to enhance the heat recovery from the exhaust gases while in latter case, the mass split reduces the irreversibility in recuperative heat exchangers (HTR and LTR).

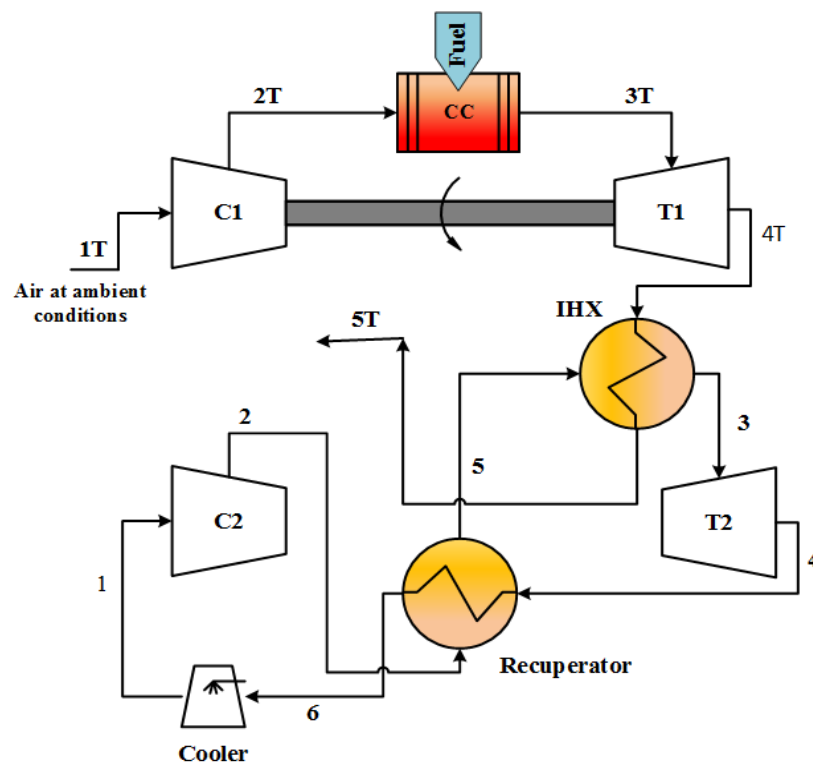


FIGURE 3.1: Schematic of combined gas turbine simple regenerative  $s\text{CO}_2$  cycle (CGTSRC).

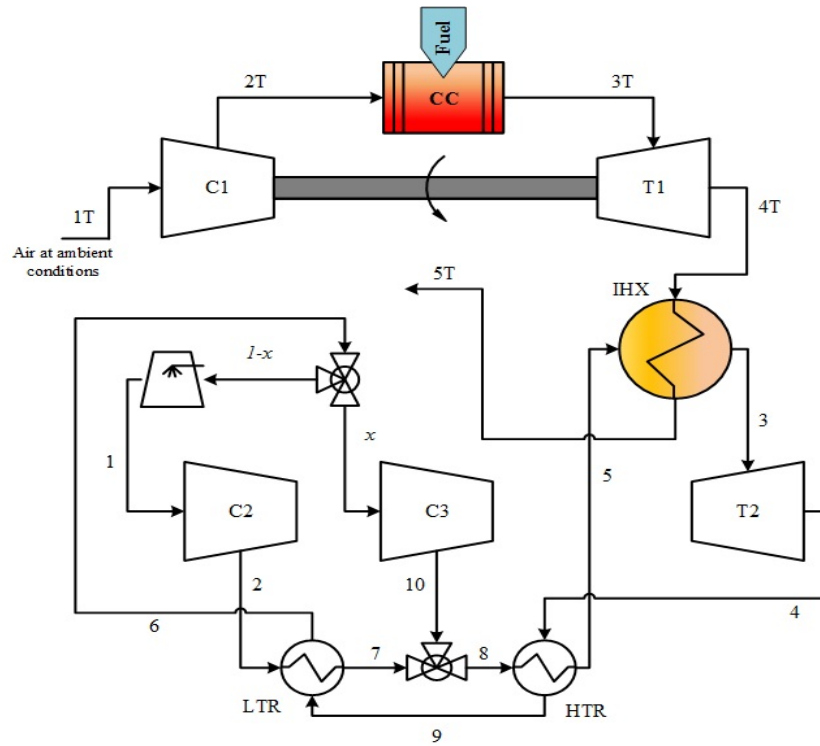


FIGURE 3.2: Schematic of combined gas turbine recompression  $s\text{CO}_2$  cycle (CGTREC).

## 3.2 Thermodynamic Modeling

The combined cycles, described earlier are modeled by applying first law and second law of thermodynamics on individual components of the power cycles to produce the thermodynamic equations. The following assumptions have been made for the modeling and analysis:

- All processes are steady state in nature.
- Compression, expansion and heat exchanger processes are adiabatic.
- Compression and expansion processes are non-isentropic.
- Pressure drops in recuperator and heat exchangers are negligible.

The thermophysical properties of  $s\text{CO}_2$  at each state are retrieved using equation of state developed by Span and Wagner [72] available in Engineering Equation



due to intrinsic irreversibilities in real processes. The exergy balance of general system can be written as:

Exergy Input - Exergy Output - Exergy destroyed = Exergy increase

In rate basis for a steady state system, the following balance can be applied to each component of the power system:

$$\sum \left( \dot{E}_{Q,in} - \dot{E}_{Q,out} \right) + \sum \left( \dot{E}_{W,in} - \dot{E}_{W,out} \right) + \sum \dot{m} \left( \dot{E}_{f,in} - \dot{E}_{f,out} \right) - \dot{E}_d = \frac{dE_{sys}}{dt} \quad (3.1)$$

$\dot{E}_Q$  and  $\dot{E}_W$  are the exergy rate associated with heat transfer and work respectively. Whereas,  $\dot{E}_f$  is the specific exergy of a fluid steam at particular state, i.e. inlet or outlet of a component. After neglecting the kinetic and potential energies, it is defined as:

$$E_f = h_f - h_0 - T_0 (s_f - s_0) \quad (3.2)$$

### 3.2.2 Turbomachinery Thermodynamic Model

Turbomachinery includes compressors and turbines of topping and bottoming sCO<sub>2</sub> power cycles. The energy balance, exergy balance and isentropic efficiency equation in conjunction with fluid property library in EES are used to compute the inlet states, outlet states and work of the turbomachinery. The model equations for turbomachinery of topping and bottoming power cycles are given below.

#### 3.2.2.1 Topping Cycle Compressor (CI)

$$W_{c1} = \dot{m}_{air} [h_{2,T} - h_{1,T}] \quad (3.3)$$

$$\eta_{c1} = \frac{h_{2s,T} - h_{1,T}}{h_{2,T} - h_{1,T}} \quad (3.4)$$

$$E_{d,c1} = \dot{m}_{air} T_0 (s_{2,T} - s_{1,T}) \quad (3.5)$$

### 3.2.2.2 Topping Cycle Turbine (T1)

$$\eta_{t1} = \frac{h_{3,T} - h_{4,T}}{h_{3,T} - h_{4,Ts}} \quad (3.6)$$

$$W_{t1} = \dot{m}_g [h_{3,T} - h_{4,T}] \quad (3.7)$$

$$E_{d,t1} = \dot{m}_g T_0 (s_{4,T} - s_{3,T}) \quad (3.8)$$

### 3.2.2.3 Bottoming sCO<sub>2</sub> Cycle Compressor (C2)

$$\eta_{c2} = \frac{h_{2s} - h_1}{h_2 - h_1} \quad (3.9)$$

$$W_{c2} = (1 - x) \dot{m}_{\text{CO}_2} (h_2 - h_1) \quad (3.10)$$

$$E_{d,c2} = W_{c2} + \dot{m}_{\text{CO}_2} (1 - x) [h_1 - h_2 - T_0 (s_1 - s_2)] \quad (3.11)$$

### 3.2.2.4 Bottoming sCO<sub>2</sub> Cycle Recompressor (C3)

$$W_{c3} = x \dot{m}_{\text{CO}_2} (h_{10} - h_6) \quad (3.12)$$

$$\eta_{c3} = \frac{h_{10s} - h_6}{h_{10} - h_6} \quad (3.13)$$

$$E_{d,c3} = W_{c3} + \dot{m}_{\text{CO}_2} x [h_6 - h_{10} - T_0 (s_6 - s_{10})] \quad (3.14)$$

### 3.2.2.5 Bottoming sCO<sub>2</sub> Cycle Turbine (T2)

$$\eta_{t2} = \frac{h_3 - h_4}{h_3 - h_{4s}} \quad (3.15)$$

$$W_{t2} = \dot{m}_{\text{CO}_2} (h_3 - h_4) \quad (3.16)$$

$$E_{d,t2} = -W_{t2} + \dot{m}_{\text{CO}_2} x [h_3 - h_4 - T_0 (s_3 - s_4)] \quad (3.17)$$

## 3.2.3 Combustion Chamber Thermodynamic Model

The energy input to the combined cycle occurs due to combustion in combustion chamber. The energy balance are as follows.

$$Q_{in} = \dot{m}_f Q_{LHV} \quad (3.18)$$

$$\left[ \left( 1 + \frac{\dot{m}_f}{\dot{m}_{air}} \right) h_{3,T} \right] - h_{2,T} = \eta_{comb} \times \frac{\dot{m}_f}{\dot{m}_{air}} \times Q_{LHV} \quad (3.19)$$

The fuel consumption  $\dot{m}_f$  depends on the efficiency of the combustion chamber  $\eta_{comb}$  because the turbine inlet temperature ( $T_{3T}$ ) of topping gas turbine is fixed, i.e. 1500 K. The exergy input to the combined power cycle is computed using following equation [63, 73, 74].

$$E_{x,in} = Q_{in} \times \left[ 1 - \left( \frac{T_0}{T_{in}} \right) \right] \quad (3.20)$$

The  $E_{x,in}$  also represents the exergy of a system at ideal condition [75], where,  $T_{in}$  is assumed to be equal to  $T_{3T}$ . The exergy destruction is determined as,

$$E_{d,cc} = T_0 \left[ \dot{m}_{air} (s_{3,T} - s_{2,T}) - \frac{Q_{in}}{T_{in}} \right] \quad (3.21)$$

### 3.2.4 Integrated Heat Exchanger (IHX) Thermodynamic Model

The exhaust gases coming out of topping gas turbine at state 4T enters the heat recovery units (IHXs) where heat is exchanged between hot fluid (exhaust gases) and cold fluid (supercritical carbon dioxide). The IHX is modelled using effectiveness method [76] according to which effectiveness is defined using either of two equations.

$$\varepsilon_{IHX} = \frac{C_{b,CO_2} (T_3 - T_5)}{C_{min} (T_{4T} - T_5)} \quad (3.22)$$

or

$$\varepsilon_{IHX} = \frac{C_{exh} (T_{4T} - T_{5T})}{C_{min} (T_{4T} - T_5)} \quad (3.23)$$

Where,  $C_{min}$  is the minimum heat capacity between exhaust gases and sCO<sub>2</sub> which are computed using appropriate flow rates and temperature. In case of bottoming preheating cycle (BPHC), same heat recovery relations are employed for both IHX-1 and IHX-2.

The heat recovery is computed using energy balance as,

$$Q_{IHX} = Q_{recv} = \dot{m}_{CO_2} (h_3 - h_5) \quad (3.24)$$

The exergy input into the bottoming sCO<sub>2</sub> power cycle as a result of heat recovery is given as [63],

$$E_{x, inbot} = Q_{IHX} \times \left[ 1 - \left( \frac{T_0}{T_{avg}} \right) \right] \quad (3.25)$$

Where,

$$T_{avg} = \frac{h_{4t} - h_{5t}}{s_{4t} - s_{5t}} \quad (3.26)$$

And the exergy destruction is calculated using exergy balance as,

$$E_{d, IHX} = [\dot{m}_{CO_2} \{h_5 - h_3 - T_0 (s_5 - s_3)\} + \dot{m}_g \{h_{4T} - h_{5T} - T_0 (s_{4T} - s_{5T})\}] \quad (3.27)$$

### 3.2.5 Recuperators Thermodynamic Model

The recuperators include HTR, LTR and cooler. The thermodynamic models for recuperators include the effectiveness equation, energy balance and exergy balance relations as given below.

#### 3.2.5.1 HTR

$$h_4 - h_9 = h_5 - h_8 \quad (3.28)$$

$$\varepsilon_{HTR} = \frac{h_5 - h_8}{h_4 - h_9} \quad (3.29)$$

$$E_{d,HTR} = [\dot{m}_{CO_2} \{h_4 - h_9 - T_0 (s_4 - s_9)\} + \dot{m}_{CO_2} \{h_8 - h_5 - T_0 (s_8 - s_5)\}] \quad (3.30)$$

#### 3.2.5.2 LTR

$$(1 - x)(h_7 - h_2) = h_9 - h_6 \quad (3.31)$$

Where 'x' is the mass split for recompression. Its value ranges from 0.20 to 0.80.

$$\varepsilon_{LTR} = \frac{h_7 - h_2}{h_9 - h_6} \quad (3.32)$$

$$E_{d,LTR} = [\dot{m}_{CO_2} (1 - x) \{h_2 - h_7 - T_0 (s_2 - s_7)\} + \dot{m}_{CO_2} \{h_9 - h_6 - T_0 (s_9 - s_6)\}] \quad (3.33)$$

#### 3.2.5.3 Cooler

$$Q_{cooler} = (1 - x) \dot{m}_{CO_2} (h_6 - h_1) \quad (3.34)$$

$$E_{d,cooler} = [\dot{m} (1 - x) \{h_6 - h_1 - T_0 (s_6 - s_1)\} + \dot{m}_w \{h_{w,in} - h_{w,out} - T_0 (s_{w,in} - s_{w,out})\}] \quad (3.35)$$

### 3.2.5.4 Mixer Model

Mixer is present between HTR and LTR for mixing two flow streams coming from compressor and recompressor. The energy and exergy balance are applied to mixer as shown below [57].

$$h_8 = xh_{10} + (1 - x) h_7 \quad (3.36)$$

$$E_{d,mix} = \left( (\dot{m}_{CO_2} s_8) - (\dot{m}_{CO_2} (1 - x) s_{10}) - (x \dot{m}_{CO_2} s_7) - \frac{Q_{mixer}}{T_8} \right) T_0 \quad (3.37)$$

## 3.3 Performance Parameters

### 3.3.1 Energy Efficiency

For parametric analysis, mass flow rate ratio (MFRR) is defined as the mass flow rate in the bottoming cycle with the mass flow rate of topping cycle as,

$$MFRR = \frac{\dot{m}_{CO_2}}{\dot{m}_{air,topping}} \quad (3.38)$$

The net work produced by topping cycle gas turbine and thermal efficiency are calculated as,

$$W_{net,T} = W_{t1} - W_{c1} \quad (3.39)$$

$$\eta_T = \left[ \frac{W_{net,T}}{Q_{in}} \right] \times 100 \quad (3.40)$$

The net work output of the bottoming cycle is calculated by taking a difference of the amount of work generated by turbine and the work consumed by both compressors (C2 and C3) as shown below for CGTREC,

$$W_{net,b} = W_{t2} - W_{c2} - W_{c3} \quad (3.41)$$

The bottoming cycle energy efficiency is calculated using the net-work generated in bottoming cycle as compared to the heat recovered in IHX,

$$\eta_b = \frac{W_{net,b}}{Q_{recv}} \quad (3.42)$$

The total work generated by the plant is the summation of net-work from both topping and bottoming cycles,

$$W_{total} = W_{net,T} + W_{net,b} \quad (3.43)$$

The overall plant energy efficiency is calculated using the total work generated by the plant as compared to inlet fuel power.

$$\eta_b = \frac{W_{total}}{Q_{in}} \quad (3.44)$$

### 3.3.2 Exergy Efficiency

The combined cycle irreversibilities are calculated by the sum of individual irreversibilities (or exergy destruction) of each component as,

$$IRR = E_{d,IHX} + E_{d,LTR} + E_{d,HTR} + E_{d,T2} + E_{d,c2} + E_{d,cooler} + E_{d,c3} + E_{d,t1} + E_{d,c1} + E_{d,cc} \quad (3.45)$$

The bottoming and combined cycle exergy efficiencies are computed using following relations:

$$\eta_{II,b} = \frac{E_{x,inbot} - IRR_b}{E_{x,inbot}} \quad (3.46)$$

$$\eta_{II,c} = \frac{E_{x,in} - E_{x,out} - IRR}{E_{x,in}} \quad (3.47)$$

Where,  $IRR_b$  and  $IRR$  represent the total irreversibilities or total exergy destruction due to entropy production in cycle components for bottoming sCO<sub>2</sub> cycle and the combined cycles, respectively.  $E_{x,out}$  represent the exergy loss to environment which cannot be recoverable.

### 3.3.3 Environmental Impact

There are no harmful emissions from bottoming supercritical CO<sub>2</sub> cycles since they are closed cycles. Owing to waste heat recovery, they can aptly benefit earth's ecosystem in the form of reducing greenhouse emissions compared to fossil fuel combined cycles of same power rating. To evaluate the environmental benefits, the bottoming sCO<sub>2</sub> cycles analyzed in this study are compared with fossil fuel cycle in case of same power output. The reduction in emissions per hour is estimated using following relation [27, 77]:

$$M_{\text{CO}_2} = \alpha_{\text{CO}_2} W_{\text{net},b} \quad (3.48)$$

The  $\alpha_{\text{CO}_2}$  is the amount of CO<sub>2</sub> released from fossil fuel power plants for 1 kWh production. It is calculated by using Eq. (3.49). The average operating heat rate (HR) and emission factor (EF) of natural gas are attained from the latest data available on US Energy Information Administration website [78]. From the latest data, the HR and EF of natural gas are 7870 Btu/kWh and 53.07 kgCO<sub>2</sub>/millions-Btu, respectively.

$$\alpha_{\text{CO}_2} = HR_{\text{naturalgas}} \times EF_{\text{naturalgas}} \quad (3.49)$$

The emissions savings estimated from this model are compared for selected cycles in Chapter 4 to find the optimum cycle which reduce maximum emissions.

## 3.4 Calculation Methodology

The cycle calculation methodology diagram for CGT-sCO<sub>2</sub> cycle is outlined in Figure 3.4 to illustrate how the cycle thermodynamic analysis is conducted. The input parameters of topping and bottoming cycles are specified separately. Firstly, the topping cycle (gas turbine) state points are calculated using energy balance relations of topping cycle. The bottoming cycle calculation started with the assumption of temperature inlet of IHX, i.e.  $T_8$  in case of BPHC,  $T_5$  in case of BREC

and BSRC. Based on component wise energy balance relations as discussed in previous section along with supercritical CO<sub>2</sub> property data from EES software, the thermodynamic properties at each state are calculated. During each iteration heat recovery in IHX(s) is computed and if the difference of heat recovery between two iterations is less than 1e-3, the code iterations are converged, and combined cycle energy and exergy parameters are calculated at the end. Else, the assumed value is updated, and cycle calculations are repeated until convergence. After that, the thermodynamic properties at each state are gathered and energy efficiency, exergy efficiency and exergy destruction in each component are calculated. Furthermore, exergetic optimization of the combined cycle is performed to find the optimum performance point at which exergy destruction and losses are minimum or exergy efficiency is maximum. The entire calculation and optimization are carried out using Engineering Equation Solver (EES) software. The basic assumptions and operating parameters for the analysis are outlined in Table 3.1, adopted from Refs. [10, 36]. The EES code for CGTREC is available in Appendix A1 for validation and testing purposes.

TABLE 3.1: Operating parameters for combined cycle calculations.

Parameters	Value
<b>Topping Conventional Gas Turbine Cycle [10]</b>	
Compression ratio ( $R_c$ )	14
Turbine inlet temperature (TIT)	1500 K
Efficiency of combustion chamber ( $\eta_{comb}$ )	0.98
Isentropic efficiency of compressor ( $C_1$ )	0.85
Isentropic efficiency of Turbine ( $T_1$ )	0.87
Temperature at inlet of compressor ( $T_{1T}$ )	303 K
Pressure at inlet of compressor ( $P_{1T}$ )	0.1 MPa
Exhaust gases temperature $T_{4T}$ )	880 K
<b>Bottoming sCO<sub>2</sub> Brayton Cycle [36]</b>	
Temperature at inlet of compressor ( $T_1$ )	304.25 K
Pressure at inlet of compressor ( $P_1$ )	7.4 MPa
Isentropic efficiency of compressors ( $C_2$ and $C_3$ )	0.8
Isentropic efficiency of Turbine ( $T_2$ )	0.9
Compression ratio ( $r_c$ )	2.7
Effectiveness of IHX, recuperator, HTR ( $\varepsilon_{HTR}$ ) and LTR ( $\varepsilon_{LTR}$ )	0.85, 0.7(LTR)
Mass flow rate of exhaust gases	107.1 kg/s

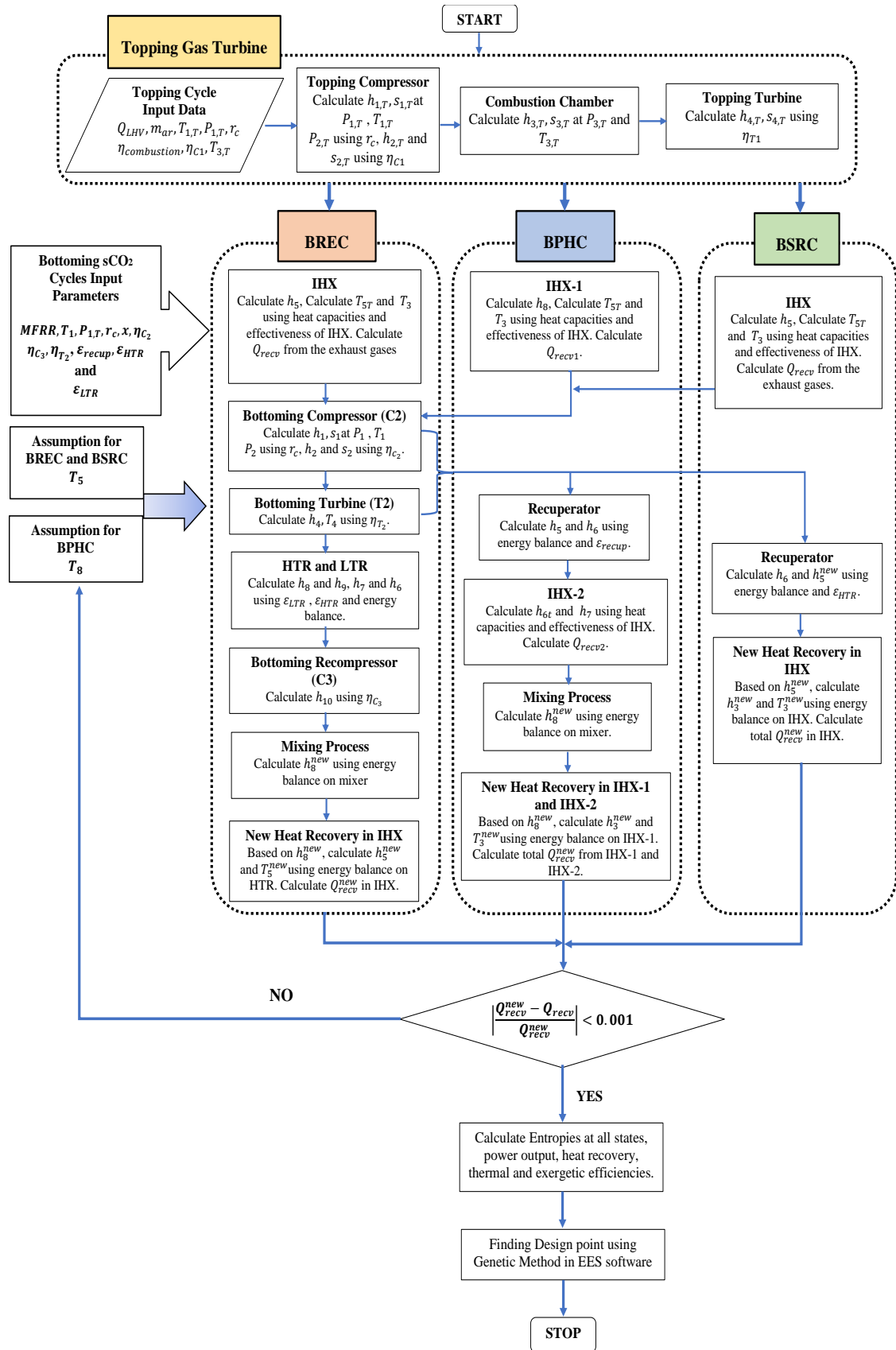


FIGURE 3.4: Methodology for thermodynamic calculations of CGT-sCO<sub>2</sub> power cycles.

### 3.5 Validation

The methodology delineated above is validated with previous research. The available results data in literature [37] are used to validate the model of bottoming sCO<sub>2</sub> recompression cycle (BREC). The graphs in the reference are digitized and used to compare with results of present research work. The comparison is made for various values of heat input. Table 3.2 presents the comparison of results and indicate the values of optimum turbine inlet temperature (TIT), first law efficiency and power output. As shown in the table, there is a good agreement between the results.

TABLE 3.2: Comparison between the present work and those of Ref. [37] for BREC.

S. No.	Q <sub>in</sub> (MW)	Present work			Ref. [37]		
		TIT (K)	$W_{net}$ (MW)	$\eta_I$ (%)	TIT (K)	$W_{net}$ (MW)	$\eta_I$ (%)
1	138	977.7	65.13	47.2	970	66	48
2	155	1056	77.6	50	1050	78	50.5
3	159	1074	81.4	51.2	1080	80.5	51

# Chapter 4

## Thermodynamic Results and Analysis

In this chapter, the thermodynamic performance analysis is carried out for selected combined sCO<sub>2</sub> power cycles using thermodynamic models and calculation methodology as described in previous chapter. The analysis is carried out in three phases: 1. Parametric analysis, 2. Thermodynamic optimization, 3. Comparison. In first phase, the combined and bottoming cycles' power output, heat recovery, energy and exergy efficiencies are investigated for variation of MFRR and recompression or mass split percentages. Moreover, the major sources of irreversibility in bottoming sCO<sub>2</sub> cycles are identified. In second phase, exergy optimization is done to find optimum performance point using the Genetic Method under certain decision parameters. The Genetic Method is a robust optimization method which finds the global optimum point using the procedure of biological evolution and it is available in Engineering Equation Solver (EES) software. In last phase, comparative analysis is carried out to decide the best possible option for waste heat recovery of gas turbine based on specified selection parameters. The results after parametric analysis of each combined cycle are described one by one in following subsections.

## 4.1 Combined Gas Turbine Recompression Brayton Cycle

The energy efficiency and power output of bottoming recompression and combined recompression cycle is illustrated in Figure 4.1. The combined cycle power output and energy efficiency is greater than the bottoming cycle's. The power output of the combined and bottoming recompression cycle increases first and then reduces slightly, thus, give the maxima at one point. Since, the large increase in the mass flow rate (or MFRR) of bottoming cycle decreases its potential to elevate its temperature from integrated heat exchanger (IHX); therefore, the power output decreases slightly at MFRR greater than 2.8. The variation of specific heat ' $C_p$ ' of sCO<sub>2</sub> stream in IHX, heat recovery ' $Q_{recv}$ ' and turbine inlet temperature ' $T_3$ ' of BREC are shown in Figure 4.2. The increase in MFRR increases the heat recovery but the  $C_p$  also increases which results in the decrease in turbine inlet temperature  $T_3$ . Furthermore, the increase in heat recovery with MFRR resulted in drop of bottoming cycle energy efficiency according to the definition (see Eq. 3.42).

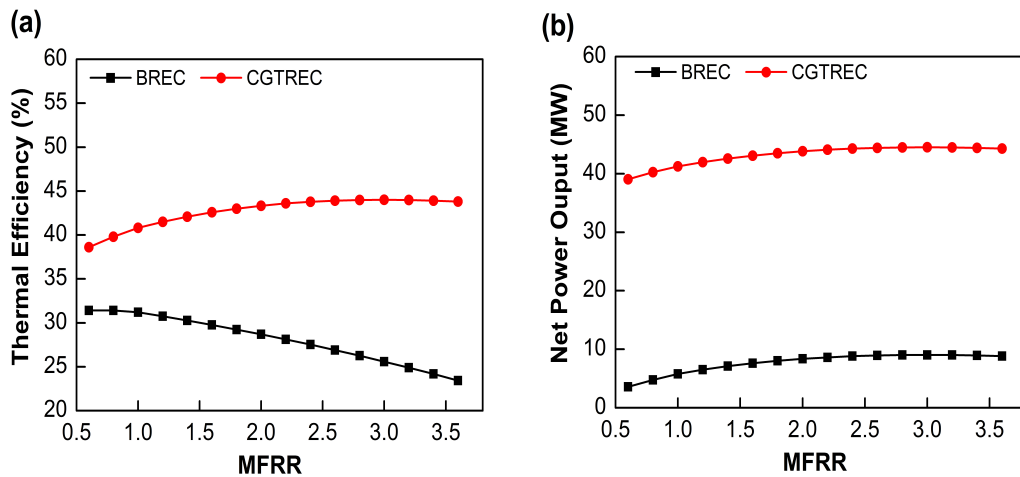


FIGURE 4.1: Behavior of (a) thermal efficiency and (b) net power output of bottoming recompression cycle (BREc) and combined gas turbine recompression cycle (CGTREC) with change in MFRR, keeping ' $x$ ' constant ( $x = 60\%$ ).

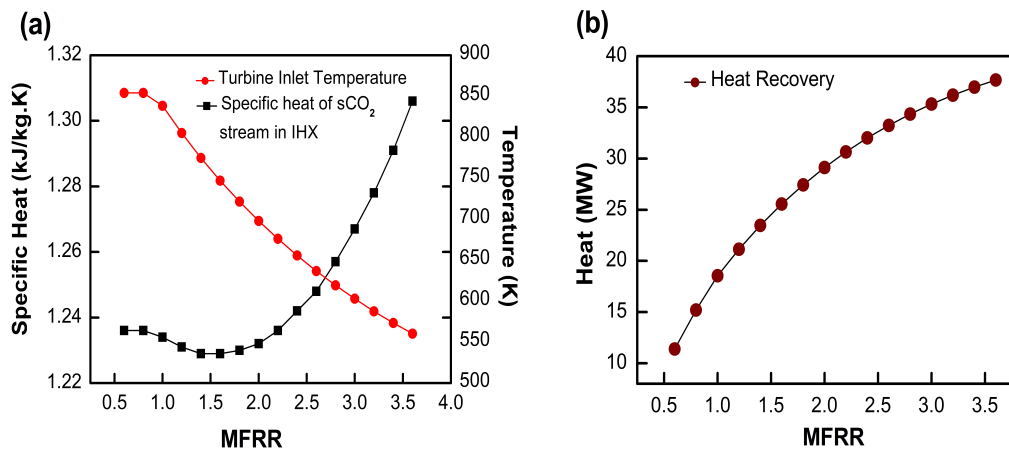


FIGURE 4.2: Behavior of (a) specific heat  $C_p$  of  $s\text{CO}_2$  in BREC, turbine inlet temperature ( $T_3$ ) and (b) heat recovery of BREC with change in MFRR keeping ‘ $x$ ’ constant ( $x = 60\%$ ).

The performance of the combined cycle is also studied for variation in both MFRR and recompression percentage  $x$ . Energy efficiency and exergy efficiency for varying MFRR and  $x$  are shown in Figure 4.3. It is evident that both efficiencies are increasing with decrease in  $x$  (i.e., performance at  $x = 55\%$  is greater than performance at  $x = 70\%$ ). Moreover, with increase in MFRR, the maxima points for each  $x$  are moving towards left direction. It explains that the energy and exergy efficiencies of CGTREC are maximum for greater mass flow rates (MFRR) and smaller mass recompression percentage  $x$ .

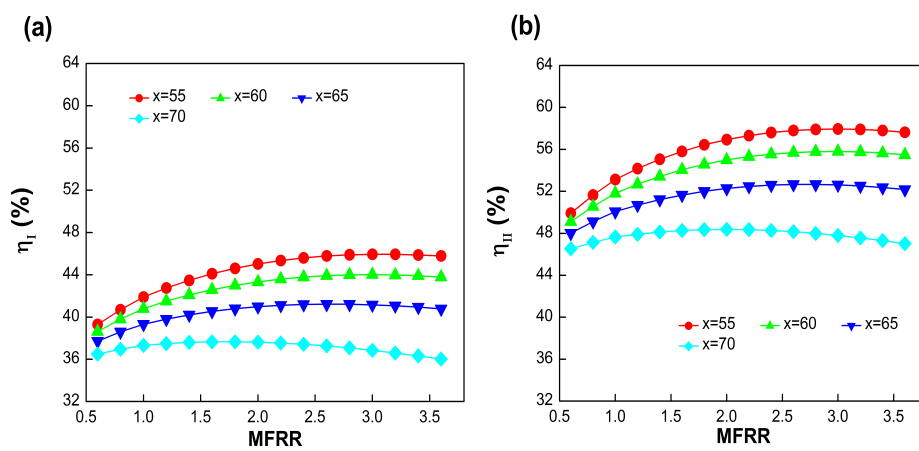


FIGURE 4.3: Variation of (a) energetic and (b) exergetic efficiencies with change in both MFRR and  $x$  for CGTREC.

To find the design point, optimization is done which provide the optimum point at which irreversibilities in the combined cycle are minimum or the exergy efficiency is maximum. The optimization is performed using Genetic method in EES and three decision parameters are selected; they are MFRR,  $x$  and  $r_c$ . The ranges of decision parameters and objective function for optimization are shown in Table 4.1.

TABLE 4.1: Objective function and ranges of decision parameters for BREC.

Parameter	Range	Objective Function
$x$	$55\% \leq x \leq 75\%$	Maximize $\eta_{II}$ of the combined cycle
MFRR	$1.4 \leq \text{MFRR} \leq 3$	
$r_c$	$2.5 \leq r_c \leq 3.5$	

The optimum results and corresponding T-s diagram are shown in Table 4.2 and Figure 4.4, respectively. These results illustrated the first law and second law efficiencies along with exergy input, exergy out, net power output and irreversibilities in components. Maximum combined cycle thermal efficiency is found to be 45.67% at CO<sub>2</sub> mass flow rate of 168 kg/s (MFRR = 1.6) and recompression percentage ‘ $x$ ’ of 45%. As shown in the Table 4.2, the total exergy input for combined cycle is 80.9 MW, out of which 13.1 MW goes out after interaction in IHX identified as exergy loss, 21.1 MW is associated with exergy destruction due to component irreversibilities and 46.2 MW is produced as power output from the combined system, resulted in 57.74% exergetic efficiency of CGTREC according to Eq. (3.47).

TABLE 4.2: Optimum results of CGTREC.

First law Analysis (Energy Analysis)	
Parameter	Optimum Value
$T_3$	739.1 K
Heat Recovery	27.2 MW
Combined power output	46.2 MW
Bottoming power output	10.7 MW
Combined Thermal Efficiency	45.67%

Parameter	Optimum Value
Bottoming Thermal Efficiency	39.4%
<b>Second law Analysis (Exergy Analysis)</b>	
Exergy input in combined cycle	80.9 MW
Exergy input in bottoming cycle	16.5 MW
Combined cycle exergy destruction	21.1 MW
Bottoming cycle exergy destruction	6.28 MW
Exergy loss	13.1 MW
Bottoming cycle exergetic Efficiency	61.9%
Combined cycle exergetic Efficiency	57.74%
<b>Optimum values of decision parameters</b>	
MFRR	1.6
$x$	45%
$r_c$	2.5

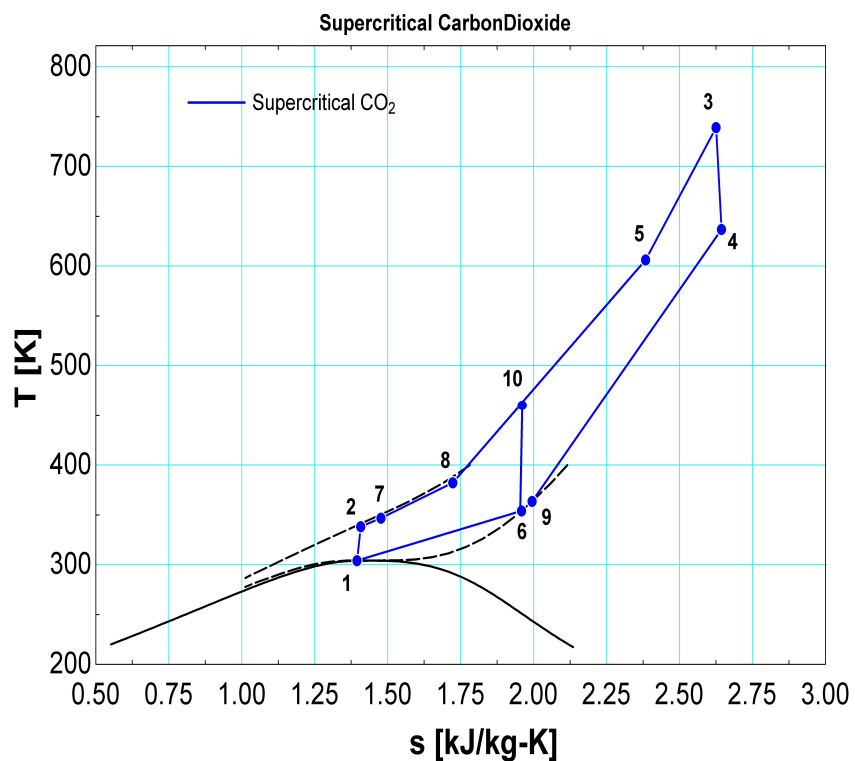


FIGURE 4.4: Optimum T-s diagram of BREC.

Figure 4.5(a) illustrate the component level exergy destruction in bottoming recompression cycle (BREC). The main sources of exergy destruction are IHX, turbine ( $T_2$ ) and HTR. In Figure 4.5(b), the sum of exergy destruction and exergy loss in CGTREC are compared with simple gas turbine cycle to elaborate the essence of heat recovery. A significant outcome is that the sum of exergy destruction and exergy loss of simple gas turbine (topping cycle) is greater than that of CGTREC. The value in simple gas turbine topping cycle is 44.34 MW while for CGTREC, it is 34.19 MW, i.e. 22.89% decrease in total cycle irreversibilities in CGTREC compared to SGT cycle. This is the manifestation of the exhaust exergy recovery in the BREC. In case of simple gas turbine, the exhaust exergy is completely wasted by the mixing of the exhaust gases into the atmosphere. By converting the simple gas turbine into combined gas turbine recompression cycle, the sum of exergy destruction and exergy losses reduce. It can be said that the total exergy destruction is decreased by the exhaust exergy recovery. Due to lower exergy destruction in the CGTREC, a greater amount of exergy input in combustion chamber ( $Q_{in}$ ) is converted into work. As a result, the thermal efficiency and exergetic efficiency enhance as compared to simple gas turbine. The percentage increase in  $\eta_I$  and  $\eta_{II}$  of CGTREC compared to simple gas turbine are 30.22% and 31.9%, respectively.

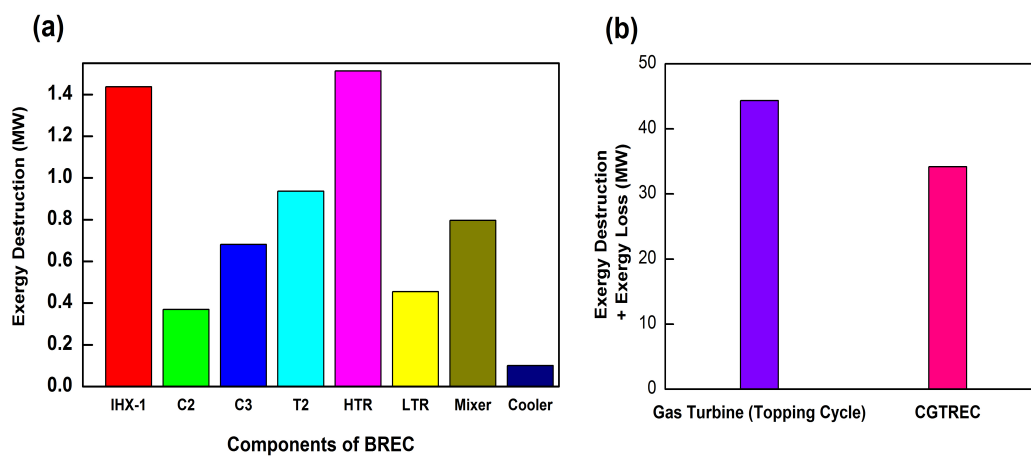


FIGURE 4.5: (a) Component level exergy destruction in BREC (b) Exergy destruction and exergy loss in CGTREC compared to SGT.

## 4.2 Combined Gas Turbine Preheating Brayton Cycle

The results of combined gas turbine-preheating sCO<sub>2</sub> bottoming cycle are shown in the following figures. Figure 4.6(a and b) shows the thermal efficiency and net power output of the combined and bottoming cycle with variation in MFRR for  $x = 65\%$ . It is apparent that the performance of combined cycle is enhanced as compared to performance of bottoming cycles. The bottoming cycle efficiency remains constant for a while, after that the decrease in efficiency is manifested by the decrease of bottoming turbine inlet temperature ' $T_3$ ' as shown in Figure 4.6(c). The heat recovery from exhaust gases ' $Q_{recv}$ ' and bottoming turbine inlet temperature ' $T_3$ ' changes because of variation in specific heats ' $C_p$ ' of cold and hot side of the exhaust heat recovery units (IHX). The IHX-1 absorbed more heat and plays dominant role in heat recovery due to larger s<sub>2</sub> mass flow as compared to that in IHX-2 as shown in Figure 4.6(d). Because of two heat recovery heat exchangers, more heat is recovered which resulted in decrease of exhaust gas temperature  $T_{6T}$ , hence, delivery of comparatively greater energy and exergy efficiencies. Using Quadratic approximation method in EES software, the maximum combined heat recovery for  $x = 65\%$  is found at MFRR = 0.81. Similarly,  $\eta_I$  and  $\eta_{II}$  are also maximum at MFRR = 0.81.

The performance of the CGTPHC is also investigated for variation in mass split percentage ' $x$ '. With increase in mass split percentage, the thermal efficiency of BPHC and the CGTPHC decreases slightly as depicted in Figure 4.7(a). The heat recovery and exergetic efficiency for different mass split percentages ' $x$ ' are also shown in Figure 4.7(b). As the heat recovery from exhaust gases decreases, the exergy efficiency decreases at constant MFRR. It means, more the exhaust heat utilization more will be the combined cycle exergetic efficiency.

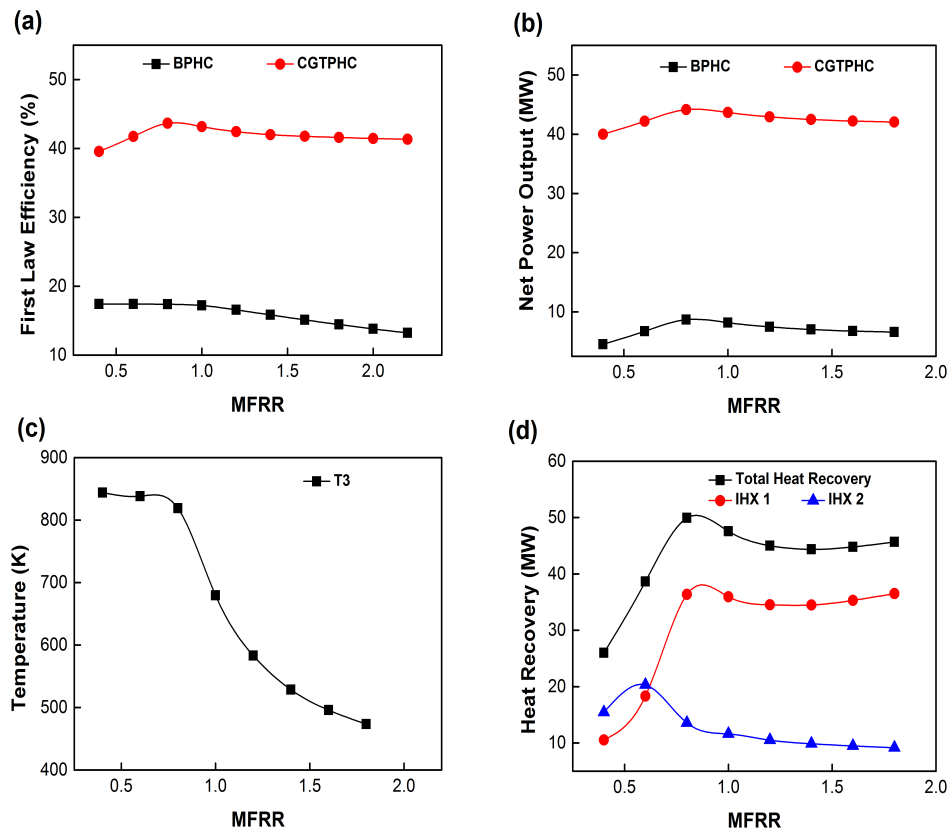


FIGURE 4.6: Variation of (a) first law efficiency, (b) net power output, (c)  $T_3$  and (d) heat recovery for CGTPHC with change in MFRR keeping ‘ $x$ ’ constant ( $x = 65\%$ ).

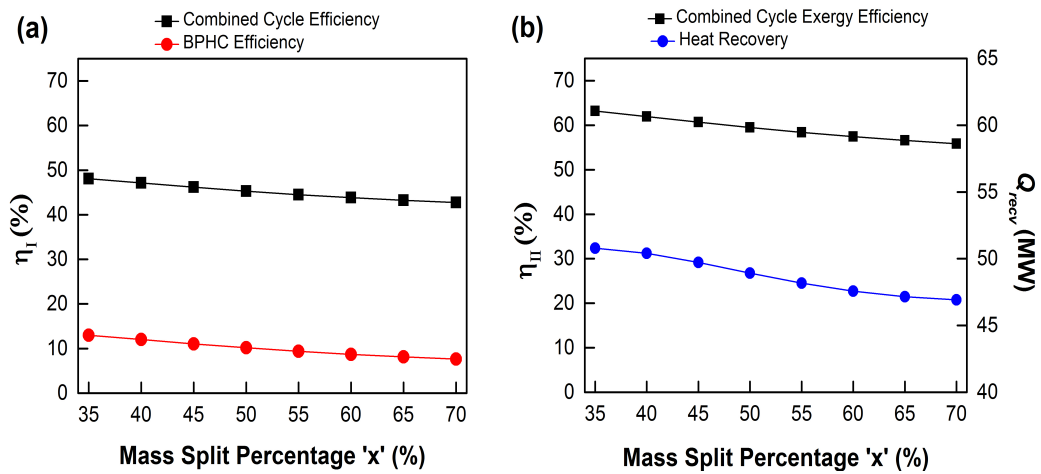


FIGURE 4.7: Variation of (a) thermal, (b) exergetic efficiency and heat recovery of CGTPHC with change in ‘ $x$ ’ at MFRR = 1.6.

The  $\eta_I$  and  $\eta_{II}$  for different MFRR and mass split percentages ‘ $x$ ’ are shown in Figure 4.8. The lines of  $\eta_I$  and  $\eta_{II}$  are going upward for decrease in mass split percentages (i.e., the combined cycle efficiency at  $x = 35\%$  is greater than at  $x =$

65%). So, the large increase in both MFRR and  $x$  simultaneously caused reduction in combined cycle energy and exergy efficiencies as depicted in Figure 4.8(a and b).

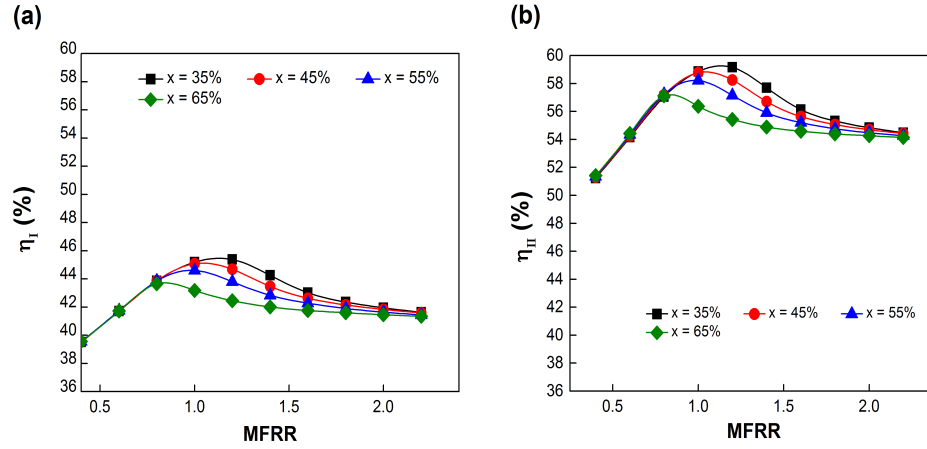


FIGURE 4.8: Variation of (a) energy efficiency and (b) exergy efficiency of CGTPHC for variation in MFRR and ‘ $x$ ’.

For optimum outcome, MFRR, mass split percentage ‘ $x$ ’ and  $r_c$  are considered as decision parameters and Genetic method in EES software is used to find optimum performance point. The bounds and function are shown in Table 4.3.

TABLE 4.3: Bounds and objective function for CGTPHC.

Parameter	Range	Objective Function
$x$	$30\% \leq x \leq 70\%$	Maximize $\eta_{II}$
MFRR	$0.5 \leq \text{MFRR} \leq 3$	
$r_c$	$2.5 \leq r_c \leq 3.5$	

The results at optimum point are given in Table 4.4 and corresponding T-s diagram in Figure 4.9. It showed the optimum energy and exergy parameters. The optimum performance is at CO<sub>2</sub> mass flow rate of 115.5 kg/s (MFRR = 1.1) and  $x = 45\%$ . Maximum combined cycle  $\eta_I$  and  $\eta_{II}$  are 46.8% and 64.8%, respectively. Compared to CGTREC, this cycle produced greater  $\eta_I$  and  $\eta_{II}$  with slightly smaller CO<sub>2</sub> mass flow rate. The exhaust exergy recovery in this cycle is also greater than CGTREC, mainly because of two heat recovery units (IHXs). The  $\eta_I$  of bottoming preheating cycle (BPHC) is lower comparatively due to larger absorbed heat in

two IHXs (See the definition of bottoming thermal efficiency in Eq. 3.42). In the waste heat recovery or cogeneration power cycles, large temperature difference in the heat recovery units (IHXs) is related to heat flowing into the bottoming power cycle. In CGTPHC cycle this temperature difference is large because of two IHXs. As a result, comparatively more power can be produced even with a lower bottoming cycle thermal efficiency because the absorbed heat is larger as compared to CGTREC (compare the values of bottoming cycle power output and thermal efficiency in Tables 4.2 and 4.4).

The total exergy input for the combined cycle is 80.9 MW, out of which, 10.8 MW goes out after interaction in IHX-1 and IHX-2 known as exergy loss, 27.4 MW is associated with exergy destruction due to component irreversibilities and 47.3 MW is produced as power output from the combined system, resulted in 64.8% combined cycle exergetic efficiency. Exergy destruction (i.e., irreversibilities) due to components of bottoming preheating cycle (BPHC) at optimum point are depicted in Figure 4.10(a). It is evident from Figure 4.10(a) and Table 4.4 that because of the presence of two heat recovery heat exchangers (IHXs), the exergy destruction due to components are greater as compared to that in BREC (shown in Table 4.2). Because, the large temperature difference and heat recovery in heat exchangers (IHX-1 and IHX-2) cause large irreversibilities. As a result, the energetic and exergetic efficiencies of BPHC are smaller than BREC (compare the values of bottoming cycle exergetic efficiency in Tables 4.2 and 4.4). However, combined energetic and exergetic performance of CGTPHC is better than CGTREC owing to larger exhaust exergy recovery.

TABLE 4.4: Optimum results of CGTPHC.

<b>First law Analysis (Energy Analysis)</b>	
<b>Parameter</b>	<b>Optimum Value</b>
$T_3$	730.4 K
Heat Recovery	49.8 MW
Combined power output	47.3 MW
Bottoming power output	1018 MW

Parameter	Optimum Value
Combined Thermal Efficiency	46.8%
Bottoming Thermal Efficiency	23.8%
<b>Second law Analysis (Exergy Analysis)</b>	
Exergy input in combined cycle	80.9 MW
Exergy input in bottoming cycle	29.1 MW
Combined cycle exergy destruction	27.4 MW
Bottoming cycle exergy destruction	12.5 MW
Exergy loss	10.8 MW
Bottoming cycle exergetic Efficiency	57%
Combined cycle exergetic Efficiency	64.8%
<b>Optimum values of decision parameters</b>	
MFRR	1.1
$x$	45%
$r_c$	3.48

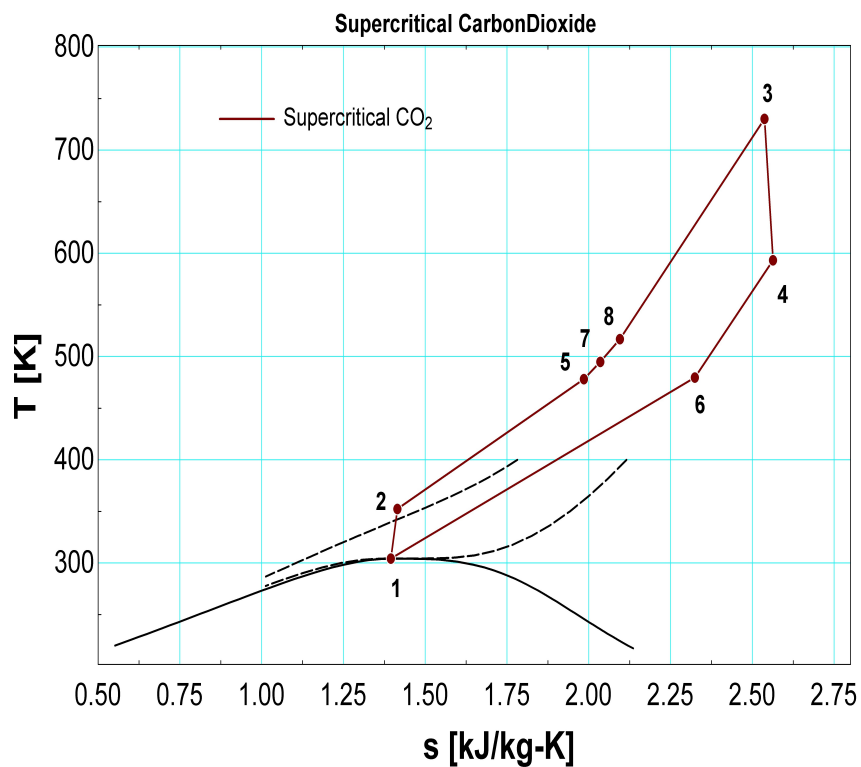


FIGURE 4.9: Optimum T-s diagram of BPHC.

The sum of exergy destruction and exergy loss in CGTPHC is compared with SGT cycle in Figure 4.10(b). Because of heat recovery by BPHC, the sum of exergy destruction and exergy loss of CGTPHC is smaller than that of simple gas turbine cycle. The sum value in simple gas turbine topping cycle is 44.34 MW while for CGTPHC, it is 28.46 MW, i.e. a decrease of 35.8% in combined cycle irreversibilities compared to SGT cycle. CGTPHC recovers larger exhaust exergy and produces larger power output compared to simple gas turbine. The percentage increase in  $\eta_I$  and  $\eta_{II}$  of CGTPHC compared to simple gas turbine are 33.4% and 48.3%, respectively. The performance gain for CGTPHC is better than CGTREC, hence, second law analysis comes out with more realistic decision taking in account the irreversibilities caused due to cycle components.

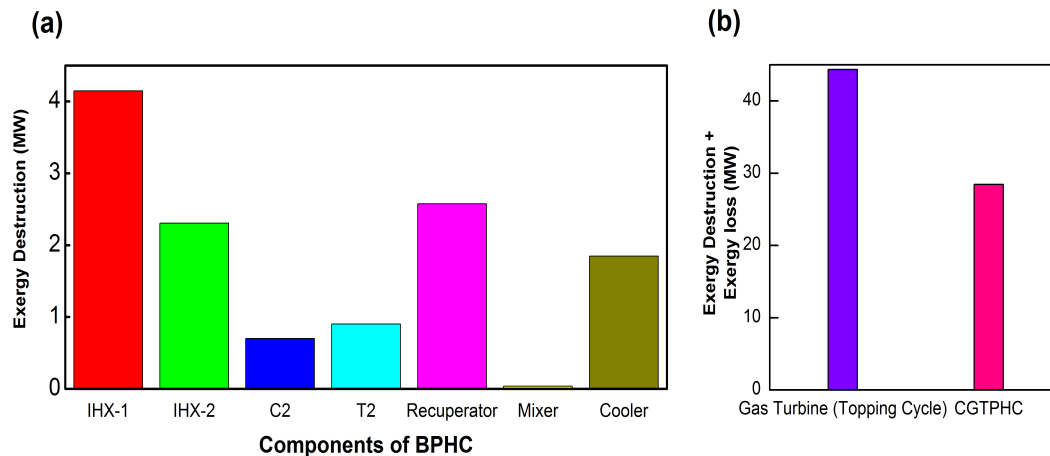


FIGURE 4.10: Component level exergy destruction in BPHC (b) Exergy destruction and exergy loss in CGTPHC compared to SGT.

## 4.3 Comparison of Results

### 4.3.1 Performance Comparison with Combined Gas Turbine Simple Regenerative Cycle (CGTSRC)

CGTSRC is considered as the reference configuration to compare the first law and second law performances of cycles with additional components and mass split;

they are: CGTREC and CGTPHC. The comparison is performed at two bottoming cycle compression ratios; they are:  $r_c = 2.7$  and  $r_c = 3$ . The main reason of the comparison is to assess the thermodynamic benefit of introducing mass split/-mass recompression percentage, recompressor and recuperators in CGTREC and CGTPHC with reference to simple regenerative cycle (CGTSRC). As depicted in Figure 4.11(a and b), the maximum combined cycle energy efficiency is given by CGTREC. While, the energy efficiency of CGTPHC and CGTSRC decreases at larger values of MFRR. Moreover, at low values of MFRR, the performance of CGTSPHC and CGTSRC approached the performance of CGTREC.

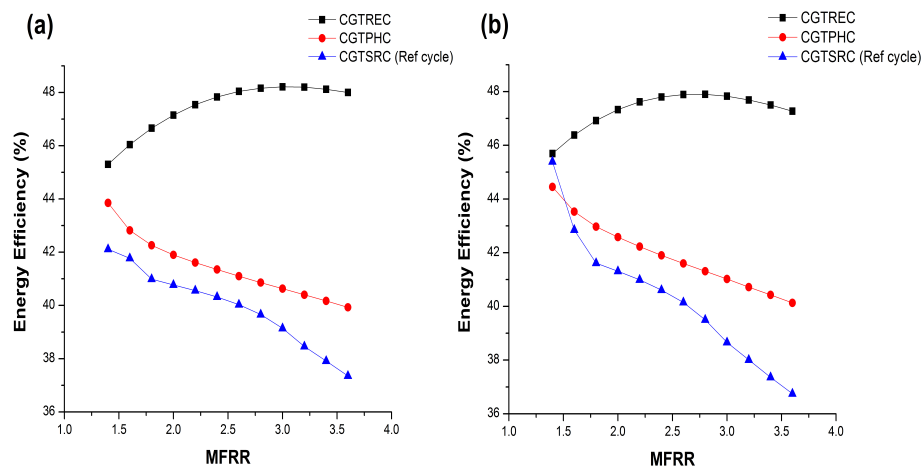


FIGURE 4.11: Comparison of combined cycle energy efficiency at (a)  $r_c = 2.7$ , (b)  $r_c = 3$ , keeping  $x = 45\%$  for CGTREC and CGTPHC.

The comparison of second law efficiency (or exergy efficiency) at  $r_c = 2.7$  and  $r_c = 3$  are shown in Figure 4.12 (a and b). At  $r_c = 2.7$ , the maximum exergy efficiency is given by CGTPHC and this is obvious owing to large exhaust exergy recovery from topping gas turbine cycle. However, at  $r_c = 3$  and smaller MFRR, the CGTPHC exhibited comparatively maximum exergy efficiency. Moreover, at larger values of MFRR, i.e.  $\text{MFRR} > 2$  the exergy efficiency of CGTREC approached near to that of CGTPHC. In general, the energy efficiency of CGTREC is maximum whereas, the second law analysis suggest CGTPHC as the one with maximum performance.

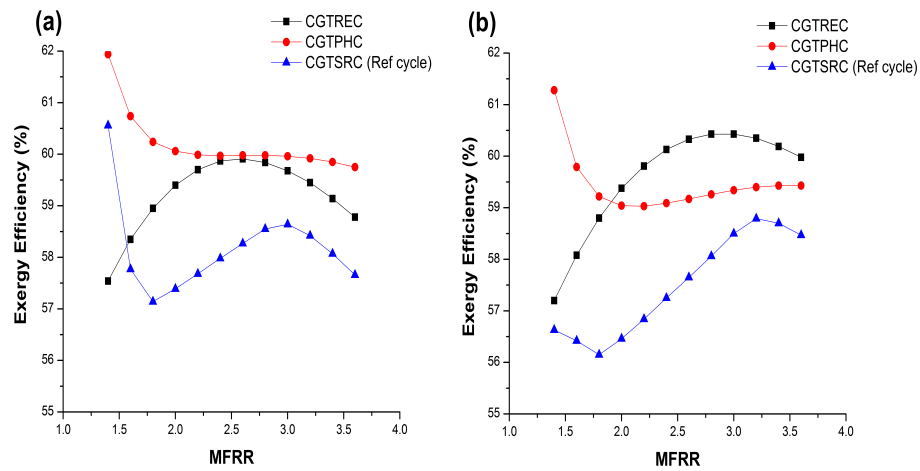


FIGURE 4.12: Comparison of combined cycle exergy efficiency at (a)  $r_c = 2.7$ , (b)  $r_c = 3$ , keeping  $x = 45\%$  for CGTREC and CGTPHC.

### 4.3.2 Performance Comparison with Air Bottoming Combined Cycle (ABC)

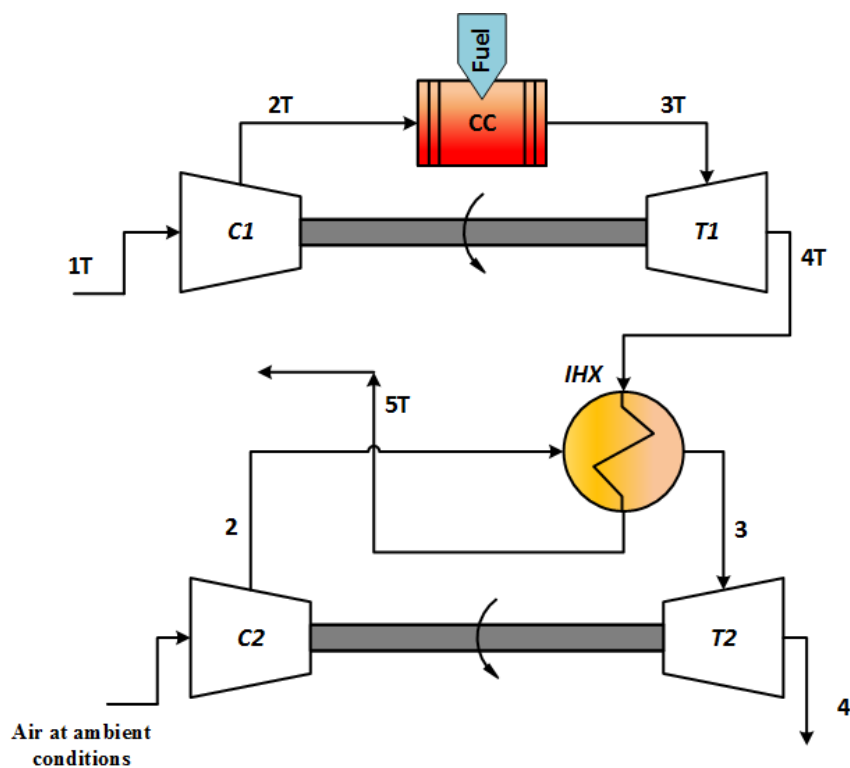


FIGURE 4.13: Schematic of Air Bottoming cycle (ABC).

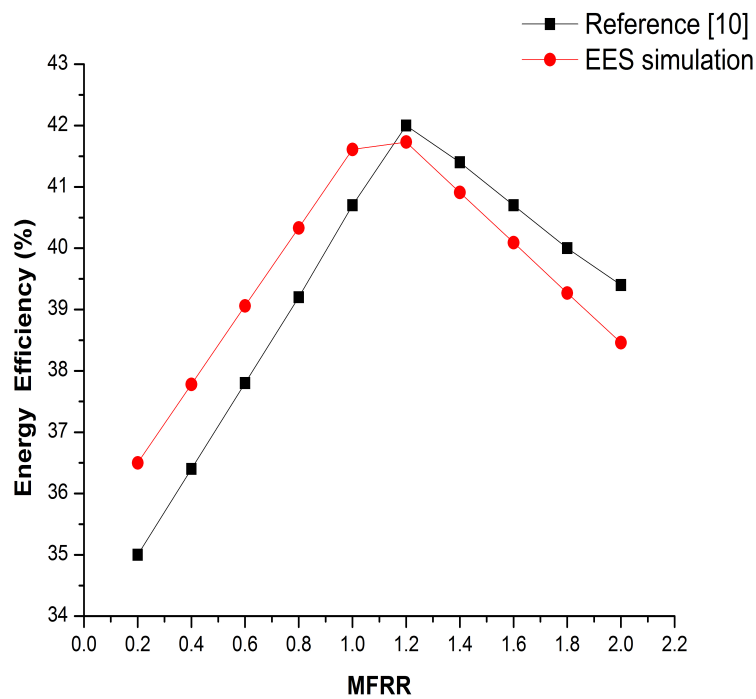


FIGURE 4.14: Results validation of ABC combined cycle.

To compare the performance of CGT-sCO<sub>2</sub> cycles, Air bottoming cycle as shown in Figure 4.13 is also used as a benchmark cycle owing to its competitive characteristics as discussed in the Introduction section. The energy and exergy analysis of ABC cycle is also carried out using EES software. The results validation is done with literature [10] and shown in Figure 4.14.

For comparative analysis, the topping gas turbine cycle is kept same for all four cycles and comparison is performed on similar operating parameters for bottoming cycles. Being air as a working fluid in ABC cycle, air at inlet enters at atmospheric conditions. The comparison is carried out at design points (optimum performance point) of all analyzed cycles. The design point for CGTSRC and ABC is also found using genetic method as adopted previously for CGTREC and CGTPHC. The main purpose of this comparison is to figure out the best possible option in terms of waste heat recovery among the considered combined cycles.

TABLE 4.5: Summary and comparison of the results.

Combined cycles Configurations	Performance of the Power Systems			Size of the Power Systems		Reduction/savings of CO <sub>2</sub> emissions (kg/h)	Priority
	$\eta_I$	$\eta_{II}$	Heat Recovery in IHX(s)	Optimum MFRR and 'x'	Number of components in bottoming cycle		
<b>CGTPHC</b>	$\eta_I = 46.8\%$ , Gain in $\eta_I$ compared to ABC is 12.68%. Gain in $\eta_I$ compared to SGT cycle is 33.44 %.	$\eta_{II} = 64.8\%$ , Gain in $\eta_{II}$ compared to ABC is 28.14%. Gain in $\eta_{II}$ compared to SGT cycle is 48.3%.	$Q_{recv} = 49.8$ MW, Gain in $Q_{recv}$ compared to ABC is 10.4 %.	MFRR = 1.1, $x = 45\%$	6 components including three heat exchangers, one cooler, one compressor and one turbine.	4947	1st
<b>CGTSRC</b>	$\eta_I = 46.26\%$ , Gain in $\eta_I$ compared to ABC is 11.4%. Gain in $\eta_I$ compared to SGT cycle is 31.9 %.	$\eta_{II} = 61.09\%$ , Gain in $\eta_{II}$ compared to ABC is 20.8%. Gain in $\eta_{II}$ compared to SGT cycle is 39.8%.	$Q_{recv} = 34.7$ MW, Reduction in $Q_{recv}$ compared to ABC is 23.1%.	MFRR = 0.98 No mass split 'x'	5 components including two heat exchangers, one cooler, one compressor and one turbine.	4719	2nd
<b>CGTREC</b>	$\eta_I = 45.67\%$ , Gain in $\eta_I$ compared to ABC is 9.96% % Gain in $\eta_I$ compared to SGT cycle is 30.22 %.	$\eta_{II} = 57.74\%$ , Gain in $\eta_{II}$ compared to ABC is 14.17 %. Gain in $\eta_{II}$ compared to SGT cycle is 31.9%.	$Q_{recv} = 27.2$ MW, Reduction in $Q_{recv}$ compared to ABC is 39.72%.	MFRR = 1.6, $x = 45\%$	7 components including three heat exchangers, one cooler, two compressors and one turbine.	4478	3rd
<b>ABC</b>	$\eta_I = 41.53\%$	$\eta_{II} = 50.57\%$	$Q_{recv} = 45.12$ MW	MFRR = 1.09 No mass split 'x'	3 components including one heat exchanger, one compressor and one turbine.	2653	Benchmark Cycle

The results are summarized in Table 4.5. The table presented the performance gain or reduction in energy efficiency, exergy efficiency and heat recovery in CGT-sCO<sub>2</sub> cycles compared to ABC and simple gas turbine cycle (SGT). The size of power cycle is also compared which is defined by the MFRR and the number of components in the sCO<sub>2</sub> cycle. Furthermore, the second last column displayed amount of reduction in greenhouse emissions because of heat recovery from topping gas turbine if the same bottoming cycle power output is produced by employing fossil fuel power cycle. The CGT-sCO<sub>2</sub> cycle with larger reduction in CO<sub>2</sub> emissions (or savings of CO<sub>2</sub> emissions) is consider as more environmental friendly cycle. The last column prioritizes the overall performance of the combined supercritical CO<sub>2</sub> cycles with reference to ABC combined cycle based on the following criteria:

1. Larger gain in  $\eta_I$  and  $\eta_{II}$  as compared to SGT and ABC.
2. Larger heat recovery compared to SGT and ABC.
3. Comparatively smaller size footprint.
4. Larger environmental advantage (i.e., larger reduction in CO<sub>2</sub> emissions).

Compared to ABC, larger gain in  $\eta_I$ ,  $\eta_{II}$  and heat recovery is achieved by CGT-PHC. The number of cycle components in CGTPHC are also lesser which also enhances its reputation in terms of plant size and initial capital and running/maintenance costs. Moreover, CGTPHC has larger environmental advantage. Hence, the CGTPHC cycle is recommended as the best combined cycle for gas turbine exhaust gases heat recovery among the nominated sCO<sub>2</sub> cycles and ABC cycle.

## 4.4 Summary

In this chapter, the thermodynamic analysis and optimization of three waste heat recovery supercritical carbon dioxide (sCO<sub>2</sub>) power systems is presented. Effects of MFRR, mass split percentage ‘ $x$ ’ and pressure ratio on the performances are

delineated. Moreover, the environmental advantage as a result of waste heat recovery with reference to fossil fuel power cycle is estimated. The prime objective here is to find the optimal combined cycle configuration for waste heat recovery based on the thermodynamic performance and environmental impact. Therefore, the optimum performance results of combined gas turbine sCO<sub>2</sub> cycles are compared with ABC and simple gas turbine cycle (SGT) to illustrate and explore the best possible configuration for gas turbine exhaust exergy recovery application.

The following can be concluded from the thermodynamic analysis and comparative analysis:

- Compared to energetic performance (1st law analysis) of simple gas turbine (SGT), there is 31.9% improvement in energetic efficiency in case of CGT-SRC, 30.22% in case of CGTREC and 33.44% in case of CGTPHC.
- Compared to exergetic performance (2nd law analysis) of simple gas turbine (SGT), there is 39.8% improvement in exergetic efficiency in case of CGTSRC, 31.9% in case of CGTREC and 48.3% in case of CGTPHC.
- Owing to exhaust exergy recovery, the sum of exergy destruction and exergy loss in combined supercritical CO<sub>2</sub> cycles is lower as compared to the sum in simple gas turbine cycle (SGT). This reduction is 22.89% in case of CGTREC and 35.8% in case of CGTPHC.
- The energetic and exergetic performances of BREC is better than BPHC owing to lower exergy destruction in components of the BREC. Energetic and exergetic efficiencies of BPHC are 23.8% and 57%, respectively. Whereas, energetic and exergetic efficiencies of BREC are 39.4% and 61.9%, respectively.
- Energetic and exergetic performance of combined supercritical CO<sub>2</sub> cycles are better than Air bottoming cycle (ABC).

- Comparative analysis based on optimum heat recovery, size, energetic efficiency, exergetic efficiency and environmental benefit revealed that CGT-PHC is selected as the optimum combined cycle and BPHC as the appropriate option for gas turbine exhaust exergy recovery.

# Chapter 5

## Turbomachinery Design

In this chapter, the compressor and turbine are designed for the optimum bottoming sCO<sub>2</sub> power cycle decided in Chapter 4. Two design methodologies are adopted, they are: 1) Preliminary design and 2) 1D mean line design. The preliminary design method is based on empirical charts and it facilitates in estimating the revolution speed, stages and impeller tip diameter of the turbomachinery. The 1D mean line design is rather more accurate; it computes the geometry as well as the efficiency of the turbomachinery. More specifically, this method computes the efficiency of turbomachinery based on enthalpy loss correlations. The turbomachinery design method is coded in MATLAB linked with REFPROP property library for retrieval of thermodynamic properties of sCO<sub>2</sub>. Finally, to evaluate the effect of turbomachinery design, the efficiency of turbomachinery calculated from the design code is transferred to thermodynamic analysis code (described in chapter 3) for determination of updated sCO<sub>2</sub> power cycle performance.

### 5.1 Compressor Design

The main compressor in sCO<sub>2</sub> cycle requires less compression work because of incompressible nature (higher density) of supercritical CO<sub>2</sub> near critical point, as a result, there is higher net efficiency of the cycle. Therefore, to ensure efficient

cycle performance, the compressor inlet conditions should be near to critical point. But, the sharp variation of properties near the critical point is the challenge for compressor designer which demands sophisticated design method that accounts for large variations in properties especially density of CO<sub>2</sub>. The commercial compressor design tools adopted to date are not applicable for design of sCO<sub>2</sub> compressor because they are based on ideal gas assumption. Hence, a revised methodology is required which should consider the impact of enthalpy and pressure losses in different sections of the compressor on the performance of the compressor. The method should be devoid of ideal gas assumption for accurate prediction of the performance of sCO<sub>2</sub> compressor. Therefore, in this chapter an iterative methodology known as 1D mean line method is applied for design of compressor. It is important to note that the efficiency of main compressor has significant effect on the cycle efficiency. Figure 5.1 illustrates the dependence of compressor isentropic efficiency on first law efficiency of BPHC. It can be observed that for increase in 15% (65% to 75%) in isentropic efficiency of compressor results in increase of 25% (10% to 12.5%) in first law efficiency of BPHC. Hence, rather than assuming the isentropic efficiency as done previously during thermodynamic analysis, it is crucial to determine the actual efficiency based on losses that are happening inside the compressor as a result of fluid flow.

The design method is carried out for bottoming cycle compressor of optimum sCO<sub>2</sub> cycle configuration decided at the end of Chapter 4, i.e. CGTPHC. The whole design procedure is divided into three phases:

1. Selection of type of Compressor
2. Preliminary sizing
3. 1D mean line design

The static and stagnation properties required during design are obtained from Reference Fluid Thermodynamic and Transport Properties Database (REFPROP) [24].

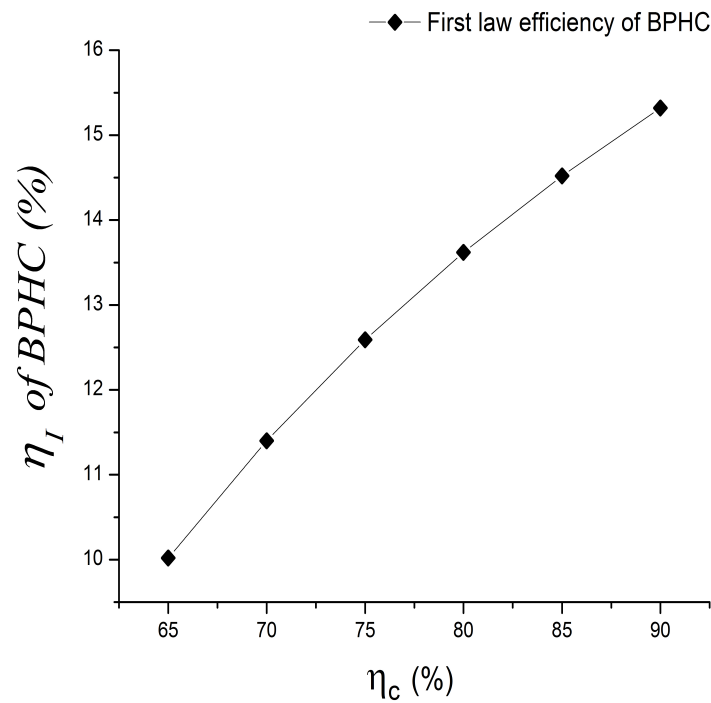


FIGURE 5.1: Effect of compressor's isentropic efficiency on the first law efficiency of BPHC.

### 5.1.1 Selection of Type of Compressor

In general, the choice among radial and axial turbomachinery depends on the mass flow rate and power output of the thermodynamic power system [65, 79]. Radial compressors are more appropriate instead of axial one owing to following reasons [80]:

1. Radial compressors are comparatively more compact because they present small number of stages compared to axial counterpart.
2. Fit for low mass flow rate and high-pressure ratio applications.
3. They are more robust, cheaper, easier to maintain and manufacture.

The power output in case of BPHC is 11.8 MW with  $s\text{CO}_2$  mass flow of 115.5 kg/s, hence, radial compressor is selected. Moreover, single stage compression is adopted instead of multi stage compression to avoid complex flow path of working fluid and

cooling flow which necessitate difficult manufacturing process and subsequently larger capital cost. A radial compressor consists of three parts: 1) a rotating impeller which imparts kinetic energy to the flow, 2) a stationary diffuser which converts the kinetic energy into increase in pressure and 3) volute section which smoothly discharges the flow. The single stage radial compressor in radial plane is shown in Figure 5.2.

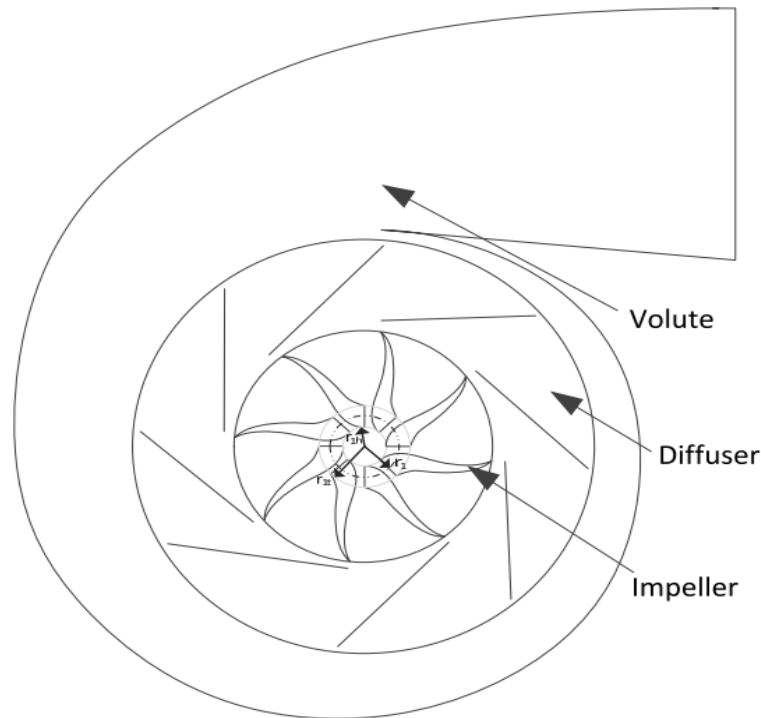


FIGURE 5.2: Single stage radial compressor in r-plane [69].

### 5.1.2 Preliminary Sizing

The design of radial compressor starts with one of the most useful method for turbomachinery selection and sizing known as Balje's  $N_S$ - $D_S$  diagram method [81, 82]. The  $N_S$ - $D_S$  diagram for single stage compressor is shown in Figure 5.3. The diagram depicts the efficiency curves of different types of compressors in terms of two dimensionless parameters, they are: Specific speed ( $N_S$ ) which is on x-axis and specific diameter ( $D_S$ ) which is on y-axis. The definition of  $N_S$  and  $D_S$  are given in Eqs. (5.1) and (5.2).

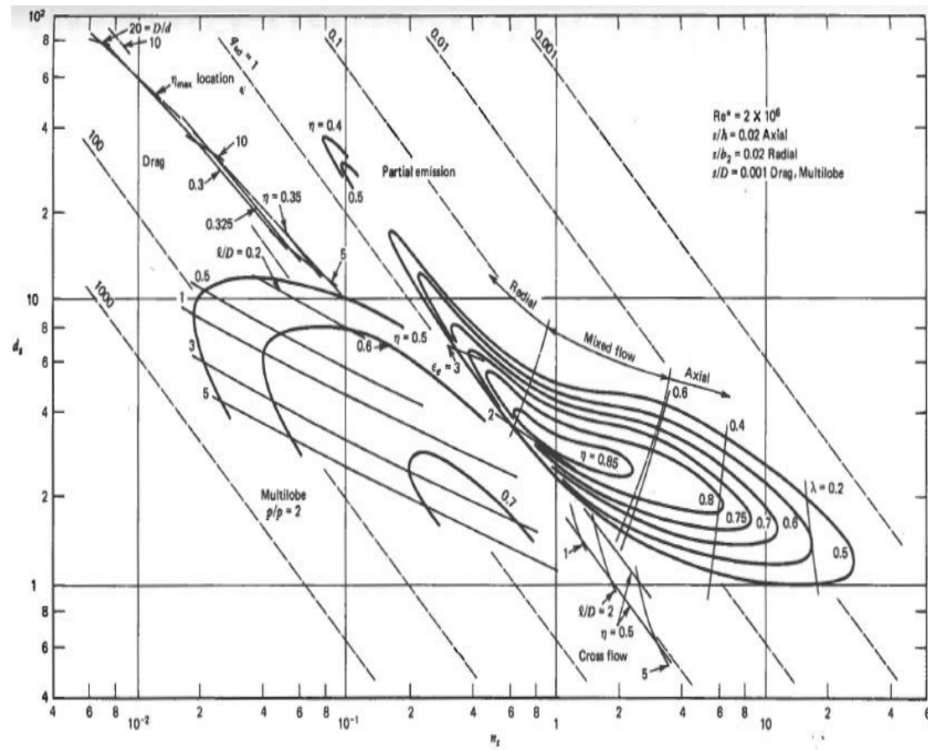


FIGURE 5.3: Balje's  $N_S$ - $D_S$  diagram for compressors [81].

Each contour line in Balje's diagram depicts the constant total to static efficiency for a given compressor type. Moreover, the efficiency increases from outer contour line towards inner; the most center contour line is the highest efficiency line. The intent of preliminary sizing is to find the couple of  $N_S$  and  $D_S$  which provides maximum efficiency.

$$N_S = \frac{N\sqrt{Q}}{\Delta H^{\frac{3}{4}}} \quad (5.1)$$

$$D_S = \frac{D_c \Delta H^{\frac{1}{4}}}{\sqrt{Q}} \quad (5.2)$$

Where,

$$Q = \dot{m}_{CO_2} \times \rho_1 \quad (5.3)$$

The  $N_S$  and  $D_S$  depends on the volumetric flow rate ' $Q$ ', thermodynamic enthalpy rise ' $\Delta H$ ', revolution speed ' $N$ ' and impeller tip diameter ' $D_c$ ' of the compressor [81]. From literature, the recommended value of  $N_S$  for radial compressors is 0.6 to 0.77 [65, 71]. The  $D_S$  is selected against  $N_S$  from Balje's diagram on maximum

efficiency line. The revolution speed ' $N$ ' and impeller tip diameter ' $D_c$ ' of radial compressor are decided using following procedure:

1. The isentropic enthalpy rise ' $\Delta H$ ' and compressor inlet density ' $\rho_{\text{CO}_2}$ ' is acquired from thermodynamic analysis of compressor and REFPROP respectively.
2. The optimum performance point (optimum  $N_S$ ) is searched by studying the specific speed ' $N_S$ ' at number of revolution speeds ' $N$ '.
3. The specific diameter  $D_S$  at optimum  $N_S$  are determined using Cordier's lines derived from Balje's diagram. These Cordier's line provide the value of  $D_S$  against  $N_S$  for maximum compressor efficiency. The equation of Cordier's line is given as [55],

$$D_{S,comp} = 2.719N_{S,comp}^{-1.092} \quad (5.4)$$

4. Finally, the impeller tip diameter ' $D_c$ ' is computed using relation of specific diameter (Eq. 5.2).

By utilizing the above described procedure using Balje's diagram, the value of revolution speed is found to be 32000 rpm for specific speed ' $N_S$ ' = 0.72 (It lie in optimum range for radial compressors). The preliminary design results for radial compressor of BPHC are summarized in Table 5.1.

TABLE 5.1: Preliminary design results of the radial compressor of BPHC.

Parameter	Value
$N_S$	0.72
$N$	32000 rpm
$D_S$	3.89
Impeller tip diameter ( $D_t$ )	141 mm
Number of stages	Single stage
Turbine expected efficiency from Baljes charts	>90%

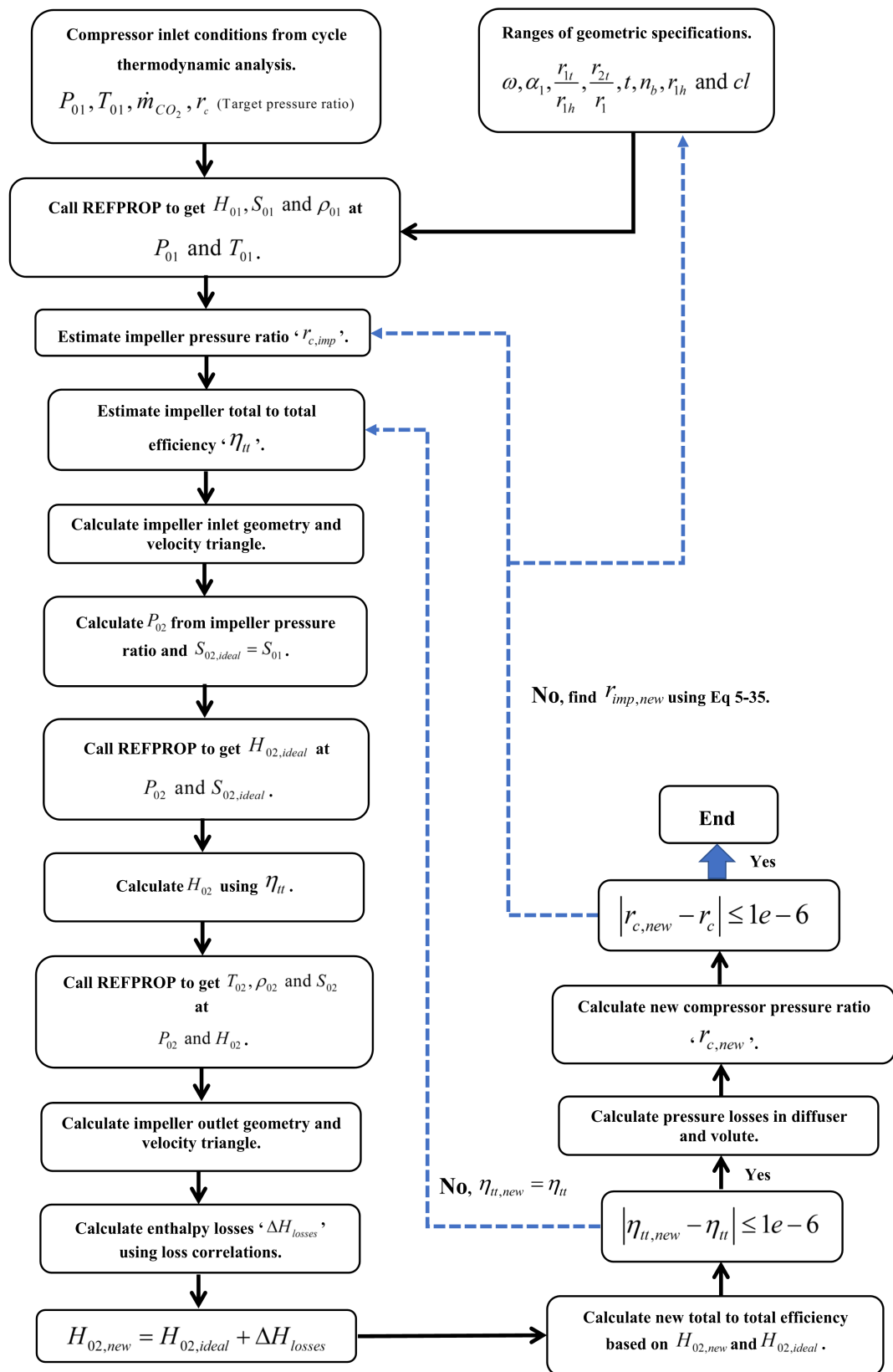


FIGURE 5.4: 1D Mean line design methodology.

### 5.1.3 1D Mean Line Compressor Design

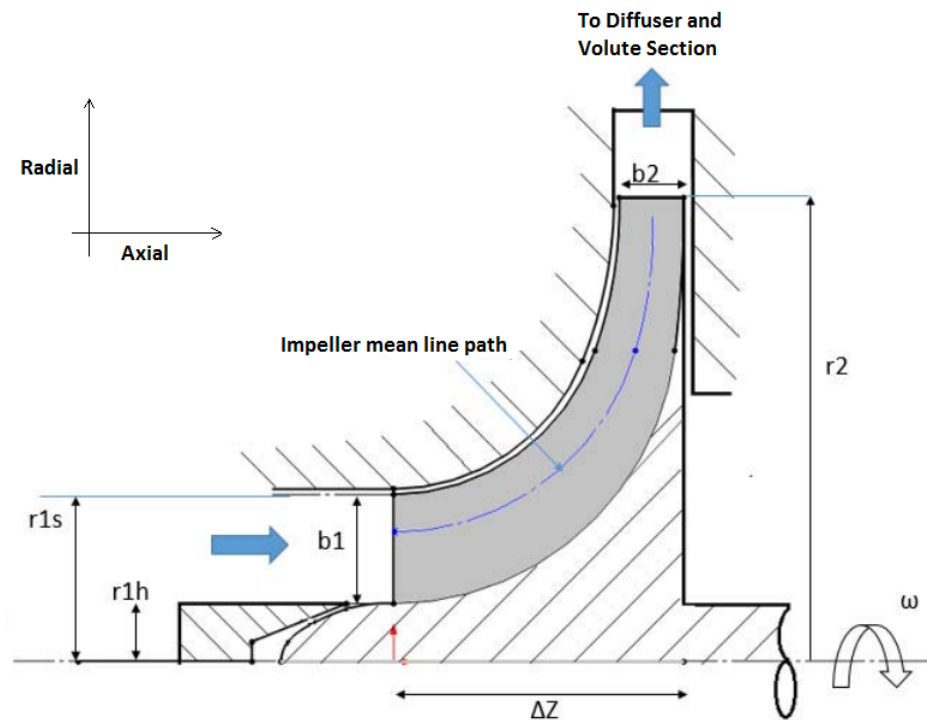


FIGURE 5.5: 1D Mean line path of a radial compressor [67].

The efficiency and impeller tip diameter estimated from Balje's  $N_S$ - $D_S$  diagram are not the exact values; they are just an estimate of compressor size and performance based on empirical data. The more precise value can be obtained by an advanced design process like 1D Mean line analysis and Computation Fluid Dynamics (CFD) tools. The 1D mean line design method compute the velocities and enthalpy losses at each segment of the compressor starting from impeller inlet and proceeds towards the volute section. The mean line or meridional view of radial compressor is illustrated in Figure 5.5. The complete methodology is illustrated in Figure 5.4 and the input geometric and thermodynamic parameters needed to start the design are shown in Tables 5.2 and 5.3. The calculations are carried out in MATLAB (R2016b) in conjunction with REFPROP to get accurate thermophysical properties during calculations. The complete code is available in Appendix A2; however, it will produce output only when user link the MATLAB with REFPROP library. The output of mean line design code are impeller geometry, inlet and outlet thermodynamics properties, inlet and outlet velocity triangles,

actual pressure ratio and actual total to total efficiency of the radial compressor. The calculations at each segment along the mean line path are delineated in the following sub sections.

TABLE 5.2: Input thermodynamic parameters from BPHC.

Input parameter	Value
$P_{01}$	7400 kPa
$T_{01}$	304.25 K
$\dot{m}_{\text{CO}_2}$	115.5 kg/s
$r_c$ (Target pressure ratio)	3.48
$\eta_{tt}$ (Assumed)	90%

TABLE 5.3: Input geometric parameters [65, 71].

Geometric parameter	Range
$\alpha_1$	0-10 <sup>0</sup>
$r_{1t}/r_{1h}$	1.5-3.5
$r_{2t}/r_1$	1.6-3.3
$r_{1h}$	15-20 mm
$t$	2.4-3.0 mm
$Z_c$	15-20
$cl$	0-2.5 mm

#### 5.1.4 Impeller Inlet

Firstly, the impeller inlet geometry which includes mean ( $r_1$ ), hub ( $r_{1h}$ ) and tip ( $r_{1t}$ ) radii are determined using given ratios in Table 5.3. The range of values in Table 5.3 for sCO<sub>2</sub> compressors are taken from literature and in each iteration parameter value is selected from the given ranges so as to find one specific value at the end which provide the target pressure ratio and maximum total to total efficiency. The impeller inlet height and area are calculated using following relations,

$$b_1 = r_{1s} - r_{1h} \quad (5.5)$$

$$A_1 = \pi r_{1s}^2 - \pi r_{1h}^2 \quad (5.6)$$

The total enthalpy, total density and total entropy are retrieved using REFPROP with the help of total input properties at impeller inlet. The axial velocity  $C_{a1}$  at impeller inlet is computed using continuity equation i.e. mass flowrate  $\dot{m}_{CO_2}$ .

$$\dot{m}_{CO_2} = \rho_1 A_1 C_{a1} = \rho_1 A_1 C_1 \cos \alpha \quad (5.7)$$

Where,  $\alpha$  is inlet swirl angle and  $A_1$  is the impeller inlet area. The static density  $\rho_1$  is required in Eq. (5.7), which is calculated using inlet total density and total to static conversion method. The procedure to calculate static density is as follows (also shown in Fig. 5.6):

1.  $C_1$  is estimated using inlet total density in Eq. (5.7).
2. Static enthalpy is calculated based on estimated  $C_1$  using total to static conversion as shown below.

$$h_0 = h_s + \frac{C_1^2}{2} \quad (5.8)$$

3. Retrieve static density from REFPROP using static enthalpy and entropy.
4. The first value of density is updated and process is continued until convergence.

The value of compressor rotational speed ' $\omega$ ' is decided in preliminary design, so,  $U_1$  is determined using Eq. (5.9).

$$U_1 = r_1 \omega \quad (5.9)$$

The relative velocity  $W_1$  and angle of relative velocity  $\beta_1$  are determined using absolute  $C_1$  and tangential velocities  $U_1$  at impeller inlet. Thus, the velocity triangle at mean radius of impeller inlet ( $r_1$ ) is constructed and shown in Figure

5.7. In the same way, the velocity triangles at impeller inlet shroud and tip can also be constructed with change only in magnitude of tangential velocities, i.e.  $U_{1S} = r_{1S}\omega$  and  $U_{1t} = r_{1t}\omega$ .

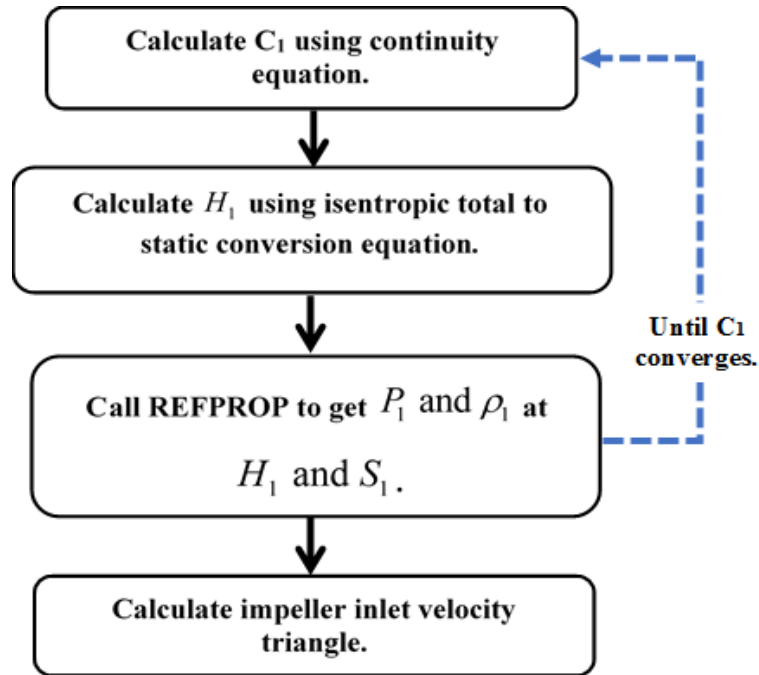


FIGURE 5.6: Method to compute impeller inlet static density.

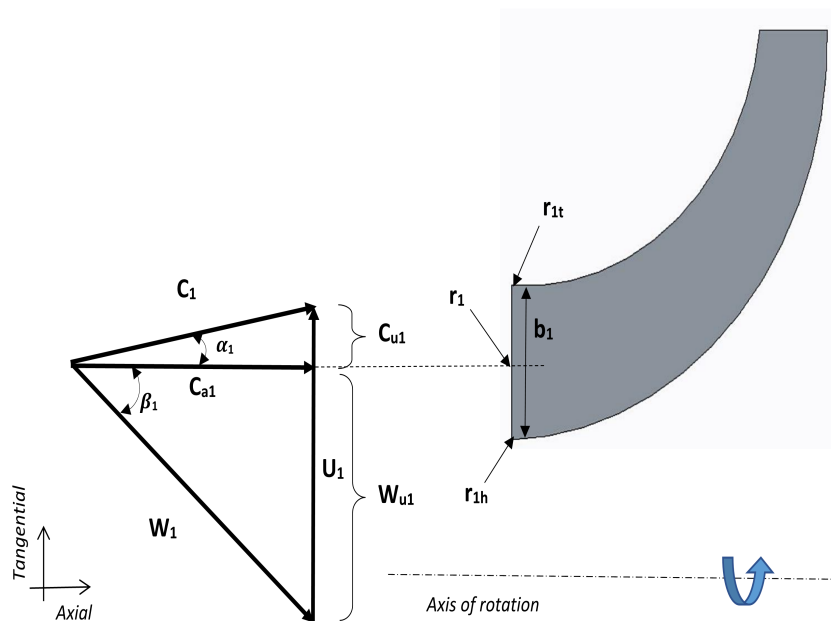


FIGURE 5.7: Impeller inlet velocity triangle.

### 5.1.5 Impeller Outlet

The impeller outlet tip radius is decided using given ratio, i.e.  $r_{2t}/r_1$  in Table 5.3. The parameter value is selected from given range in each iteration until the specified value is attained which provide target pressure ratio and maximum total to total efficiency. The blade thickness is kept same at impeller inlet and outlet, i.e.  $t_1 = t_2$  and impeller height at outlet is assumed to be 40% of inlet impeller height, i.e.  $b_2 = 0.4b_1$ .

The total pressure at impeller outlet ' $P_{02}$ ' is calculated using assumed impeller pressure ratio  $r_{c,i}$ . Next,  $H_{02,ideal}$  is determined using isentropic assumption ( $S_{02,ideal} = S_{01}$ ). Then, total to total efficiency of impeller is assumed, i.e.  $\eta_{tt} = 90\%$  to calculate the actual  $H_{02}$ .

$$H_{02} = H_{01} + \frac{H_{02,ideal} - H_{01}}{\eta_{II}} \quad (5.10)$$

The actual entropy at impeller outlet  $S_{02}$  is calculated using  $H_{02}$  and  $P_{02}$  by calling REFPROP. The absolute velocity at outlet is estimated using continuity equation given by,

$$\dot{m}_{CO_2} = \rho_2 A_2 C_{r2} \quad (5.11)$$

Where  $A_2$  is the area at impeller outlet given by,

$$A_2 = (2\pi r_2 - Zt_1) b_2 \quad (5.12)$$

The absolute fluid velocity at impeller outlet  $C_2$  is the combined effect of radial velocity  $C_{r2}$  and tangential  $C_{U2}$  velocities given by,

$$C_2 = \sqrt{(C_{U2})^2 + (C_{r2})^2} \quad (5.13)$$

Where,  $C_{U2}$  is computed using Euler equation,

$$H_{02} - H_{01} = U_2 C_{U2} - U_1 C_{U1} \quad (5.14)$$

The static density at impeller outlet, i.e.  $\rho_2$  is computed using total conditions and following steps similar to that illustrated in Figure 5.3:

1. Impeller outlet density ' $\rho_{02}$ ' is estimated using  $H_{02}$  and  $P_{02}$ .
2.  $C_{r2}$  is calculated using Eq. (5.11) and estimated total density.
3. Eqs. (5.13) and (5.14) are solved to compute  $C_2$ .
4. Total to static conversion is used to compute static enthalpy  $H_2$  at impeller outlet.
5. Static density  $\rho_2$  is retrieved using REFPROP at  $H_2$  and entropy  $S_{02}$ .
6. The density from REFPROP is compared with estimated density in step 1, the previous value is updated and process from step 1 to 5 continues till convergence of static density.

The impeller tangential velocity  $U_2$  is computed using  $r_2$  and  $\omega$ . Since,  $C_2$ ,  $U_2$  and  $C_{r2}$  are known, the full velocity triangle at impeller outlet can be drawn and illustrated in Figure 5-8, consequently, the relative velocity angle  $\beta$  and absolute velocity angle  $\alpha_2$  are determined using trigonometry.

### 5.1.6 Enthalpy Loss Models

Enthalpy losses occurring in the impeller of compressor are calculated using loss correlations available in literature [64, 67]. After calculating losses, new enthalpy at impeller outlet  $H_{02,new}$  is computed based on which new total to total efficiency  $\eta_{II,new}$  is calculated. The guessed value of the efficiency is updated and process continues until the efficiency converges. The enthalpy loss models for radial compressors are classified into internal and external loss models. The internal loss models quantify the non-isentropic behavior of the fluid when passing through the impeller. Whereas, the external losses measure the energy loss occurring outside the impeller.

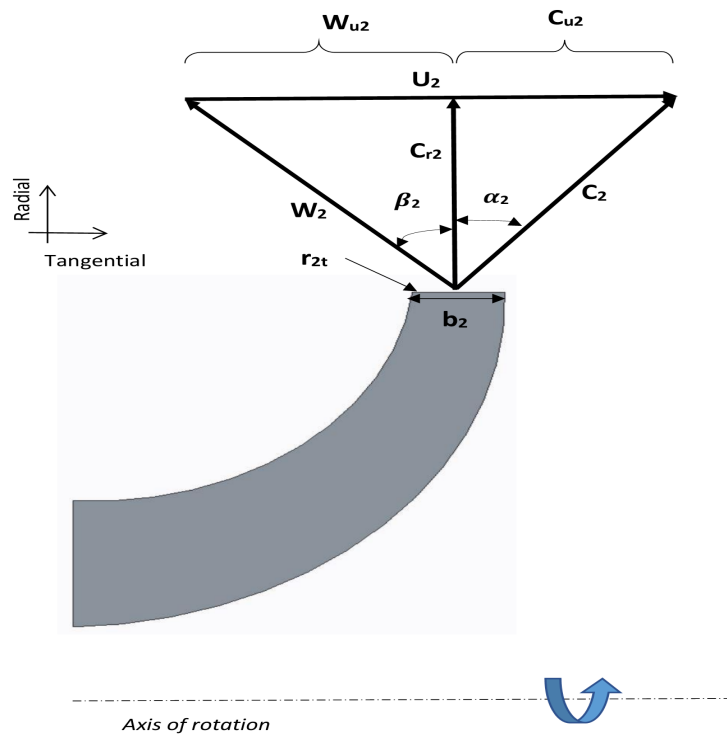


FIGURE 5.8: Impeller outlet velocity triangle.

### 5.1.7 Internal Loss Models

For quantifying internal losses, four loss models are selected. Their names and definitions are as follows,

#### 5.1.7.1 Incidence Loss

The incidence loss occurs due to difference between relative velocity and blade angle at leading edge of the impeller or in other words, there is misalignment of flow with blade angle. The loss model given by Conrad et al. [83] is used.

$$\Delta H_{inc} = f_{inc} \frac{W_{u1}}{2} \quad (5.15)$$

Where,  $f_{inc} = 0.5-0.7$

### 5.1.7.2 Blade Loading Loss

Supercritical CO<sub>2</sub> on contact with impeller blade experiences momentum loss. This loss is mainly due to boundary layer growth on the blade surfaces as well as separation and deceleration of the flow. The loss model given by Coppage et al. [84] is implemented in which the diffusion factor  $D_f$  measures the extent of flow deceleration.

$$\Delta H_{BL} = 0.05 D_f^2 U_2^2 \quad (5.16)$$

$$D_f = 1 - \frac{W_2}{W_{1t}} + 0.75 \frac{\Delta H/U_2^2}{(W_{1s}/W_2) [(Z/\pi)(1 - r_{1s}/r_2) + 2r_{1s}/r_2]} \quad (5.17)$$

### 5.1.7.3 Skin Friction Loss

Skin friction losses accounts for frictional losses which occur due shear stress exerted on the fluid as a result of boundary layer growth. The model devised by Jansen [85] is adopted.

$$\Delta H_{sf} = 2C_f \frac{L_b}{D_{hyd}} \overline{W}^2 \quad (5.18)$$

Where,

$$L_b = r_{1,t} + 2r_2 - 2r_{1,h} \quad (5.19)$$

$$D_{hyd} = \pi \times \frac{(2r_{1,tip})^2 - (2r_{1,h})^2}{\pi(2r_{1,t}) + 4Z(r_{1,t} - r_{1,h})} \quad (5.20)$$

and,

$$\overline{W} = \frac{C_{1,s} + C_2 + W_{1,s} + 2W_{1,h} + 3W_2}{8} \quad (5.21)$$

### 5.1.7.4 Clearance Loss

The presence of gap or clearance between impeller and shroud allows some fluid to leak and flow towards low pressure side (suction side) of the compressor; this

process results in clearance loss. The correlation developed by Jansen [85] is used to quantify loss due to leakage.

$$\Delta H_{cl} = 0.6 \frac{\varepsilon}{b_2} C_{U2} \sqrt{\frac{4\pi}{b_2 Z} \left[ \frac{r_{1,t}^2 - r_{1,h}^2}{(r_2 - r_{1,t})(1 + \rho_2/\rho_1)} \right]} \quad (5.22)$$

### 5.1.8 External Loss Models

Two external loss models are selected. Their names and definitions are as follows,

#### 5.1.8.1 Recirculation Loss

After leaving the impeller outlet, the low momentum fluid starts recirculating back into the impeller. The extent of this recirculation depends on the value of  $\alpha_2$  and diffusion factor  $D_f$  defined earlier. To estimate this loss, correlation provided by Oh et al. [86] is adopted.

$$\Delta H_{rc} = 8 \times 10^{-5} \sinh(3.5\alpha_2^3) D_f^2 U_2^2 \quad (5.23)$$

#### 5.1.8.2 Disc Friction Loss

Disc friction loss occur due to friction between back face of the impeller and the stationary surface faced by it. The loss model formulated by Daily and Neca [87] is selected to quantify this loss.

$$\Delta H_{df} = f_{df} \frac{\bar{\rho} r) 2^2 U_2^3}{4\dot{m}} \quad (5.24)$$

Where,

$$f_{df} = \begin{cases} \frac{2.67}{Re_{df}^{0.5}} & Re_{df} < 3 \times 10^5 \\ \frac{0.0622}{Re_{df}^{0.5}} & Re_{df} \geq 3 \times 10^5 \end{cases}$$

$$Re_{df} = \rho_2 U_2 \frac{r_2}{\mu_2} \quad (5.25)$$

### 5.1.8.3 Mixing Loss

Mixing occurs because of distorted flow inside the rotating impeller. There occurs mixing of high momentum fluid (distorted flow) with lower momentum fluid adjacent to passage walls. The loss model given by Johnston and Dean [88] based on abrupt expansion losses is adopted.

$$\Delta H_{mix} = \frac{C_2^2}{2 + 2 \tan^2 \alpha_2} \left[ \frac{1 - \varepsilon_{wake} - b_3/b_2}{1 - \varepsilon_{wake}} \right] \quad (5.26)$$

where,  $\varepsilon_{wake}$  is the wake fraction of blade to blade space and it is estimated using method given by Lieblein [89].

$$\varepsilon_{wake} = 1 - \frac{C_{m,wake}}{C_{m,mix}} \quad (5.27)$$

Where,  $C_{m,wake}$  and  $C_{m,mix}$  depends on separation velocity  $W_{sep}$  which in turn depends on diffusion factor  $D_{eq}$ .

$$D_{eq} = \frac{W_1 + W_2 + 4\pi r_2 \left[ \frac{U_2 C_{U2} - U_1 C_{U1}}{U_2 Z L_b} \right]}{2} \quad (5.28)$$

and  $W_{sep}$  depends on following conditions.

For  $D_{eq} \leq 2$

$$W_{sep} = W_2$$

And for  $D_{eq} > 2$

$$W_{sep} = W_2 \frac{D_{eq}}{2}$$

And the meridional velocities can be determined using,

$$C_{m,wake} = \sqrt{W_{sep}^2 - W_{U2}^2} \quad (5.29)$$

$$C_{m,mix} = \frac{C_{m2}A_2}{2\pi r_2 b_2} \quad (5.30)$$

### 5.1.9 Updated Compressor Efficiency

The actual enthalpy at impeller outlet is obtained after including internal and external losses.

$$H_{02,new} = H_{02,ideal} + (\Delta H_{losses})_{internal} + (\Delta H_{losses})_{external} \quad (5.31)$$

As a result, the updated total to total efficiency is,

$$\eta_{II,new} = \frac{H_{02,ideal} - H_{01}}{H_{02,new} - H_{01}} \quad (5.32)$$

The updated efficiency is compared with assumed one, if the difference is very small (i.e. Error < 1e-6) it means the efficiency converges and the process proceed towards diffuser and volute section. If the difference is large the assumed efficiency is replaced with updated one and the iteration is repeated until convergence.

### 5.1.10 Diffuser and Volute Section

The diffuser and volute section are stationary so it is assumed that no energy is added after outlet of the impeller i.e.  $H_{03} = H_{02}$ , where,  $H_{03}$  is the total enthalpy after diffuser and volute section. The loss in total pressure in diffuser and volute section is estimated using appropriate value of loss factor from literature. So, the total pressure after diffuser and volute section is given by,

$$P_{03} = P_{02} - K_{D,V} (P_{02} - P_2) \quad (5.33)$$

### 5.1.11 Pressure Ratio Convergence

After calculation of pressure at compressor exit, the compressor pressure ratio is calculated using Eq. (5.34) and compared with target pressure ratio (i.e. required pressure ratio from cycle thermodynamic analysis).

$$r_{c,iteration} = \frac{P_{03}}{P_{01}} \quad (5.34)$$

If the values are closed enough or error  $< 1e-6$ , the code completes the iteration and results are attained otherwise impeller pressure ratio is updated using,

$$r_{c,impnew} = r_{c,imp} \frac{r_c}{r_{c,iteration}} \quad (5.35)$$

### 5.1.12 Compressor Design Results

The 1D mean line design method described so far in this chapter is applied to compressor design of supercritical CO<sub>2</sub> BPHC and the geometry and performance results are summarized in Table 5.4.

TABLE 5.4: Compressor geometry and performance results for supercritical CO<sub>2</sub> BPHC.

Geometric Parameter	Value	Geometric Parameter	Value	Performance Parameter	Value
$r_{1h}$	15 mm	$b_2$	13.2 mm	$r_{c,imp}$	3.53
$r_1$	35.7 mm	$L_b$	196.6 mm	$r_c$	3.48
$r_{1t}$	48 mm	$\beta_1$	72.88 <sup>0</sup>	$\eta_{tt}$	81.2%
$t_1$	2.5 mm	$\beta_2$	82.1 <sup>0</sup>		
$b_1$	33 mm	$Z_c$	14		
$r_2$	89.3 mm				

### 5.1.13 Validation of Compressor Design Code

The experiments on thermodynamic performance of  $sCO_2$  cycle and the performance of its turbomachinery are going on in Sandia National Laboratory [52]. The  $sCO_2$  cycle experimental test loop comprises of compressor with mass flow of 3.53 kg/s and revolution speed of 75000 rpm. The geometric parameters and target pressure ratio of the compressor under test are used as input to validate the 1D mean line design code developed in this study. The input geometric parameters and operating conditions of the compressor are shown in Table 5.5.

TABLE 5.5: Geometry and operating conditions of the compressor in Sandia National Laboratory [52].

Input Parameter	Value
$P_{01}$	7687 kPa
$T_{01}$	305.30 K
$P_{02}$	1398 kPa
$\dot{m}_{CO_2}$	3.53 kg/s
$\omega$	75000 rpm
$r_{1h}$	2.5 mm
$t_1$	0.762 mm
$Z$	17
$cl$	0.00025 mm

Under given operating conditions, the target pressure ratio of the compressor for validation is  $P_{02}/P_{01} = 1.82$ . The comparison of results from 1D mean line design code and experimental results from the compressor of Sandia National Laboratory are shown in Table 5.6.

TABLE 5.6: Comparison of results from 1D Mean line design code with experimental results.

Geometry Comparison			Efficiency Comparison			
Parameter	1D mean line design code	Sandia National Laboratory [52]	Parameter	1D mean line design code	CFD [55]	Sandia National Laboratory [52]
$r_{1t}$	9.4 mm	9.4 mm	$\eta_{tt}$	77.5%	76%	66.38%
$r_2$	18.7 mm	18.68 mm				
$b_2$	1.7 mm	1.7mm				

The geometry results from 1D mean line design are in close agreement with experimental results; there is very negligible error. Whereas, the significant difference is observed when total to total efficiency of the compressor is compared. The main reason is the presence of windage losses in experimental test loop because the compressor is running at very high revolution speed i.e. 75000 rpm. The mean line design code in this study predict efficiency for low speed compressors (at low speeds windage losses are minimal) since, it does not consider the windage losses. Therefore, more accurate design code is required which accounts for extra losses occur due to high speed of the compressor. Even though, the CFD analysis done so far in literature also predicted the efficiency in the range of 76% [55] as predicted by 1D mean line design code in this study.

## 5.2 Turbine Design

The turbine (T2) is designed for optimum waste heat recovery cycle i.e. Bottoming Preheating sCO<sub>2</sub> cycle (BPHC) using similar procedure as adopted for compressor design. The design includes the calculation of nozzle geometry, rotor geometry and efficiency of the turbine. Firstly, preliminary design procedure is used to estimate the stages, revolution speed ' $N$ ' and rotor diameter  $D_t$  of the turbine with the help of Balje's turbine diagram as shown in Fig. 5.9. Then, 1D mean line design method is used to determine more size parameters and accurate turbine efficiency.

The turbine design is easier compared to compressor design because it works far away from the critical point (at high temperature and pressure) and variation of properties like specific heat and density are not abrupt as illustrated in introduction chapter. The properties of  $s\text{CO}_2$  where required during the design process are retrieved from REFPROP library as it has been done in case of compressor design.

Both radial and axial turbines are used in  $s\text{CO}_2$  cycles depending on the mass flow rate and power production capacity. Comparatively, radial turbines are easier to manufacture and they show higher reliability in low power production applications [65]. In case of BPHC, the radial turbine is more appropriate because the optimum power output is 11.8 MW as shown in Table 4.4.

### 5.2.1 Preliminary Sizing

The equations of specific speed and specific diameter (Eqs. 5.1 and 5.2) are used to determine the revolution speed and rotor diameter of the radial turbine (only replace  $D_c$  with  $D_t$  in Eq. 5.2). The empirical studies on large number of turbines shows that the optimum range of specific speed in which performance of the radial turbine is maximum is 0.4 to 0.7. Based on that, the revolution speed and stages of the turbine are decided using following steps:

1. The isentropic enthalpy drop ' $\Delta H_d$ ' and turbine outlet density  $\rho_4$  is acquired from thermodynamic analysis of turbine and REFPROP respectively. The turbine outlet density is used to determine volume flow rate ' $Q$ '.
2. The optimum performance point (optimum  $N_S$ ) is searched by studying the specific speed ' $N_S$ ' at number of revolution speeds.
3. The specific diameter  $D_S$  at optimum  $N_S$  are determined using Cordier's lines derived from Balje's turbine diagram. These Cordier's line provide the value of  $D_S$  against  $N_S$  for maximum turbine efficiency. The equation of

Cordier's line is given as [55],

$$D_{S,comp} = 2.056 N_{S,turb}^{-0.812} \tag{5.36}$$

4. Finally, the turbine rotor tip diameter ' $D_t$ ' is computed using relation of specific diameter (Eq. 5.2).

By utilizing the above described procedure using Balje's diagram, the value of revolution speed is found to be 32000 rpm for specific speed ' $N_S$ ' = 0.57. The preliminary design results for radial turbine of BPHC are summarized in Table 5.7.

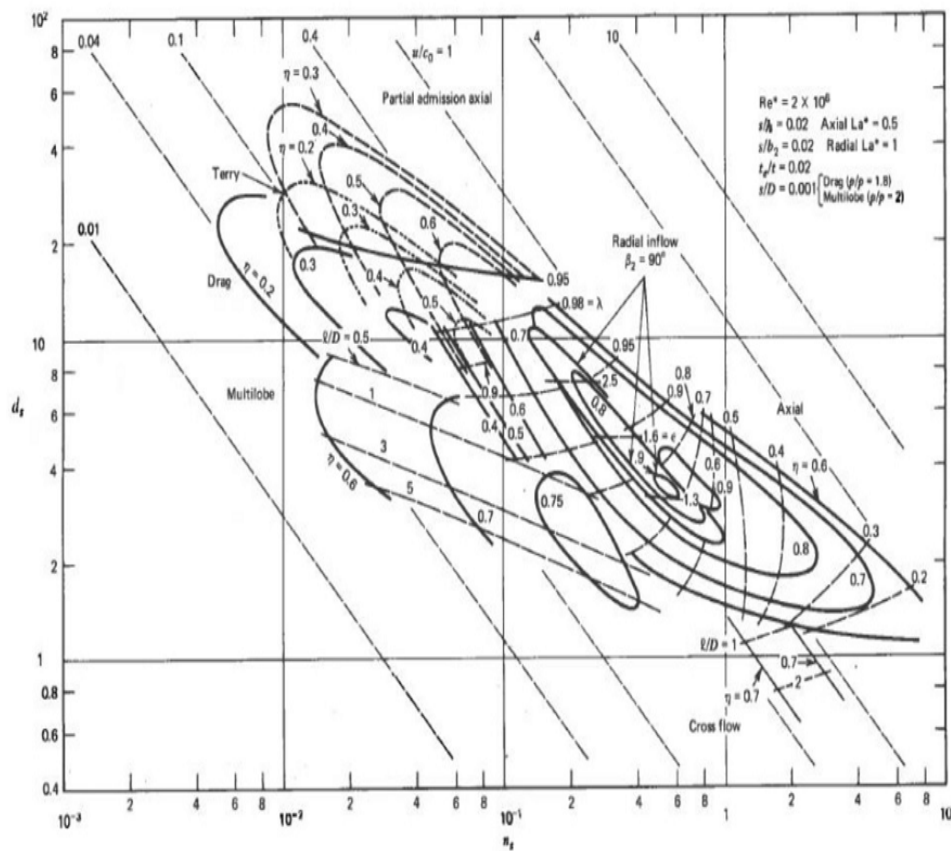


FIGURE 5.9: Balje's  $N_S$ - $D_S$  diagram for Turbines.

TABLE 5.7: Preliminary design results of the radial turbine of BPHC.

Parameter	Value
$N_S$	0.57
$N$	32000 rpm
$D_S$	3.25
Rotor tip diameter ( $D_t$ )	215 mm
Number of stages	Single stage
Turbine expected efficiency from Baljes charts	$\sim 90\%$

### 5.2.2 1D Mean Line Turbine Design

The 1D mean line design process starts with value of estimated efficiency and revolution speed found from preliminary sizing (shown in Table 5.7) as an input value. The thermodynamic properties and geometry are computed at each section of the turbine. Then, efficiency is corrected based on enthalpy losses occurring in it and the process continues until the convergence of efficiency. In addition to geometry of the rotor, velocities at rotor inlet and outlet are also calculated and velocity triangles are constructed to illustrate the nature and direction of the flow across the radial turbine rotor. The input parameters and design conditions required for the design process are given in Table 5.8. The detail design procedure is described in following steps:

1. The estimated efficiency i.e. 90% in this case (from preliminary design) is used to calculate exit total enthalpy of the turbine using,

$$h_{04} = h_{01} - \Delta H_d \eta_s \quad (5.37)$$

2. The fluid velocity (also known as discharge spouting velocity) and the rotor inlet tangential velocity are calculated using following relations,

$$C_{os} = \sqrt{2\Delta H_d} \quad (5.38)$$

$$U_{3b} = v_s C_{os} \quad (5.39)$$

Where,  $v_s$  is velocity ratio whom value is taken from the best practice in literature (Its value range provided in Table 5.8).

TABLE 5.8: Input parameters and design conditions for turbine 1D mean line design code.

<b>Turbine Parameters</b>	<b>Value</b>
Inlet total pressure ( $P_{03}$ )	25.75 MPa
Outlet total pressure ( $P_{04}$ )	7.4 MPa
Inlet total temperature ( $T_{03}$ )	730.4 K
Mass flow rate ( $\dot{m}$ )	115.5 kg/s
Velocity ratio ( $v_s$ )	0.6-0.8
Turbine efficiency ( $\eta_s$ ) from Preliminary sizing	90%

3. Using rotor inlet tangential velocity, rotor inlet radius  $r_{3b}$  is calculated using

$$r_{3b} = \frac{U_{3b}}{\omega} \quad (5.40)$$

4. The component of fluid velocity in tangential direction  $C_{3bu}$  is computed using Eq. (5.41) and  $C_{3b}$  is computed using trigonometry. The rotor inlet and outlet thicknesses along with rotor outlet hub and shroud radiuses are calculated using Eqs. (5.43) to (5.46).

$$C_{3bu} = \frac{U_{3b}\eta_s}{2v_s^2} \quad (5.41)$$

$$C_{3b} = \frac{C_{3bu}}{\sin(\alpha_3)} \quad (5.42)$$

$$t_{3b} = 0.04r_3 \quad (5.43)$$

$$t_4 = 0.02r_3 \quad (5.44)$$

$$r_{h4} = 0.22r_3 \quad (5.45)$$

$$r_{s4} = 0.7r_3 \quad (5.46)$$

5. Pressure losses occur from turbine inlet volute section till rotor inlet. This pressure loss is estimated using Eq. (5.47).

$$P_{03b} = P_{03} - \frac{\rho_{03}\Delta H_d(1 - \eta_s)}{4} \quad (5.47)$$

6. The known thermodynamic properties at rotor inlet ( $P_{03b}$  and  $h_{03b}$ ) and rotor inlet fluid velocity  $C_{3b}$  are used to compute the static properties ( $h_{3b}$  and  $\rho_{3b}$ ) at rotor inlet.
7. The rotor inlet width is calculated using Eq. (5.48).

$$b_3 = \frac{\dot{m}}{2\pi r_{3b}\rho_{3b}C_{m3b}} \quad (5.48)$$

8. The density at rotor outlet  $\rho_4$  is assumed to find outlet fluid velocity  $C_{m4}$  using Eqs. (5.49) and (5.50) is used to compute static enthalpy  $h_4$  at rotor outlet. Using  $h_4$  and outlet pressure  $P_4$ , the density value is corrected.

$$C_{m4} = \frac{\dot{m}}{2\pi r_4\rho_4 b_4} \quad (5.49)$$

$$h_4 = h_{04} - \frac{1}{2}C_{m4}^2 \quad (5.50)$$

9. The rotor outlet radius and width are calculated using Eqs. (5.51) and (5.52).

$$r_4 = \frac{r_{h4} + r_{s4}}{2} \quad (5.51)$$

$$b_4 = r_{s4} - r_{h4} \quad (5.52)$$

10. The tangential velocity at rotor outlet is calculated using Eq. (5.53) and number of turbine blades are estimated using Eq. (5.54).

$$U_4 = r_4 \omega \quad (5.53)$$

$$Z_t = \frac{\pi}{30} (110 - \alpha_{3b}) \tan \alpha_{3b} \quad (5.54)$$

11. The nozzle exit and inlet radius are then computed using Eqs. (5.55) and (5.56).

$$r_{3a} = r_{3b} + 2b_3 \cos \alpha_3 \quad (5.55)$$

$$\frac{r_3}{r_{3a}} = 1.3 \quad (5.56)$$

The velocity triangles at rotor inlet and outlet are drawn with the help of calculated velocities and angles. The meridional view of the sCO<sub>2</sub> cycle turbine along with the velocity triangles are shown Figure 5.10.

12. The enthalpy losses occur in the turbine are calculated and outlet enthalpy is updated using Eq. (5.57). The passage loss ( $\Delta h_{pass}$ ), exit loss ( $\Delta h_{exit}$ ), nozzle loss ( $\Delta h_{nozz}$ ) and tip clearance ( $\Delta h_{tipcl}$ ) loss are considered. The correlations available in literature [64, 90, 91] are used to compute these losses.

$$\Delta h_{loss,turb} = \Delta h_{tipcl} + \Delta h_{exit} + \Delta h_{nozz} + \Delta h_{pass} \quad (5.57)$$

13. The updated turbine efficiency based on updated outlet enthalpy is calculated using,

$$\eta_s^{corr} = \frac{\Delta H_d}{\Delta H_d + \Delta h_{loss,turb}} \quad (5.58)$$

14. The updated turbine efficiency is compared with the estimated efficiency specified at the start of the turbine design code. If the difference is small i.e.  $\leq 1e-3$  then code stops and output geometry and efficiency are saved otherwise code repeats with  $\eta_s = \eta_s^{corr}$  until convergence. The final converged results are summarized in Table 5.9.

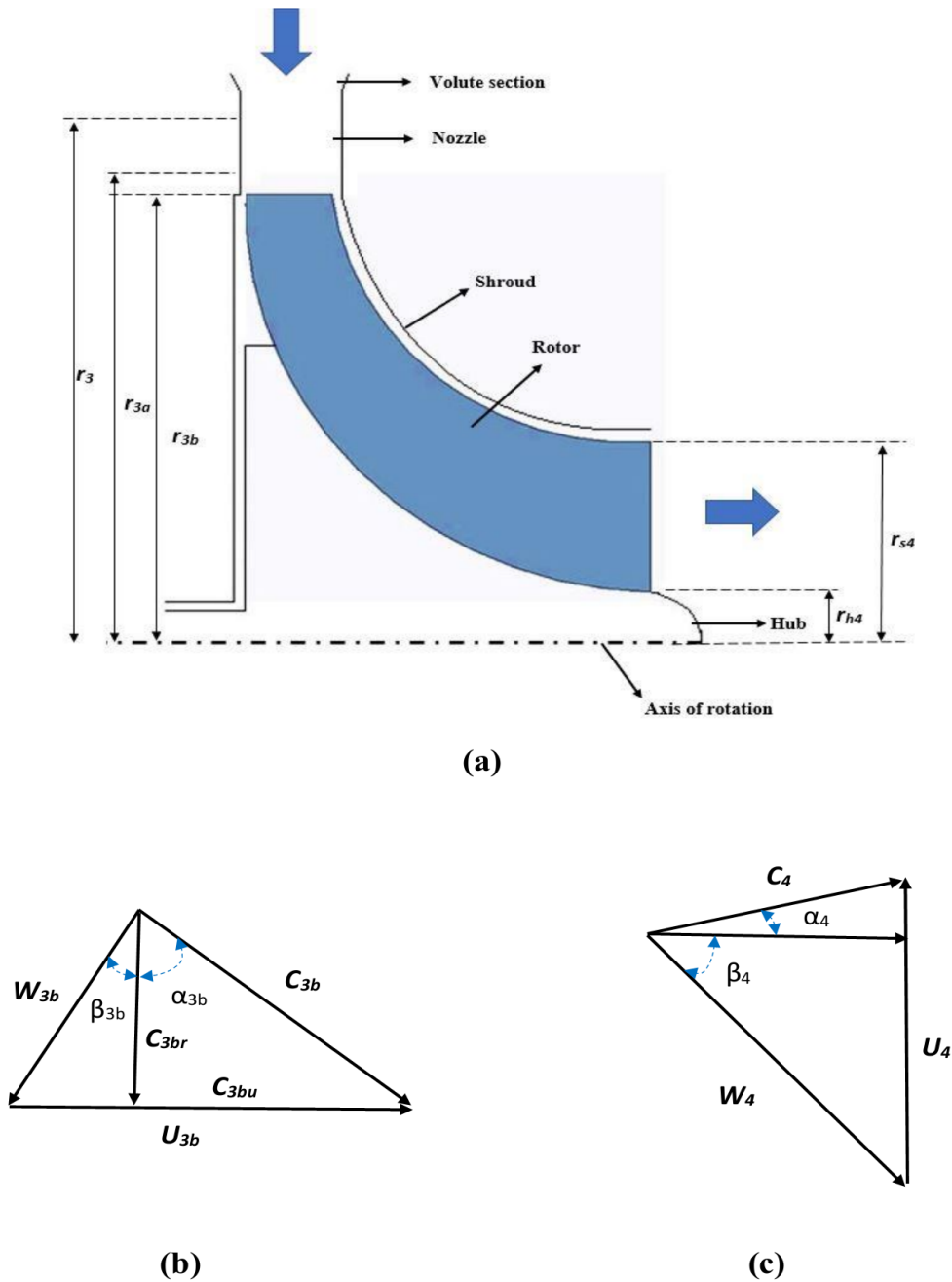


FIGURE 5.10: (a) Meridional view showing main stations of the radial turbine; (b) Rotor inlet velocity triangle;(c) Rotor outlet velocity triangle.

TABLE 5.9: Radial turbine design results for BPHC.

Turbine Geometry		Turbine Efficiency	
$r_3$	160 mm	$\eta_s$	86.17%
$r_{3a}$	123 mm		
$r_{3b}$	115.8 mm		
$r_4$	53.3 mm		
$b_3$	14.1 mm		
$b_4$	55.6 mm		
$t_{3b}$	4.6 mm		
$t_4$	2.3 mm		
$\beta_{3b}$	$27.14^\circ$		
$\beta_4$	$62.54^\circ$		
$Z_t$	14		

### 5.2.3 Revised Performance Evaluation of BPHC and CGTPHC

The compressor and turbine design codes are linked with cycle thermodynamic analysis for precise calculation of cycle energy and exergy efficiencies. The optimum cycle configuration decided at the end of Chapter 4 is combined gas turbine preheating cycle (CHTPHC). So, the assumed efficiencies specified prior in Table 3.1 are replaced with updated efficiency computed from 1D mean line design code and thermodynamic results of BPHC and CGTPHC are updated. The updated results of optimum cycle configuration are shown in Table 5.10. The updated performance slightly decreases, however, the difference between two methods is very small because the assumption was quite reasonable in simple uncoupled thermodynamic analysis as compared to coupled one. It does not indicate that the turbomachinery design code has no significance; these design methods helps in prediction of cycle performance during off-design conditions especially when there

are fluctuations in compressor inlet conditions during real time operation of sCO<sub>2</sub> compressors.

TABLE 5.10: Comparison of thermodynamic results of CGTPHC from two methods (a) Assumed compressor efficiency method (b) Predicted compressor efficiency using 1D mean line design method.

Thermodynamic analysis with assumed turbomachinery efficiency		Thermodynamic analysis coupled with compressor and turbine design code
$\eta_c$	80%	81.2% (Calculated from compressor design code)
$\eta_t$	90%	86.17% (Calculated from 1D turbine design code)
$\eta_{I,combined}$	46.8%	46.27%
$\eta_{II,combined}$	64.8%	64.3%
$\eta_{I,bottoming}$	23.8%	22.7%
$\eta_{II,bottoming}$	57%	55.8%

# Chapter 6

## Conclusion and Recommendations

Waste heat recovery is one of the alternatives for increasing the energy efficiency of the power cycles and sustaining the future energy demands. In this thesis, supercritical carbon dioxide power cycles are employed as bottoming cycles to recover the waste heat from topping gas turbine cycle and utilize it effectively to produce more power. Three combined cycle configurations which comprises of topping gas turbine cycle and bottoming sCO<sub>2</sub> Brayton cycle are evaluated using thermodynamic analysis, size and environmental impact. The thermodynamic analysis (energy and exergy analysis) and optimization of the combined cycles are carried out using Genetic method available in Engineering Equation Solver (EES) to find the optimum point at which the power production as well as the exergetic efficiency are maximum.

The performances of the combined cycles are compared with performance of simple gas turbine cycle and the conventional air bottoming combined cycle (ABC). The energy and exergy efficiency of the combined and bottoming sCO<sub>2</sub> cycles, size and mass flow rate and savings in exhaust emissions as a result of waste heat recovery are considered as the key measures during comparison for selecting the optimum combined cycle. It is found that, CGT-sCO<sub>2</sub> cycles performed better than ABC

and simple gas turbine cycle (SGT). Moreover, the optimum combined cycle having maximum exergetic efficiency and environmental advantage is CGTPHC. The energy and exergy efficiency of the CGTPHC are 46.8% and 64.8%, respectively.

After thermodynamic analysis and comparison, this study focused on design of turbomachinery for optimum bottoming sCO<sub>2</sub> cycle using preliminary and 1D mean line design methodologies. The design is divided into three phases: 1) Selection of type of turbomachinery, 2) Preliminary design to compute the stages, revolution speed and impeller tip diameter of the turbomachinery and 3) 1D mean line design for calculating the complete geometry and performance of the turbomachinery. The objective in turbomachinery design is to determine the geometry, stages and efficiency of the compressor and the turbine based on internal and external losses associated with the turbomachinery. The design calculations are performed in MATLAB combined with REFPROP fluid property library in order to get thermodynamic data of sCO<sub>2</sub> at each stage. In addition, turbomachinery design code is coupled with thermodynamic analysis calculations to determine the updated cycle performance. The compressor design code is also validated with experimental results and reasons of deviation is also discussed.

The thermodynamic analysis and turbomachinery design code developed in this study are robust and adaptive that is, they can be applied to other heat sources and operating environment like geothermal, biomass and solar energy sources.

On the basis of theoretical analysis and comparison with conventional power systems, the supercritical CO<sub>2</sub> power cycles proves to be a promising technology for waste heat recovery applications. However, the analysis and design codes can be made more realistic if following steps are taken:

1. The integrated performance analysis code should be developed which incorporate the design and sizing of turbomachinery, regenerators, recuperators and piping system for sCO<sub>2</sub> power cycles.

2. The theoretical design codes should investigate the response of the cycles in off-design conditions. Data-driven mathematical models can also be implemented to forecast the performance of the supercritical CO<sub>2</sub> cycles.
3. Life cycle cost analysis should be done which can further clarify the details on economics of this power system.
4. With the advancement of state-of-the-art turbomachinery and heat exchangers, experimental testing loop of large scale (i.e.,  $\approx 40$  MW) should be established which will help in validation and improvement of the design codes. Some of the small-scale test loops under consideration are developed by various institutes and companies [92, 93]. For large capacity testing loops, there are challenges like material selection, improvements in design of bearing and seals and innovations required in structure design of heat exchangers.

# Bibliography

- [1] A. Poullikkas, “An overview of current and future sustainable gas turbine technologies,” *Renewable and Sustainable Energy Reviews*, vol. 9, no. 5, pp. 409–443, 2005.
- [2] A. Polyzakis, C. Koroneos, and G. Xydis, “Optimum gas turbine cycle for combined cycle power plant,” *Energy Conversion and Management*, vol. 49, no. 4, pp. 551–563, 2008.
- [3] A. Poullikkas, “Parametric study for the penetration of combined cycle technologies into cyprus power system,” *Applied Thermal Engineering*, vol. 24, no. 11-12, pp. 1697–1707, 2004.
- [4] M. Ghazikhani, I. Khazaei, and E. Abdekhodaie, “Exergy analysis of gas turbine with air bottoming cycle,” *Energy*, vol. 72, pp. 599–607, 2014.
- [5] M. Korobitsyn, “Industrial applications of the air bottoming cycle,” *Energy Conversion and Management*, vol. 43, no. 9-12, pp. 1311–1322, 2002.
- [6] M. A. Korobitsyn and M. A. Korobitsyn, “New and advanced conversion technologies: Analysis of cogeneration, combined and integrated cycles,” 1998.
- [7] W. M. Farrell, “Air cycle thermodynamic conversion system,” Jun. 21 1988, uS Patent 4,751,814.
- [8] Y. S. Najjar and M. S. Zaamout, “Performance analysis of gas turbine air-bottoming combined system,” *Energy Conversion and Management*, vol. 37, no. 4, pp. 399–403, 1996.

- 
- [9] M. Ghazikhani, I. Khazaei, and E. Abdekhodaie, “Exergy analysis of gas turbine with air bottoming cycle,” *Energy*, vol. 72, pp. 599–607, 2014.
- [10] M. Saghaffar and A. Poullikkas, “Thermo-economic optimization of air bottoming cycles,” *Journal of power technologies*, vol. 95, 2015.
- [11] A. Alklaibi, M. Khan, and W. Khan, “Thermodynamic analysis of gas turbine with air bottoming cycle,” *Energy*, vol. 107, pp. 603–611, 2016.
- [12] O. Bolland, M. Forde, and B. Hande, “Air bottoming cycle: use of gas turbine waste heat for power generation,” *Journal of Engineering for Gas Turbines and Power*, vol. 118, no. 2, pp. 359–368, 1996.
- [13] A. Ayub, N. Sheikh, R. Tariq, and M. Khan, “Thermodynamic optimization of air bottoming cycle for waste heat recovery,” in *2<sup>nd</sup> International Conference on Energy Systems for Sustainable Development (ESSD-2018)*, 2018, pp. 59–62.
- [14] M. Astolfi, M. C. Romano, P. Bombarda, and E. Macchi, “Binary ORC (organic rankine cycles) power plants for the exploitation of medium–low temperature geothermal sources—Part A: Thermodynamic optimization,” *Energy*, vol. 66, pp. 423–434, 2014.
- [15] Y. Chen, P. Lundqvist, A. Johansson, and P. Platell, “A comparative study of the carbon dioxide transcritical power cycle compared with an organic Rankine cycle with R123 as working fluid in waste heat recovery,” *Applied Thermal Engineering*, vol. 26, no. 17–18, pp. 2142–2147, 2006.
- [16] H. Yagli, A. Koc, C. Karakus, and Y. Koc, “Comparison of toluene and cyclohexane as a working fluid of an organic rankine cycle used for reheat furnace waste heat recovery,” *International Journal of Exergy*, vol. 19, no. 3, pp. 420–438, 2016.
- [17] M. Yari and S. Mahmoudi, “A thermodynamic study of waste heat recovery from GT-MHR using organic Rankine cycles,” *Heat and Mass Transfer*, vol. 47, no. 2, pp. 181–196, 2011.

- [18] N. Shokati, F. Mohammadkhani, M. Yari, S. Mahmoudi, and M. A. Rosen, “A comparative exergoeconomic analysis of waste heat recovery from a gas turbine-modular helium reactor via organic Rankine cycles,” *Sustainability*, vol. 6, no. 5, pp. 2474–2489, 2014.
- [19] J. Roy, M. Mishra, and A. Misra, “Performance analysis of an Organic Rankine Cycle with superheating under different heat source temperature conditions,” *Applied Energy*, vol. 88, no. 9, pp. 2995–3004, 2011.
- [20] A. Algieri and P. Morrone, “Comparative energetic analysis of high-temperature subcritical and transcritical Organic Rankine Cycle (ORC). A biomass application in the Sibari district,” *Applied Thermal Engineering*, vol. 36, pp. 236–244, 2012.
- [21] H. Yağlı, Y. Koç, A. Koç, A. Görgülü, and A. Tandiroğlu, “Parametric optimization and exergetic analysis comparison of subcritical and supercritical organic Rankine cycle (ORC) for biogas fuelled combined heat and power (CHP) engine exhaust gas waste heat,” *Energy*, vol. 111, pp. 923–932, 2016.
- [22] H. Chen, D. Y. Goswami, and E. K. Stefanakos, “A review of thermodynamic cycles and working fluids for the conversion of low-grade heat,” *Renewable and Sustainable Energy Reviews*, vol. 14, no. 9, pp. 3059–3067, 2010.
- [23] B.-T. Liu, K.-H. Chien, and C.-C. Wang, “Effect of working fluids on organic Rankine cycle for waste heat recovery,” *Energy*, vol. 29, no. 8, pp. 1207–1217, 2004.
- [24] E. Lemmon, M. Huber, and M. McLinden, “NIST standard reference database 23: Reference fluid thermodynamic and transport properties-REFPROP, Version 9.1, National Institute of Standards and Technology, Standard Reference Data Program, Gaithersburg,” See <http://www.nist.gov/srd/nist23.cfm>, 2013.
- [25] J. M. Calm and G. C. Hourahan, “Refrigerant data summary,” *Engineered Systems*, vol. 18, no. 11, pp. 74–77, 2001.

- [26] V. Dostal, M. Driscoll, and P. Hejzlar, “A supercritical carbon dioxide cycle for next generation nuclear reactors. Massachusetts Institute of Technology, MA 2004,” Ph.D. dissertation, PhD Thesis.
- [27] H. Yamaguchi, X. Zhang, K. Fujima, M. Enomoto, and N. Sawada, “Solar energy powered rankine cycle using supercritical CO<sub>2</sub>,” *Applied Thermal Engineering*, vol. 26, no. 17-18, pp. 2345–2354, 2006.
- [28] Y. Ahn, S. J. Bae, M. Kim, S. K. Cho, S. Baik, J. I. Lee, and J. E. Cha, “Review of supercritical CO<sub>2</sub> power cycle technology and current status of research and development,” *Nuclear Engineering and Technology*, vol. 47, no. 6, pp. 647–661, 2015.
- [29] G. Sulzer, “Process for generating work from heat (in swiss),” *Swiss Patent CH269599*, vol. 15, 1950.
- [30] E. G. Feher, “The supercritical thermodynamic power cycle,” *Energy conversion*, vol. 8, no. 2, pp. 85–90, 1968.
- [31] S. F. M. H. H. L. A. Werner, G. Klemencic, “Comparison of conventional and CO<sub>2</sub> power generation cycles for waste heat recovery,” in *5th International Symposium, Supercritical CO<sub>2</sub> Power Cycles*, 2016, pp. 1–15.
- [32] M. Kulhanek and V. Dostal, “Supercritical carbon dioxide cycles thermodynamic analysis and comparison,” in *Supercritical CO<sub>2</sub> Power Cycle Symposium, Boulder, CO, May*, 2011, pp. 24–25.
- [33] —, “Thermodynamic analysis and comparison of supercritical carbon dioxide cycles,” in *Proceedings of Supercritical CO<sub>2</sub> Power Cycle Symposium*, 2011, pp. 24–25.
- [34] S. J. Bae, J. Lee, Y. Ahn, and J. I. Lee, “Preliminary studies of compact Brayton cycle performance for small modular high temperature gas-cooled reactor system,” *Annals of Nuclear Energy*, vol. 75, pp. 11–19, 2015.

- [35] H. J. Yoon, Y. Ahn, J. I. Lee, and Y. Addad, "Potential advantages of coupling supercritical CO<sub>2</sub> Brayton cycle to water cooled small and medium size reactor," *Nuclear Engineering and Design*, vol. 245, pp. 223–232, 2012.
- [36] G. Angelino, "Carbon dioxide condensation cycles for power production," *Journal of Engineering for Power*, vol. 90, no. 3, pp. 287–295, 1968.
- [37] F. A. Al-Sulaiman and M. Atif, "Performance comparison of different supercritical carbon dioxide Brayton cycles integrated with a solar power tower," *Energy*, vol. 82, pp. 61–71, 2015.
- [38] Y. H. Ahn, S. J. Bae, M. S. Kim, S. K. Cho, S. J. Baik, J. I. Lee, and J. E. Cha, "Cycle layout studies of S-CO<sub>2</sub> cycle for the next generation nuclear system application," in *The Korean Nuclear Society Autumn Meeting (2014)*. The Korean Nuclear Society, 2014.
- [39] J. Sarkar and S. Bhattacharyya, "Optimization of recompression S-CO<sub>2</sub> power cycle with reheating," *Energy Conversion and Management*, vol. 50, no. 8, pp. 1939–1945, 2009.
- [40] J. Sarkar, "Second law analysis of supercritical CO<sub>2</sub> recompression Brayton cycle," *Energy*, vol. 34, no. 9, pp. 1172–1178, 2009.
- [41] A. D. Akbari and S. M. Mahmoudi, "Thermoeconomic analysis & optimization of the combined supercritical CO<sub>2</sub> (carbon dioxide) recompression Brayton/organic Rankine cycle," *Energy*, vol. 78, pp. 501–512, 2014.
- [42] M. Reyes-Belmonte, A. Sebastián, M. Romero, and J. González-Aguilar, "Optimization of a recompression supercritical carbon dioxide cycle for an innovative central receiver solar power plant," *Energy*, vol. 112, pp. 17–27, 2016.
- [43] X. Wang, Q. Liu, Z. Bai, J. Lei, and H. Jin, "Thermodynamic analysis of the cascaded supercritical CO<sub>2</sub> cycle integrated with solar and biomass energy," *Energy Procedia*, vol. 105, pp. 445–452, 2017.

- [44] D. V. Di Maio, A. Boccitto, and G. Caruso, "Supercritical carbon dioxide applications for energy conversion systems," *Energy Procedia*, vol. 82, pp. 819–824, 2015.
- [45] M. Wang, P. Zhao, J. Wang, H. Li, and Y. Dai, "Conceptual design and parametric study of combined carbon dioxide/organic Rankine cycles," *Applied Thermal Engineering*, vol. 103, pp. 759–772, 2016.
- [46] M. S. Kim, Y. Ahn, B. Kim, and J. I. Lee, "Study on the supercritical CO<sub>2</sub> power cycles for landfill gas firing gas turbine bottoming cycle," *Energy*, vol. 111, pp. 893–909, 2016.
- [47] M. Mohagheghi and J. Kapat, "Thermodynamic optimization of recuperated S-CO<sub>2</sub> Brayton cycles for waste heat recovery applications," in *4<sup>th</sup> International Supercritical CO<sub>2</sub> Power Cycles Symposium*, 2014.
- [48] S. Wright, C. Davidson, and W. Scammell, "Thermo-economic analysis of four S-CO<sub>2</sub> waste heat recovery power systems," in *Fifth International S-CO<sub>2</sub> Symposium, San Antonio, TX, Mar, 2016*, pp. 28–31.
- [49] M. Marchionni, G. Bianchi, K. M. Tsamos, and S. A. Tassou, "Techno-economic comparison of different cycle architectures for high temperature waste heat to power conversion systems using CO<sub>2</sub> in supercritical phase," *Energy Procedia*, vol. 123, pp. 305–312, 2017.
- [50] S. K. Cho, M. Kim, S. Baik, Y. Ahn, and J. I. Lee, "Investigation of the bottoming cycle for high efficiency combined cycle gas turbine system with supercritical carbon dioxide power cycle," in *ASME Turbo Expo 2015: Turbine Technical Conference and Exposition*. American Society of Mechanical Engineers, 2015, pp. V009T36A011–V009T36A011.
- [51] G. Kimzey, "Development of a Brayton bottoming cycle using supercritical carbon dioxide as the working fluid," *Electric Power Research Institute, University Turbine Systems Research Program, Gas Turbine Industrial Fellowship, Palo Alto, CA*, 2012.

- [52] S. A. Wright, R. F. Radel, M. E. Vernon, G. E. Rochau, and P. S. Pickard, "Operation and analysis of a supercritical CO<sub>2</sub> Brayton cycle," *Sandia Report*, No. SAND2010-0171, 2010.
- [53] T. Conboy, S. Wright, J. Pasch, D. Fleming, G. Rochau, and R. Fuller, "Performance characteristics of an operating supercritical CO<sub>2</sub> Brayton cycle," in *ASME Turbo Expo 2012: Turbine Technical Conference and Exposition*. American Society of Mechanical Engineers, 2012, pp. 941–952.
- [54] M. Persichilli, A. Kacludis, E. Zdankiewicz, and T. Held, "Supercritical CO<sub>2</sub> power cycle developments and commercialization: why S-CO<sub>2</sub> can displace steam ste," *Power-Gen India & Central Asia*, 2012.
- [55] N. Holaind, G. Bianchi, M. De Miol, S. S. Saravi, S. A. Tassou, A. Leroux, and H. Jouhara, "Design of radial turbomachinery for supercritical CO<sub>2</sub> systems using theoretical and numerical CFD methodologies," *Energy Procedia*, vol. 123, pp. 313–320, 2017.
- [56] J. Y. Lee, J. I. Lee, Y. H. Ahn, S. G. Kim, and J. E. Cha, "Conceptual design of supercritical CO<sub>2</sub> Brayton cycle radial turbomachinery for SMART application," 2012.
- [57] S. Banik, S. Ray, and S. De, "Thermodynamic modelling of a recompression CO<sub>2</sub> power cycle for low temperature waste heat recovery," *Applied Thermal Engineering*, vol. 107, pp. 441–452, 2016.
- [58] M. Marchionni, G. Bianchi, and S. A. Tassou, "Techno-economic assessment of Joule-Brayton cycle architectures for heat to power conversion from high-grade heat sources using CO<sub>2</sub> in the supercritical state," *Energy*, vol. 148, pp. 1140–1152, 2018.
- [59] S. Hou, Y. Zhou, L. Yu, F. Zhang, and S. Cao, "Optimization of the combined supercritical CO<sub>2</sub> cycle and organic Rankine cycle using zeotropic mixtures for gas turbine waste heat recovery," *Energy Conversion and Management*, vol. 160, pp. 313–325, 2018.

- [60] S. Hou, S. Cao, L. Yu, Y. Zhou, Y. Wu, and F. Zhang, "Performance optimization of combined supercritical CO<sub>2</sub> recompression cycle and regenerative organic Rankine cycle using zeotropic mixture fluid," *Energy Conversion and Management*, vol. 166, pp. 187–200, 2018.
- [61] Y. Zhang, H. Li, W. Han, W. Bai, Y. Yang, M. Yao, and Y. Wang, "Improved design of supercritical CO<sub>2</sub> Brayton cycle for coal-fired power plant," *Energy*, vol. 155, pp. 1–14, 2018.
- [62] S. Park, J. Kim, M. Yoon, D. Rhim, and C. Yeom, "Thermodynamic and economic investigation of coal-fired power plant combined with various supercritical CO<sub>2</sub> Brayton power cycle," *Applied Thermal Engineering*, vol. 130, pp. 611–623, 2018.
- [63] K. Manjunath, O. Sharma, S. Tyagi, and S. Kaushik, "Thermodynamic analysis of a supercritical/transcritical CO<sub>2</sub> based waste heat recovery cycle for shipboard power and cooling applications," *Energy Conversion and Management*, vol. 155, pp. 262–275, 2018.
- [64] J. Lee, J. I. Lee, H. J. Yoon, and J. E. Cha, "Supercritical carbon dioxide turbomachinery design for water-cooled small modular reactor application," *Nuclear Engineering and Design*, vol. 270, pp. 76–89, 2014.
- [65] S. Spazzoli, "Supercritical CO<sub>2</sub> power cycle for solar applications thermodynamic analysis and 1D turbo-machinery design," *MS-Thesis, Faculty of Mechanical, Maritime and Materials Engineering*, pp. 1–115, 2016.
- [66] Z. Liu, W. Luo, Q. Zhao, W. Zhao, and J. Xu, "Preliminary design and model assessment of a supercritical CO<sub>2</sub> compressor," *Applied Sciences*, vol. 8, no. 4, p. 595, 2018.
- [67] M. M. A. Khadse, L. Blanchette and J. Kapat, "Impact of S-CO<sub>2</sub> properties on centrifugal compressor impeller: Comparison of two loss models for mean line analyses," in *5<sup>th</sup> International Symposium, Supercritical CO<sub>2</sub> Power Cycles*, 2016, pp. 1–20.

- [68] J. Lee, J. I. Lee, Y. Ahn, and H. Yoon, "Design methodology of supercritical CO<sub>2</sub> Brayton cycle turbomachineries," in *ASME Turbo Expo 2012: Turbine Technical Conference and Exposition*. American Society of Mechanical Engineers, 2012, pp. 975–983.
- [69] S. S. Sanghera, "Centrifugal compressor meanline design using real gas properties," *Department of Mechanical and Aerospace Engineering*, pp. 1–37, 2013.
- [70] H. W. Oh, E. S. Yoon, and M. Chung, "An optimum set of loss models for performance prediction of centrifugal compressors," *Proceedings of the Institution of Mechanical Engineers, Part A: Journal of Power and Energy*, vol. 211, no. 4, pp. 331–338, 1997.
- [71] B. Monje, D. Sánchez, M. Savill, P. Pilidis, and T. Sánchez, "A design strategy for supercritical CO<sub>2</sub> compressors," in *ASME Turbo Expo 2014: Turbine Technical Conference and Exposition*. American Society of Mechanical Engineers, 2014, pp. V03BT36A003–V03BT36A003.
- [72] R. Span and W. Wagner, "A new equation of state for carbon dioxide covering the fluid region from the triple-point temperature to 1100 K at pressures up to 800 MPa," *Journal of Physical and Chemical Reference Data*, vol. 25, no. 6, pp. 1509–1596, 1996.
- [73] X. Zhang, L. Wu, X. Wang, and G. Ju, "Comparative study of waste heat steam SRC, ORC and S-ORC power generation systems in medium-low temperature," *Applied Thermal Engineering*, vol. 106, pp. 1427–1439, 2016.
- [74] N. M. Jubeh, "Exergy analysis and second law efficiency of a regenerative Brayton cycle with isothermal heat addition," *Entropy*, vol. 7, no. 3, pp. 172–187, 2005.
- [75] K. Brun, P. Friedman, and R. Dennis, *Fundamentals and applications of supercritical carbon dioxide (S-CO<sub>2</sub>) based power cycles*. Woodhead publishing, 2017.

- [76] T. L. Bergman, F. P. Incropera, D. P. DeWitt, and A. S. Lavine, *Fundamentals of heat and mass transfer*. John Wiley & Sons, 2011.
- [77] S. M. Bina, S. Jalilinasrabad, and H. Fujii, “Energy, economic and environmental (3E) aspects of internal heat exchanger for ORC geothermal power plants,” *Energy*, vol. 140, pp. 1096–1106, 2017.
- [78] “U.S. energy information administration, independent statistics & analysis.”
- [79] D. Fleming, T. Holschuh, T. Conboy, G. Rochau, and R. Fuller, “Scaling considerations for a multi-megawatt class supercritical CO<sub>2</sub> Brayton cycle and path forward for commercialization,” in *ASME Turbo Expo 2012: Turbine Technical Conference and Exposition*. American Society of Mechanical Engineers, 2012, pp. 953–960.
- [80] Y. Gong, N. Carstens, M. Driscoll, and I. Matthews, “Analysis of radial compressor options for supercritical CO<sub>2</sub> power conversion cycles,” *Center for Advanced Nuclear Energy Systems, MIT Department of Nuclear Science and Engineering: Cambridge, MA, USA*, 2006.
- [81] O. Balje, *Turbomachines-A guide to design, selection, and theory*. John Wiley & Sons, 1981, no. Book.
- [82] E. Kenneth and P. Nichols, “How to select turbomachinery for your application,” *Barber-Nichols Inc*, pp. 5–6, 2012.
- [83] O. Conrad, K. Raif, and M. Wessels, “The calculation of performance maps for centrifugal compressors with vane-island diffusers,” in *Performance Prediction of Centrifugal Pumps and Compressors*, 1979, pp. 135–147.
- [84] J. Coppage and F. Dallenbach, “Study of supersonic radial compressors for refrigeration and pressurization systems,” Sarrett Corp Los Angeles CA Airesearch MFG Div, Tech. Rep., 1956.
- [85] W. Jansen, “A method for calculating the flow in a centrifugal impeller when entropy gradient are present,” *Inst. Mech. Eng. Internal Aerodynamics*, 1970.

- [86] H. W. Oh, "Investigation on the design and performance analysis methods of centrifugal turbomachines, Doctoral Thesis," 1999.
- [87] J. W. Daily and R. E. Nece, "Chamber dimension effects on induced flow and frictional resistance of enclosed rotating disks," *Journal of Basic Engineering*, vol. 82, no. 1, pp. 217–230, 1960.
- [88] J. Johnston and R. Dean, "Losses in vaneless diffusers of centrifugal compressors and pumps: Analysis, experiment, and design," *Journal of Engineering for Power*, vol. 88, no. 1, pp. 49–60, 1966.
- [89] S. Lieblein, F. C. Schwenk, and R. L. Broderick, "Diffusion factor for estimating losses and limiting blade loadings in axial-flow-compressor blade elements," National Advisory Committee for Aeronautics Cleveland OH Lewis Flight Propulsion Lab, Tech. Rep., 1953.
- [90] K. Rahbar, S. Mahmoud, and R. K. Al-Dadah, "Mean-line modeling and CFD analysis of a miniature radial turbine for distributed power generation systems," *International Journal of Low-Carbon Technologies*, vol. 11, no. 2, pp. 157–168, 2016.
- [91] H.-C. Jung and S. Krumdieck, "Meanline design of a 250 kW radial inflow turbine stage using R245fa working fluid and waste heat from a refinery process," *Proceedings of the Institution of Mechanical Engineers, Part A: Journal of Power and Energy*, vol. 230, no. 4, pp. 402–414, 2016.
- [92] S. A. Wright, T. M. Conboy, E. J. Parma, T. G. Lewis, and A. J. Suo-Anttila, "Summary of the sandia supercritical CO<sub>2</sub> development program." Sandia National Lab.(SNL-NM), Albuquerque, NM (United States), Tech. Rep., 2011.
- [93] M.-J. Li, H.-H. Zhu, J.-Q. Guo, K. Wang, and W.-Q. Tao, "The development technology and applications of supercritical CO<sub>2</sub> power cycle in nuclear energy, solar energy and other energy industries," *Applied Thermal Engineering*, vol. 126, pp. 255–275, 2017.

# EES Code for CGTREC

\$REFERENCE CarbonDioxide IIR

FUNCTION Cmin(C\_b,C\_exh)

IF(C\_exh>C\_b) THEN C\_min = C\_b ELSE C\_min = C\_exh ENDIF

Cmin:=C\_min END

FUNCTION Tfive(T\_1, P\_1, P\_2,m\_dot, eff\_comp1, eff\_comp2, eff\_turb, eff\_htr,  
eff\_ltr, eff\_regen,T\_4t, C\_exh, x\_max,m\_dot\_ta)

“Initial Guess”

T\_5:= 700

REPEAT

h\_5:= ENTHALPY(CarbonDioxide,T=T\_5,P=P\_2)

“Finding h\_1 and h\_2, First Compression Process”

h\_1:= ENTHALPY(CarbonDioxide,T=T\_1,P=P\_1)

s\_1:= ENTROPY(CarbonDioxide,T=T\_1,P=P\_1)

s\_2: = s\_1

h\_2a:= ENTHALPY(CarbonDioxide,s=s\_2,P=P\_2)

h\_2: = ((h\_2a - h\_1) / eff\_comp1 ) + h\_1

T\_2:=Temperature(CarbonDioxide,h=h\_2,P=P\_2)

“Integrated Heat Exchanger”

$$h_{4t} := \text{Enthalpy}(\text{Air}, T = T_{4t})$$

$$C_{b.} := (\text{Cp}(\text{CarbonDioxide}, T = T_{.5}, P = P_{.2})) * m_{\text{dot}}$$

$$C_{\text{min}} := \text{Cmin}(C_{b.}, C_{\text{exh}})$$

$$T_{.3} := (\text{eff}_{\text{regen}} * (C_{\text{min}} / C_{b.}) * (T_{4t} - T_{.5})) + T_{.5}$$

$$h_{.3} := \text{ENTHALPY}(\text{CarbonDioxide}, T = T_{.3}, P = P_{.2})$$

$$Q1 := m_{\text{dot}} * (h_{.3} - h_{.5})$$

“Finding  $h_{.4}$ , Expansion Process”

$$s_{.3} := \text{Entropy}(\text{CarbonDioxide}, h = h_{.3}, P = P_{.2})$$

$$s_{.4} := s_{.3}$$

$$h_{4a} := \text{Enthalpy}(\text{CarbonDioxide}, s = s_{.4}, P = P_{.1})$$

$$h_{.4} := h_{.3} - (\text{eff}_{\text{turb}} * (h_{.3} - h_{4a}))$$

$$T_{.4} := \text{Temperature}(\text{CarbonDioxide}, h = h_{.4}, P = P_{.1})$$

“Finding  $h_{.8}$  and  $h_{.9}$ , High temperature recuperation process”

$$h_{.8} := (h_{.5} - (h_{.4} * \text{eff}_{\text{htr}})) / (1 - \text{eff}_{\text{htr}})$$

$$h_{.9} := h_{.4} - h_{.5} + h_{.8}$$

$$T_{.9} := \text{Temperature}(\text{CarbonDioxide}, h = h_{.9}, P = P_{.1})$$

“Finding  $h_{.7}$  and  $h_{.6}$ , Low temperature recuperation process”

$$C_{b.9} := (\text{Cp}(\text{CarbonDioxide}, h = h_{.9}, P = P_{.1})) * m_{\text{dot}}$$

$$C_{b.2} := (\text{Cp}(\text{CarbonDioxide}, h = h_{.2}, P = P_{.2})) * m_{\text{dot}} * x_{\text{max}}$$

$$C_{\text{min.ltr}} := \text{Cmin}(C_{b.9}, C_{b.2})$$

$$h_{.7} := (\text{eff}_{\text{ltr}} * ((C_{\text{min.ltr}} / m_{\text{dot}}) * (T_{.9} - T_{.2}))) + h_{.2}$$

---

```

h_6:= h_9 - (x_max * (h_7 - h_2))

“Finding h_10, Second Compression process”

s_6:= ENTROPY(CarbonDioxide,h=h_6,P=P_1)

s_10:= s_6

h_10a:=Enthalpy(CarbonDioxide,s=s_10,P=P_2)

h_10:= ((h_10a - h_6) +(h_6* eff.comp2)) / (eff.comp2)

“Finding h_8, Mixing process”

h_8_new:= ((1- x_max) * h_10) + (x_max * h_7)

h_5_new:= h_4 - h_9 + h_8_new

T_5_new:=Temperature(CarbonDioxide,h=h_5_new,P=P_2)

C_b_new:=(Cp(CarbonDioxide,T=T_5_new,P=P_2)) * m_dot

C_min_new:= Cmin(C_b_new,C_exh)

T_3_new:= (eff.regen * (C_min_new/C_b_new) * (T_4t - T_5_new)) + T_5_new

h_3_new:= ENTHALPY(CarbonDioxide,T=T_3_new,P=P_2)

Q1_new:= m_dot * (h_3_new - h_5_new)

Error:= abs((Q1_new - Q1)/Q1_new)

T_5:= T_5_new

UNTIL(Error<0.0001)

Tfive:=T_5

END

“Base INPUT Parameters”

T_1 = 304.25[K]

```

$$P_{.1} = 7.4[\text{MPa}]$$

$$r_{.c} = 2.5$$

$$P_{.2} = r_{.c} * P_{.1}$$

$$\text{eff}_{\text{comp1}} = 0.80$$

$$\text{eff}_{\text{comp2}} = 0.80$$

$$m_{\text{dot}_{\text{ta}}} = 105[\text{kg/s}]$$

$$\text{MFRR} = 1.6 \text{ Input parameter}$$

$$m_{\text{dot}} = \text{MFRR} * m_{\text{dot}_{\text{ta}}}$$

$$\text{"eff}_{\text{turb}} = 0.90\text{"}$$

$$\text{eff}_{\text{htr}} = 0.85$$

$$\text{eff}_{\text{ltr}} = 0.7$$

$$\text{"x}_{\text{max}} = 0.55\text{" Input parameter}$$

$$\text{eff}_{\text{regen}} = 0.85$$

$$C_{\text{exh}} = 117.2$$

$$C_{\text{p}_{\text{exh}}} = 1.116$$

$$T_{.4t} = 880 [\text{K}]$$

$$m_{\text{dot}_{\text{g}}} = 107.1[\text{kg/s}]$$

$$P_{.4t} = 0.101325 [\text{MPa}]$$

“CALCULATIONS”

$$h_{.4t} = \text{Enthalpy}(\text{Air}, T = T_{.4t})$$

$$T_{.5_{\text{corr}}} = \text{Tfive}(T_{.1}, P_{.1}, P_{.2}, m_{\text{dot}}, \text{eff}_{\text{comp1}}, \text{eff}_{\text{comp2}}, \text{eff}_{\text{turb}}, \text{eff}_{\text{htr}}, \text{eff}_{\text{ltr}}, \text{eff}_{\text{regen}}, T_{.4t}, C_{\text{exh}}, x_{\text{max}}, m_{\text{dot}_{\text{ta}}})$$

$$h_{.5} = \text{ENTHALPY}(\text{CarbonDioxide}, T=T_{.5\_corr}, P=P_{.2})$$

$$s_{.5} = \text{ENTROPY}(\text{CarbonDioxide}, T=T_{.5\_corr}, P=P_{.2})$$

$$s_{.4t} = \text{ENTROPY}(\text{Air}, T=T_{.4t}, P=P_{.4t})$$

“ExhaustOUT”

$$C_{p.b} = (\text{Cp}(\text{CarbonDioxide}, T=T_{.5\_corr}, P=P_{.2}))$$

$$C_{.b} = (C_{p.b} * m_{.dot})$$

$$C_{.min} = \text{Cmin}(C_{.b}, C_{.exh})$$

$$“T_{.5t} = T_{.4t} - (\text{eff\_regen} * (C_{.min}/C_{.exh}) * (T_{.4t} - T_{.5\_corr}))”$$

$$s_{.5t} = \text{ENTROPY}(\text{Air}, T=T_{.5t}, P=P_{.4t})$$

$$h_{.5t} = h_{.4t} - (\text{eff\_regen} * ((C_{.min}/m_{.dot\_g}) * (T_{.4t} - T_{.5\_corr})))$$

$$“h_{.5t} = \text{Enthalpy}(\text{Air}, T=T_{.5t})”$$

$$T_{.5t} = \text{Temperature}(\text{Air}, h=h_{.5t})$$

“Finding  $h_{.1}$  and  $h_{.2}$ , First Compression Process”

$$h_{.1} = \text{ENTHALPY}(\text{CarbonDioxide}, T=T_{.1}, P=P_{.1})$$

$$s_{.1} = \text{ENTROPY}(\text{CarbonDioxide}, T=T_{.1}, P=P_{.1})$$

$$s_{.2} = s_{.1}$$

$$h_{.2a} = \text{ENTHALPY}(\text{CarbonDioxide}, s=s_{.2}, P=P_{.2})$$

$$h_{.2} = ((h_{.2a} - h_{.1}) / \text{eff\_comp1}) + h_{.1}$$

$$T_{.2} = \text{Temperature}(\text{CarbonDioxide}, h=h_{.2}, P=P_{.2})$$

$$s_{.2a} = \text{Entropy}(\text{CarbonDioxide}, h=h_{.2}, P=P_{.2})$$

$$\rho_{.1} = \text{Density}(\text{CarbonDioxide}, T=T_{.1}, P=P_{.1})$$

$$\rho_{.2} = \text{Density}(\text{CarbonDioxide}, T=T_{.2}, P=P_{.2})$$

“Integrated Heat Exchanger”

$$T_{.3} = (\text{eff\_regen} * (C_{\text{min}}/C_{\text{b}}) * (T_{.4t} - T_{.5\_corr})) + T_{.5\_corr}$$

$$h_{.3} = \text{ENTHALPY}(\text{CarbonDioxide}, T=T_{.3}, P=P_{.2})$$

$$Q_{\text{absorbed}} = m_{\text{dot}} * (h_{.3} - h_{.5})$$

$$Cp_{.b2} = (Cp(\text{CarbonDioxide}, T=T_{.3}, P=P_{.2}))$$

$$Cp_{\text{avg}} = (Cp_{\text{.b}} + Cp_{.b2}) / 2$$

“Finding h<sub>.4</sub>, Expansion Process”

$$s_{.3} = \text{Entropy}(\text{CarbonDioxide}, h=h_{.3}, P=P_{.2})$$

$$s_{.4} = s_{.3}$$

$$h_{.4a} = \text{Enthalpy}(\text{CarbonDioxide}, s=s_{.4}, P=P_{.1})$$

$$h_{.4} = h_{.3} - (\text{eff\_turb} * (h_{.3} - h_{.4a}))$$

$$T_{.4} = \text{Temperature}(\text{CarbonDioxide}, h=h_{.4}, P=P_{.1})$$

$$s_{.4a} = \text{Entropy}(\text{CarbonDioxide}, h=h_{.4}, P=P_{.1})$$

$$\rho_{.3} = \text{Density}(\text{CarbonDioxide}, T=T_{.3}, P=P_{.2})$$

$$\rho_{.4} = \text{Density}(\text{CarbonDioxide}, T=T_{.4}, P=P_{.1})$$

“Finding h<sub>.8</sub> and h<sub>.9</sub>, High temperature recuperation process”

$$h_{.8} = (h_{.5} - (h_{.4} * \text{eff\_htr})) / (1 - \text{eff\_htr})$$

$$T_{.8} = \text{Temperature}(\text{CarbonDioxide}, h=h_{.8}, P=P_{.2})$$

$$s_{.8} = \text{ENTROPY}(\text{CarbonDioxide}, h=h_{.8}, P=P_{.2})$$

$$h_{.9} = h_{.4} - h_{.5} + h_{.8}$$

$$T_{.9} = \text{Temperature}(\text{CarbonDioxide}, h=h_{.9}, P=P_{.1})$$

$$s_{.9} = \text{ENTROPY}(\text{CarbonDioxide}, h=h_{.9}, P=P_{.1})$$

“Finding h<sub>7</sub> and h<sub>6</sub>, Low temperature recuperation process”

$$C_{b_9} = (C_p(\text{CarbonDioxide}, h=h_9, P=P_1)) * m_{\text{dot}}$$

$$C_{b_2} = (C_p(\text{CarbonDioxide}, h=h_2, P=P_2)) * m_{\text{dot}} * x_{\text{max}}$$

$$C_{\text{min\_ltr}} = \text{Cmin}(C_{b_9}, C_{b_2})$$

$$h_7 = (\text{eff\_ltr} * ((C_{\text{min\_ltr}} / m_{\text{dot}}) * (T_9 - T_2))) + h_2$$

$$T_7 = \text{Temperature}(\text{CarbonDioxide}, h=h_7, P=P_2)$$

$$s_7 = \text{ENTROPY}(\text{CarbonDioxide}, h=h_7, P=P_2)$$

$$h_6 = h_9 - (x_{\text{max}} * (h_7 - h_2))$$

$$T_6 = \text{TEMPERATURE}(\text{CarbonDioxide}, h=h_6, P=P_1)$$

$$P_6 = \text{PHASE}(\text{CarbonDioxide}, T=T_6, P=P_1)$$

“Finding h<sub>10</sub>, Second Compression process”

$$s_6 = \text{ENTROPY}(\text{CarbonDioxide}, h=h_6, P=P_1)$$

$$s_{10} = s_6$$

$$h_{10a} = \text{Enthalpy}(\text{CarbonDioxide}, s=s_{10}, P=P_2)$$

$$h_{10} = ((h_{10a} - h_6) + (h_6 * \text{eff\_comp2})) / (\text{eff\_comp2})$$

$$T_{10} = \text{Temperature}(\text{CarbonDioxide}, h=h_{10}, P=P_2)$$

$$s_{10a} = \text{ENTROPY}(\text{CarbonDioxide}, h=h_{10}, P=P_2)$$

$$\rho_6 = \text{Density}(\text{CarbonDioxide}, T=T_6, P=P_1)$$

$$\rho_{10} = \text{Density}(\text{CarbonDioxide}, T=T_{10}, P=P_2)$$

“Q<sub>out</sub>”

$$Q_{\text{out}} = x_{\text{max}} * m_{\text{dot}} * (h_6 - h_1)$$

“Power Out and Efficiencies”

$$W_c = x_{\max} * m_{\dot{}} * (h_2 - h_1)$$

$$W_{c2} = (1 - x_{\max}) * m_{\dot{}} * (h_{10} - h_6)$$

$$W_{in,b} = W_c + W_{c2}$$

$$W_t = m_{\dot{}} * (h_3 - h_4)$$

$$W_{net,b} = W_t - W_c - W_{c2}$$

$$W_{net,t} = 35469[\text{kW}]$$

$$Q_{input} = 101130[\text{kW}]$$

$$Q_{recovery\_exh} = m_{\dot{}} * g * (h_{4t} - h_{5t})$$

$$W_{net,out} = W_{net,t} + W_{net,b}$$

$$\text{THERMALeff}_{combined} = ((W_{net,b} + W_{net,t}) / Q_{input}) * 100$$

$$\text{ThermEff}_b = (W_{net,b} / Q_{absorbed}) * 100$$

$$\text{ThermEff}_{b2} = (W_{net,b} / Q_{input}) * 100$$

$$\text{ThermEff}_t = (W_{net,t} / Q_{input}) * 100$$

$$\text{deltaT}_{cold} = T_3 - T_{5\_corr}$$

$$x = 1 - x_{\max}$$

“Cooling water in cooler”

$$m_w = 120[\text{kg/s}]$$

$$P_w = 0.101325 [\text{MPa}]$$

$$T_{w\_in} = 298[\text{K}]$$

$$h_{w\_in} = \text{Enthalpy}(\text{Water}, T = T_{w\_in}, P = P_w)$$

$$h_{w\_out} = h_{w\_in} + (Q_{out} / m_w)$$

$$T_{w\_out} = \text{Temperature}(\text{Water}, P = P_w, h = h_{w\_out})$$

$$sw\_in = \text{Entropy}(\text{Water}, T = T_{w\_in}, P = P_w)$$

$$sw\_out = \text{Entropy}(\text{Water}, h = h_{w\_out}, P = P_w)$$

“EXERGY ANALYSIS”

“TOPPING CYCLE”

$$s_{1t} = 5.712$$

$$h_{1t} = 303.4$$

$$Ed_{c1} = 2861[\text{kW}]$$

$$Ed_{t1} = 4193[\text{kW}]$$

$$Ed_{cc} = 7803 [\text{kW}]$$

“BOTTOMING CYCLE”

$$T_o = 298[\text{K}]$$

$$T_{1t} = 303.4[\text{K}]$$

$$T_{oair} = T_o$$

$$ExIN = 80904$$

$$ExINnet = (m_{\dot{g}} * (h_{4t} - h_{5t} - (T_{oair} * (s_{4t} - s_{5t}))))$$

$$ExINnetA = (m_{\dot{g}} * (h_3 - h_5 - (T_o * (s_3 - s_5))))$$

$$P_o = P_{4t}$$

$$h_o = \text{Enthalpy}(\text{Air}, T = T_{oair})$$

$$s_o = \text{ENTROPY}(\text{Air}, T = T_{oair}, P = P_o)$$

$$Exinput = m_{\dot{g}} * (((h_{4t} - h_o) - (T_o * (s_{4t} - s_o))))$$

$$Exout = m_{\dot{g}} * (((h_{5t} - h_o) - (T_o * (s_{5t} - s_o))))$$

$$E_{d\_T2} = (-W_t) + (m_{\dot{g}} * (h_3 - h_4 - (T_o * (s_3 - s_{4a}))))$$

$$E_{d\_T2a} = m_{dot} * ((T_o * (s_{4a} - s_3)))$$

$$E_{d\_c2} = (W_c) + (m_{dot} * (x_{max}) * (h_1 - h_2 - (T_o * (s_1 - s_{2a}))))$$

$$E_{d\_c2a} = m_{dot} * (x_{max}) * ((T_o * (s_{2a} - s_1))) \text{ Checking of two methods}$$

$$E_{d\_c3} = (W_{c2}) + (m_{dot} * (1 - x_{max}) * (h_6 - h_{10} - (T_o * (s_6 - s_{10a}))))$$

$$E_{d\_c3a} = m_{dot} * (1 - x_{max}) * ((T_o * (s_{10a} - s_6))) \text{ Checking of two methods}$$

$$E_{d\_IHX} = (m_{dot} * (h_5 - h_3 - (T_o * (s_5 - s_3)))) + ExINnet$$

$$E_{d\_IHXa} = (((m_{dot} * (s_3 - s_5)) + (m_{dot\_g} * (s_5 - s_4))) * T_o)$$

$$E_{d\_LTR} = (m_{dot} * (x_{max}) * ((h_2 - h_7) - (T_o * (s_2 - s_7)))) + (m_{dot} * ((h_9 - h_6) - (T_o * (s_9 - s_6))))$$

$$E_{d\_LTRa} = ((m_{dot} * x_{max} * (s_7 - s_2)) + (m_{dot} * (s_6 - s_9))) * T_o$$

$$E_{d\_HTR} = (m_{dot} * ((h_4 - h_9) - (T_o * (s_4 - s_9)))) + (m_{dot} * ((h_8 - h_5) - (T_o * (s_8 - s_5))))$$

$$E_{d\_HTRa} = ((m_{dot} * (s_9 - s_4)) + (m_{dot} * (s_5 - s_8))) * T_o$$

$$E_{d\_cooler} = (m_{dot} * (x_{max}) * (h_6 - h_1 - (T_o * (s_6 - s_1)))) + (m_w * (h_{w\_in} - h_{w\_out} - (T_o * (s_{w\_in} - s_{w\_out}))))$$

$$\text{"}E_{d\_cooler} = (m_{dot} * (x_{max}) * (h_6 - h_1 - (T_o * (s_6 - s_1)))) - ((m_{dot} * (x_{max}) * (h_6 - h_1)) * (1 - (T_o / T_1)))\text{"}$$

$$Q_{mix} = (h_8 - (h_{10} * (1 - x_{max})) - (h_7 * x_{max})) * m_{dot}$$

$$Ed_{mix} = Q_{mix} / T_8$$

$$E_{d\_mix} = ((m_{dot} * (s_8)) - (m_{dot} * (1 - x_{max}) * s_{10a}) - (x_{max} * m_{dot} * s_7)) * T_o$$

"Exergetic efficiency"

$$Ex_{outA} = Ex_{input} - ExINnet$$

$$\text{IRR\_total} = \text{E\_d\_IHX} + \text{E\_d\_LTR} + \text{E\_d\_HTR} + \text{E\_d\_T2} + \text{E\_d\_c2} + \text{E\_d\_cooler} + \text{E\_d\_c3} + \text{E\_d\_t1} + \text{E\_d\_c1} + \text{E\_d\_cc} + \text{E\_d\_mix}$$

$$E = ((\text{ExIN} - \text{IRR\_total} - \text{Exout}) / \text{ExIN}) * 100$$

$$E1 = (\text{W\_net\_out}) / \text{ExIN}$$

“Exergy efficiency of bottoming cycle”

$$\text{Tavg} = ((h_{.4t} - h_{.5t}) / (s_{.4t} - s_{.5t}))$$

$$\text{ExIN\_bot} = (\text{Q\_absorbed} * (1 - (\text{T}_o / \text{Tavg})))$$

$$\text{IRR\_bot} = \text{E\_d\_IHX} + \text{E\_d\_LTR} + \text{E\_d\_HTR} + \text{E\_d\_T2} + \text{E\_d\_c2} + \text{E\_d\_cooler} + \text{E\_d\_c3} + \text{E\_d\_mix}$$

$$\text{Ef\_bot} = 1 - ((\text{IRR\_bot}) / \text{ExIN\_bot})$$

$$\text{Ef\_bot2} = (\text{W\_net\_b}) / \text{ExIN\_bot}$$

$$\text{Ef\_bot3} = 1 - ((\text{IRR\_bot}) / \text{ExINnet})$$

$$\text{Ef\_bot4} = ((\text{W\_net\_b}) / \text{ExINnet})$$

$$\text{Total} = \text{IRR\_total} + \text{Exout} + \text{W\_net\_out}$$

$$\text{Totalb} = \text{IRR\_bot} + \text{W\_net\_b}$$

“Environmental Advantage”

$$\text{HR\_gt} = 7870$$

$$\text{Ef\_gt} = 53.07$$

$$\text{aCO2\_gt} = ((\text{HR\_gt} * \text{Ef\_gt}) / 1e6) * 0.454$$

$$\text{HR\_cc} = 7870$$

$$\text{Ef\_cc} = 53.07$$

$$\text{aCO2\_cc} = ((\text{HR\_cc} * \text{Ef\_cc}) / 1e6)$$

$$MCO2 = (aCO2_{cc} * W_{net_b})$$

$$A_{pet} = 0.266 \text{ [L/kWh]}$$

$$t_{oper} = 24[h]$$

$$M_{pe} = W_{net_b} * A_{pet}$$

“Turbomachinery sizing”

Average densities

$$\rho_{avg\_1} = (\rho_{.1} + \rho_{.2})/2$$

$$\rho_{avg\_2} = (\rho_{.6} + \rho_{.10})/2$$

$$\rho_{avg\_3} = (\rho_{.3} + \rho_{.4})/2$$

Turbine

$$H_{drop} = (h_{.3} - h_{.4}) * 1000$$

$$Q_{.t} = \dot{m} / \rho_{avg\_3}$$

$$N_{rpm\_t} = 15000$$

$$S_{.t} = 4$$

$$N_{rad\_t} = 0.105 * N_{rpm\_t}$$

$$N_{s\_t} = (((Q_{.t})^{0.5}) * (N_{rad\_t})) / (H_{drop}/S_{.t})^{0.75}$$

$$D_{s\_t} = 2.056 * ((N_{s\_t})^{(-0.812)})$$

$$D_{.t} = (D_{s\_t} * (Q_{.t})^{0.5}) / ((H_{drop}/S_{.t})^{0.25})$$

Compressor

$$S_{.c} = 4$$

$$H_{rise} = (h_{.2} - h_{.1}) * 1000$$

$$Q_{.c} = (\dot{m} * x_{max}) / \rho_{avg\_1}$$

$$N_{rpm\_c} = N_{rpm\_t}$$

$$N_{rad\_c} = 0.105 * N_{rpm\_t}$$

$$N_{s\_comp} = (N_{rad\_c} * (Q\_c)^{0.5}) / (H_{rise}/S\_c)^{0.75}$$

$$D_{s\_c} = 2.719 * (N_{s\_comp})^{-1.092}$$

$$D_c = (D_{s\_c} * (Q\_c)^{0.5}) / ((H_{rise}/S\_c)^{0.25})$$

Recompressor

$$S_{rc} = 4$$

$$H_{rise\_r} = (h_{10} - h_6) * 1000$$

$$Q_{rc} = (m_{dot} * (1 - x_{max})) / \rho_{avg\_2}$$

$$N_{rpm\_rc} = N_{rpm\_t}$$

$$N_{rad\_rc} = 0.105 * N_{rpm\_t}$$

$$N_{s\_rcomp} = (N_{rad\_rc} * (Q_{rc})^{0.5}) / (H_{rise\_r}/S_{rc})^{0.75}$$

$$D_{s\_rc} = 2.719 * (N_{s\_rcomp})^{-1.092}$$

$$D_{rc} = (D_{s\_rc} * (Q_{rc})^{0.5}) / ((H_{rise\_r}/S_{rc})^{0.25})$$

# MATLAB Code for Compressor Design

```
clc

clear all;

%%

##### INPUT PARAMETERS #####

mdot = 115.5; %Mass flow rate

T1 = 304.25; %Inlet total temperature (K)

N = 32000; %Blade speed (rpm)

Nrad = 0.105 * N; %rad/s

P1 = 7400; %Inlet total pressure (kPa)

alpha = 1.4; %Inlet swirl angle (degrees)

alpha1 = alpha * (pi/180); %Inlet swirl angle (radians)

r1.h = 15e-3; %Inlet hub radius (m)

t1 = 2.5e-3; %Inlet blade thickness

Zf = 8; %Number of full blades

Zs = 6; %Number of splitter blades
```

---

```

Z_t = Z_f + Z_s; %Total number of blades

% Target Stage Pressure ratio guess value

PR_target = 3.48;

% Rotor Pressure ratio guess value

PR_est(1) = 3.5;

% Total to total efficiency (estimated)

eff_tt(1) = 0.8;

##### Impeller Geometry #####

clrn = 0.00025; % Tip clearance

r1_t = r1_h * 3.2; % r1_t/r1_h = 3 (using radius ratio in literature)

b1 = r1_t - r1_h;

r1_s = r1_t + clrn;

r1 = sqrt((0.5* r1_s^2) + (0.5 * r1_h^2)); %Mean inlet radius r1

r2 = r1 * 2.5; % r2_t/r1 = 2.4 (using outlet radius ratio in literature)

b2 = 0.4*b1;

%%

##### Impeller Inlet #####

%Impeller Total Inlet properties

H1 = refpropm('H','T',T1,'P',P1,'CO2'); %total inlet Enthalpy

S1 = refpropm('S','T',T1,'P',P1,'CO2'); %total inlet Entropy

D1 = refpropm('D','T',T1,'P',P1,'CO2'); %total inlet Density

%Inlet Area

```

---

```

A1 = (pi* r1_s^2) - (pi* r1_h^2);

%Inlet blade velocity at radius r1,r1s,r1h

U1 = r1 * Nrad;

U1s = r1_s * Nrad;

U1h = r1_h * Nrad;

U1t = r1_t * Nrad;

% Inlet static density and static enthalpy function

[rho_s1,Hs1,C1,err] = inletdensity(mdot,alpha1,D1,H1,S1,A1);

%Ps_1 = refpropm('P','H',Hs1,'D',rho_s1,'CO2'); % Inlet static pressure

Ps_1 = refpropm('P','H',Hs1,'S',S1,'CO2');

% Inlet Axial velocity

C1a = C1 *cos(alpha1);

% Inlet Relative velocity and angle beta1

C_u1 = C1* sin(alpha1);

W_u1 = U1 - C_u1;

W1 = sqrt((W_u1^2) + (C1a^2));

beta1 = (atan(W_u1/C1a))* (180/pi);

W_u1s = U1s - C_u1;

W1s = sqrt((W_u1s^2) + (C1a^2));

W_u1h = U1h - C_u1;

W1h = sqrt((W_u1h^2) + (C1a^2));

W_u1t = U1t - C_u1;

```

```

W1t = sqrt((W_u1t^2) + (C1a^2));

##### Impeller outlet #####

eff_ttnew = zeros();

PR_new = zeros();

E = zeros();

for j = 1:50 % Pressure ratio correction loop

P2(j) = PR_est(j) * P1;

for i=1:500 % Total to total efficiency correction loop

S2_isen = S1; % Isentropic outlet total entropy

H2_isent = refpropm('H','P',P2(j),'S',S2_isen,'CO2'); %Total isentropic outlet En-
thalpy

H2_act = ((H2_isent - H1)/eff_tt(i)) + H1; % Actual outlet total enthalpy

S2_act = refpropm('S','P',P2(j),'H',H2_act,'CO2'); % Actual outlet total entropy

T2 = refpropm('T','P',P2(j),'H',H2_act,'CO2'); % Actual outlet total temperature

A2 = ((2* pi * r2) - ((Z_t)*t1))*b2; % Outlet blade area

U2 = r2 * Nrad; % Outlet blade velocity

C_u2 = (H2_act - H1 + (U1 * (C1* sin(alpha1))))/U2;

% Outlet static density and static enthalpy function

D2 = refpropm('D','H',H2_act,'P',P2(j),'CO2'); %total outlet Density

[rho_s2,Hs2,C2,Cr2,err2] = outletdensity(mdot,D2,A2,C_u2,H2_act,S2_act);

Ps_2 = refpropm('P','H',Hs2,'S',S2_act,'CO2'); % Outlet static pressure

H2s_isent = refpropm('H','P',Ps_2,'S',S2_isen,'CO2'); %static isentropic outlet En-
thalpy

```

---

```

V_2 = refpropm('V','H',Hs2,'D',rho_s2,'CO2'); % Outlet viscosity

alpha2 = (acos(Cr2/C2)) * (180/pi); % alpha2 in degrees

alpha2_rad = (acos(Cr2/C2)); %alpha2 in radians

% Outlet Beta angle and Relative velocity

W_u2 = U2 - C_u2;

beta2 = (atan(W_u2/Cr2))* (180/pi);

W2 = sqrt((W_u2^2) + (Cr2^2));

##### Enthalpy Losses correlations #####

%Incidence loss

L_Inc = 0.5 * ((W_u1^2)/2);

%Blade Loading loss

deltaH = H2_act - H1;

Denom = (W1s/W2)* (((Z_t/pi)*(1-(r1_s/r2))) + ((2*r1_s)/r2));

Df = (1- (W2/W1t)) + (((0.75 * deltaH)/U2^2)/(Denom));

L_bl = 0.05 * (Df^2) * (U2^2);

%Clearence loss

L_clr = (0.6/b2) * (C_u2*clrn) * (sqrt(((4* pi) / (b2 * Z_t))*(C_u2 * C1a) *
(((r1_t^2) - (r1_h^2))/((r2 - r1_t)*(1 + (D2/D1))))));

%Skin friction loss

Cf = 0.005;

C1s = C1;

Wavg = (C1s+C2+W1s+(2*W1h)+(3*W2))/8;

```

---

```

Lb = r1_t +(2*r2) - (2*r1_h);

Lb2 = (Z_t - (b2/2))+ ((0.5)*(((2*r2)-(2*r1))/cosd(beta2)));

Dh = pi * (((r1_t*2)^2 - (r1_h*2)^2)/((pi * (2*r1_t)) + (2*Z_t * ((r1_t*2) -
(r1_h*2)))));

L_skinf = (2 * Cf * (Wavg^2) * Lb )/Dh;

%Disc friction loss

Re_df = D2 * U2 * (r2/V_2);

rho_avg = (D2+D1)/2;

if Re_df > 3e5

f_df = (0.0622 /(Re_df^0.2));

else f_df = (2.67 /(Re_df^0.5)); end

L_df = f_df * ((rho_avg * (r2^2) * (U2^3))/(4*mdot));

% Recirculation loss

L_rc = (8e-5) * (U2^2) * (Df^2) * (sinh(3.5 * (alpha2_rad^3)));

% Mixing loss

D_eq = (W1+W2 + (4*pi*r2 * (((U2*C_u2)-(U1*C_u1))/(U2*Z_t*Lb))))/2;

if D_eq <= 2

W_sep = W2;

else

W_sep = W2*(D_eq/2);

end

Cm_wake = sqrt(W_sep^2 + W_u2^2);

```

---

```

Cm_mix = ((Cr2* A2 )/ (pi * b2 * 2 * r2));

e_wake = 1-(Cm_wake/Cm_mix);

L_mix = (1 / (1+(tan(alpha2_rad))^2)) * ((C2^2) / 2) * ((1- e_wake - 0.8)/(1-
e_wake))^2;

##### Efficiency Correction #####

H2_actnew = H2_isent + (L.Inc + L_mix + L_bl + L_clr + L_skinf + L_df + L_rc);

eff_ttnew(i) = ((H2_isent - H1)/(H2_actnew - H1));

eff_ts(i) = ((H2s_isent - H1)/(H2_actnew - H1));

E(i) = abs(eff_ttnew(i) - eff_tt(i));

if E(i) < 1e-8 break else eff_tt(i+1)=eff_ttnew(i); end

end

%%

##### Pressure ratio Correction (Outer loop)#####

kd = 0.08; % Diffuser loss coefficient

P3 = P2(j) - (kd * ( P2(j) - Ps.2));

S3 = refpropm('S','P',P3,'H',H2_act,'CO2');

PR_new(j) = P3 / P1;

E2(j) = abs(PR_new(j) - PR_target);

if E2(j) < 1e-8

break

else

PR_est(j+1)=PR_est(j) * (PR_target / PR_new(j));

```

end

end